THE EFFECTS OF FATIGUE AND HEAT TREATMENT ON PLANE STRAIN FRACTURE TOUGHNESS

A THESIS

PRESENTED TO

THE FACULTY OF GRADUATE STUDIES

THE UNIVERSITY OF MANITOBA

IN PARTIAL FULFILMENT

OF THE REQUIREMENTS FOR THE DEGREE

MASTER OF SCIENCE IN ENGINEERING

BY

IVAN LEONARD PURDY

1970

TABLE OF CONTENTS

ABSTRACT

The engineering problem of fracture is investigated with the specific aims of understanding the component processes and variables affecting fracture. The effects of maximum fatigue stress intensity, specimen geometry, and heat treatment cycle on the plane strain fracture toughness of a material are studied. Compact tension specimens and single edge notch specimens, machined from plates of 18 N_i (250) maraging steel and 4340 steel, were fatigue cracked and then fractured in quasi-static tension tests. The experimental data indicate that the fracture toughness is affected by the maximum fatigue stress intensity and the heat treatment cycle. Also, the measured fracture toughness is found to depend upon the geometry of the specimen used in the fracture toughness test.

ACKNOWLEDGEMENTS

The author wishes to express his sincere gratitude to Dr. J. Shewchuk and Dr. M. Chaturvedi for their guidance, encouragement, and friendly advice given during this project. The author is also indebted to the technicians and other graduate students, especially Mr. S. Joshi, of the Department of Mechanical Engineering for their assistance. Also, the author extends his thanks to the United States Steel Corporation for their donation of the materials used, the Defence Research Board of Canada for their financial support of the project, and the Bell Canada Corporation for their fellowship awarded to the author.

LIST OF TABLES

LIST OF FIGURES

CHAPTER 1

INTRODUCTION

1.1 Introduction

The phenomenon of structural failure by catastrophic fracture at average stress levels well below the yield strength has been encountered as an engineering problem for many years. The frequency of occurrence of such failures has increased over the years as the size and load carrying requirements of the components of engineering structures have increased. Tests and procedures have been developed to counter particular problems but until recently, no generally useful approach had been developed.

Early investigations into fracture situations were, in the main, post-failure in nature. As most failures originated from stress concentrations or material inhomogenity whose presence were unknown to the designer and because the process of fracture was very rapid with little or no forewarning by general yielding, tests were required to measure fracture-resistive properties of materials to help in preventative design against fracture failure. Various impact energy, transition temperature, notch and bend tests were devised to measure a material's resistance to certain types of stress concentrators but a generally applicable test for a material parameter, or parameters, to be incorporated in design was still required.

During recent years, the demand for very high strength, light weight materials by the defense and aerospace industries has placed more importance

on the problem of fracture, and especially brittle fracture. As higher strength, lower ductility materials were brought into use, service failure of components made from these materials became a very major concern and thus emphasized the need for a quantitative approach to dealing with cracks and crack-like flaws in structures.

With the realization of the problem at hand, study was begun with the object of establishing laboratory tests and analytical techniques which could provide a measure of the crack tolerance of a material. Such knowledge would provide workable criteria for evaluating and selecting materials for a given application and, consequently, develop a rational basis for design against fracture.

As the laboratory tests were designed to model the actual situation in a structure, it was necessary to model the cracks and flaws to their same degree of severity. The actual structural components would vary, from application to application, in size, heat treatment, load history, and similar related variables. Thus it becomes desirable to determine in the laboratory how such variables affect the model to provide some information as to how the structure will behave under the application of these variables.

1.2 Statement of Problem

This thesis is primarily an experimental study of the effect on the measured plane strain fracture toughness parameter, K_{IC}, of the fatigue load history and of the heat treatment given to the material during the development of a crack-like defect.

1.3 Scope of Thesis

The thesis is divided into 6 chapters.

Chapter 1 is an introduction to the field of fracture and a statement of the problem under study.

A review of the macroscopic and microscopic methods of interpreting the factors affecting fracture is presented in Chapter 2.

Chapter 3 develops the theory of fracture mechanics approach.

The experimental study which was performed to measure the effect of fatigue load history and heat treatment on fracture toughness is described in Chapter 4.

The results and discussion of the experimental program are analyzed in Chapter 5.

Chapter 6 contains a summary of the thesis.

A bibliography is presented at the conclusion of the thesis.

CHAPTER 2

A REVIEW OF PUBLISHED LITERATURE ON FRACTURE

2.1 Introduction

The literature review which follows will attempt to present a state of the art picture of the problem of fracture as it is being handled. As a beginning, the terminology involved in fracture will be defined. With a rigorous statement of terminology as a basis, the literature review will proceed to reveal the macroscopic and microscopic features of fracture analysis and to show the effects of variables on fracture. Then, equipped with an understanding of the features of fracture and the variables involved, a review of design approaches to fracture will be presented. Chapter 2 will then conclude with a concise summary of the fracture situation.

2.2 Fracture Terminology

In the technical literature relating to the subject of fracture, a source of confusion can be the terminology. Different terms may have similar meanings or a single term may possibly have different interpretations. Therefore, terms used to describe the fracture process, the appearance of a fracture surface, laboratory test methods and measurements will be defined in this section.

As a first step, the word fracture must be clearly understood. When a solid is subjected to increasing loads, the resulting stresses will, at a certain stage, become high enough to cause the solid to break apart. If such breakage occurs before the piece has thinned down to zero thickness, the process is called fracture (26). Separation following reduction to zero thickness is termed rupture (26). Most fractures consist of three stages:

crack initiation, crack propagation, and final separation.

When analyzing a fracture, the extent of plastic strain before fracture can be employed as an indication of the circumstances preceding the failure. In assessing the amount of plastic deformation, the terms brittle and ductile are used.

Ductile fracture involves extensive prior plastic deformation. Usually the strain in the component will considerably exceed the strain associated with the material's yield strength. Figure 2.1 illustrates typical ductile behaviour in a slow bend test of a standard V-notch Charpy specimen.

In the realm of ductile fracture, the word tough often appears. Tough behaviour is descriptive of fracture occurring only after extensive plastic deformation and hence at stresses above the yield strength. Qualitatively, tough is associated with the term ductile.

The word brittle describes the behaviour of a member that fractures with negligible plastic deformation. Brittle can be arbitrarily defined as "behaviour in which the nominal plastic strain preceding fracture, at whatever stress, is less than a small but measurable value commonly taken as a few percent strain." (3). Figure 2.2 and 2.3 illustrate typical brittle and ductile failures.

Fracture appearance also required terminology. Fracture surface appearance is described with reference to (a) the macroscopic geometry of the surface (b) the texture of the surface as seen by the unaided eye and (c) the microscopic geometry of fracture as related to crystal structure and observed under a light microscope.

Macroscopic geometry employs the terms shear, ductile, tearing and

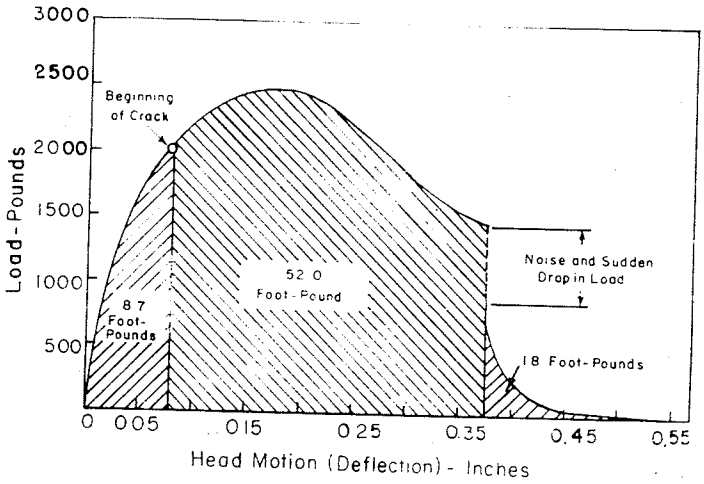

Figure 2.1 Load-deflection curve for a slow bend test of a standard 'V'-notch Charpy specimen (3)

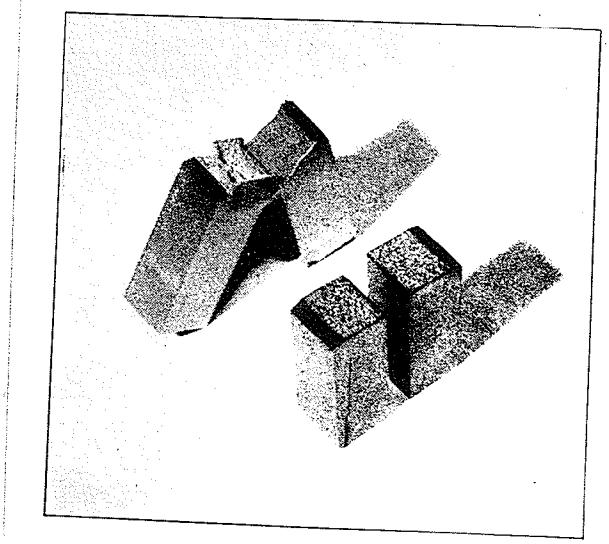

Figure 2.2 Typical brittle and ductile fractures of Charpy impact specimens (8)

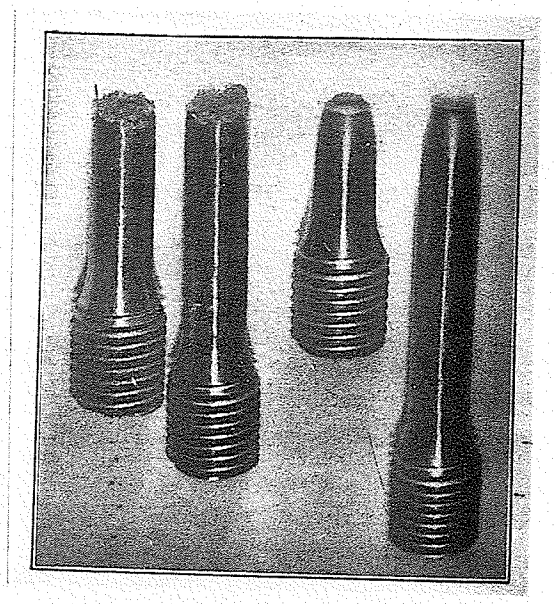

Figure 2.3 Typical tensile fractures of brittle and ductile material (8)

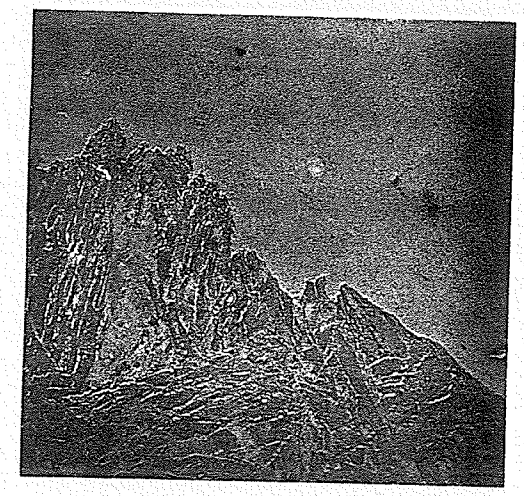

Figure 2.4 Microsection of fibrous fracture of medium carbon alloy steel (3)

slant to describe fracture where separation occurs on oblique planes of high shearing stress. The texture of such surfaces is referred to as fibrous.

The terms brittle, flat and square describe separation that occurs on a plane of high tensile stress. The texture of such a surface is described as granular or crystalline in appearance.

Microscopic observations of fracture are placed into one of three categories - fibrous, cleavage or intercrystalline. Fibrous fracture is associated with severe plastic deformation of the crystals prior to separation which causes a very jagged appearance as shown in Figure 2.4. Cleavage cracks are shown in Figure 2.5. Cleavage fracture may be defined as: "a low energy, low deformation, transgranular fracture that produces a fracture surface composed entirely, or almost entirely, of one or more flat facets, each of which is formed by the propagation of a crack through a crystal by mechanisms that do not require plastic strain in volumes of material at distances ahead of the crack equal to a major portion of the size of the crystal through which the crack is passing." (12)
Cleavage cracks are associated with particular crystallographic planes and are made up of straight segments. Individually, cleavage cracks are associated with very small plastic strains. However, the joining together of several of these cracks may involve large plastic strains and a tearing action. Finally, grain boundary or intercrystalline cracking may be caused by such various embrittling conditions as temper embrittlement from improper heat treatment and embrittlement from mercuric and hydrogen atmosphere. The relation of embrittlement to fracture will be more fully discussed later. Figure 2.6 shows grain boundary cracking due to the presence of temper embrittled tempered martensite.

Figure 2.5 Cleavage crack in a grain of coarse-grained ferrite

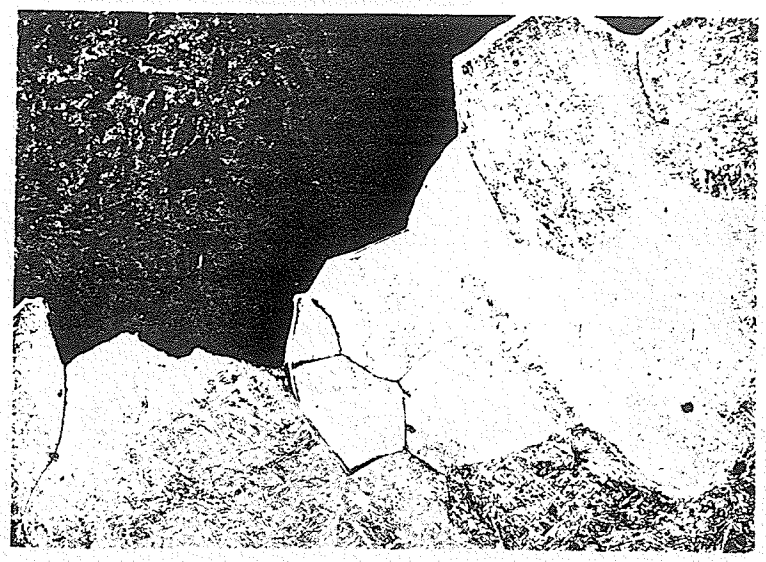

Figure 2.6 An example of grain-boundary fracture (3)

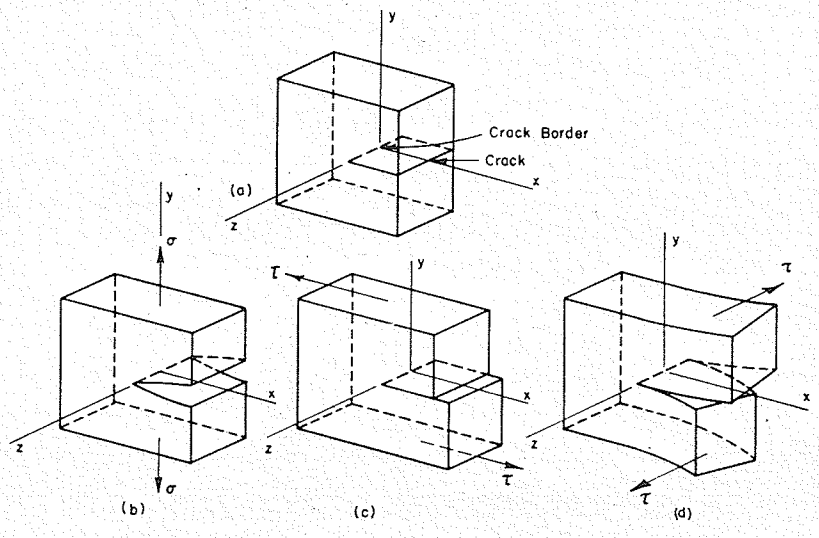

Figure 2.7 Crack surface displacements and modes of fracture (3)

(a) Member containing crack (b) Opening mode

(c) Forward shearing mode (d) Parallel shearing mode

When fracture occurs, displacements of surfaces must also occur. Fracture appearances are associated with particular displacement modes. Hence, an understanding of the three possible displacement modes will aid in comprehending fracture surface appearance. Figure 2.7 (a) shows a block of material with a crack border along the z axis. Opening mode displacements occur when the crack surfaces separate in the y direction only, as shown in Figure 2.7 (b). Forward shearing mode displacements, Figure 2.7 (c) occur when the crack surfaces slide in the x direction only. Parallel shearing mode displacements occur when the crack surfaces slide in the z direction only, as in Figure 2.7 (d). Now it can be seen that the terms brittle, flat, cleavage and square relate to an opening mode fracture. Similarily, shear, ductile, tearing and slant relate to a shearing mode of fracture. A mixed mode of fracture consists of an opening mode of fracture over the central fracture surface bounded by a shear mode of fracture or shear lips at the surfaces.

Transitions in fracture behaviour also occur and must be described. Fracture mode transition is a change in fracture mode, perhaps from shear to opening mode and can be attributed to such causes as a decrease in temperature, an increase in strain rate, or an increase in specimen size or thickness. Temperature transitions are also very important in fracture behaviour as a change in operating temperature of a component may vary its required energy to fracture and thus affect its fracture behaviour. Hence we have particular transition temperatures identified by 1) a change from tough to brittle behaviour, 2) a change from a shear to an opening mode fracture, 3) a marked change in the fracture stress, or 4) a definite change in the ability of the material to arrest a running crack.

2.3 Macroscopic Features of Fracture Analysis

2.3.1 Brittle Fracture

The fractures in structural materials, which have caused so much concern, have all the characteristics of brittle fracture. These failures occur quite suddenly, usually without warning, and propagation to total failure is limited to fractions of a second. Such fractures show no apparent deformation of the component as a whole or only very localized yielding in the vicinity of the fracture origin.

Numerous examples of catastrophic fracture have been observed and recorded. Figure 2.8 shows a ship which fractured in two while in port when the nominal stress in the deck was less than 10 k.s.i. Figure 2.9 reveals the wreckage produced when an East Ohio Gas Company liquid storage tank fractured. The brittle fracture of this large tank allowed the escape of gas into a heavily populated industrial area of Cleveland, Ohio in 1944, claiming over 130 lives and property damage estimated in excess of seven million dollars. Shown in Figure 2.10 is the havoc created in the Ridgeland power station in Chicago in 1954 when the low pressure spindle of a 165 M.W. steam turbine burst. These examples all reveal the very dangerous and harmful consequences of brittle fracture.

A remarkable feature of most of these service fractures is the apparent absence of ductility, while a normal tensile test on the same material at the same temperature of the casualty may show an extension of 20 to 30%. Investigations of the casualty material did not reveal an abnormally high tensile strength nor exceptional hardness which are both somewhat indicative of brittleness. Explanations for such failures can usually be found only after detailed investigations into the microstructure of the fracture and

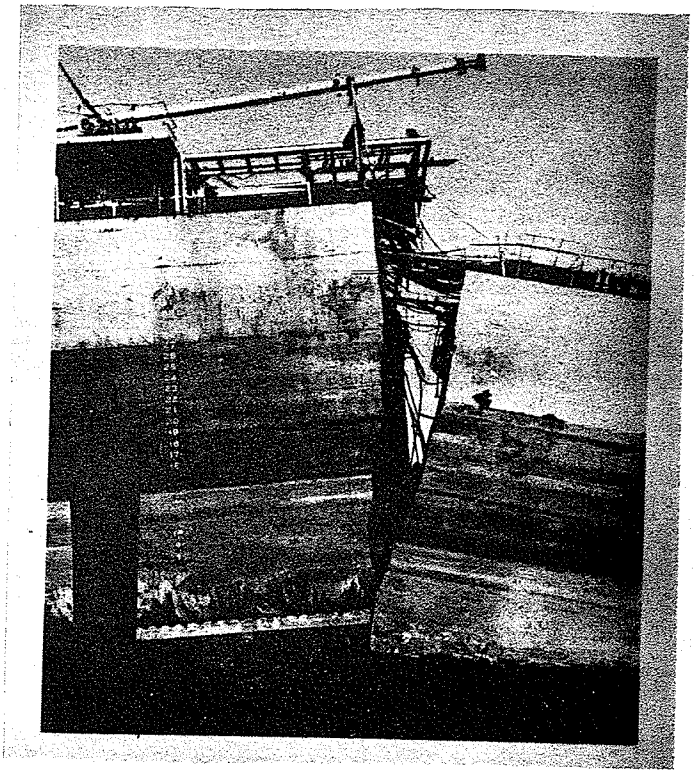

Figure 2.8 A ship which fractured while in port (9)

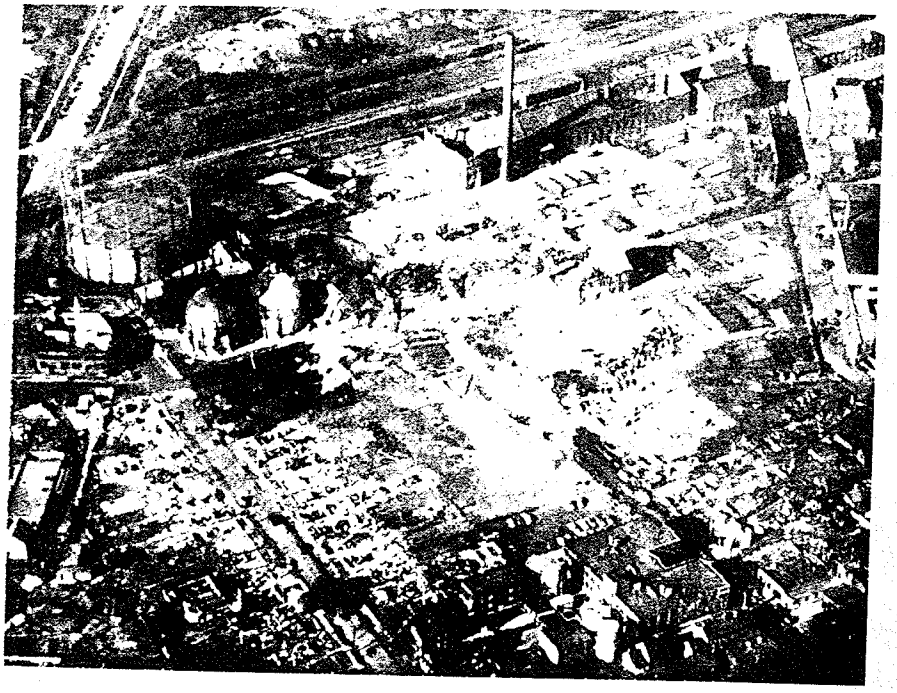

Figure 2.9 Wreckage produced by liquid storage tank fracture (3)

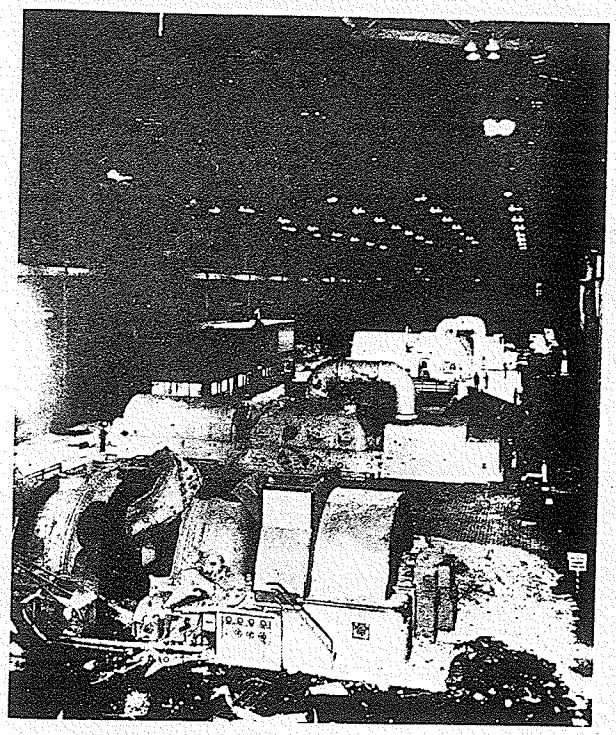

Figure 2.10 View of Ridgeland power station following turbine spindle failure (6)

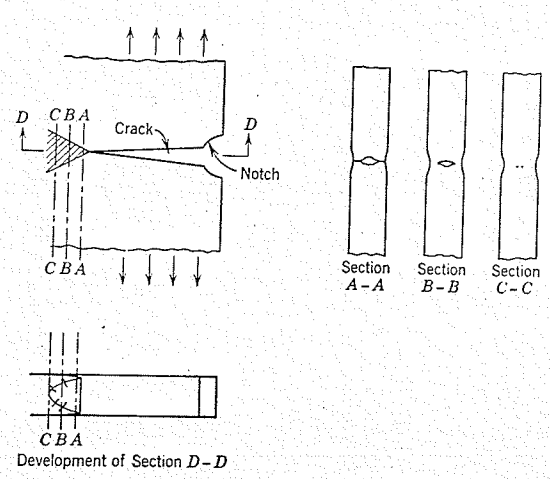

Figure 2.11 Mode of failure of a notched plate in tension (8)

and the adjacent material. The correlation of this information to the temperature, constraints, stress concentrations and loads that were present at the time of the fracture will yield a possible explanation for the fracture failure.

When considering fracture on the microscale, surfaces will separate due to (a) shear forces producing slip movement along certain crystallographic planes and/or (b) tensile forces causing cleavage or splitting. In most fractures, both modes will be present in varying degrees. Since maximum tensile, compressive and shear forces are oriented in a characteristic way for each manner of load application, identification of the basic mechanism is often useful in determining the type of load that initiated fracture. On the other hand a knowledge of the manner of load application with reference to a fracture can aid in determining whether the fracture was brittle or ductile in nature.

Shear fractures are predominantly dull gray and fibrous in appearance and have edges which are usually deformed plastically. Such fractures are promoted by the action of shear forces and may be compared to the separation of cards in a deck when one part of the deck slides over the other until translation separates the deck in two stacks.

Conversely, brittle fractures are generally crystalline in appearance. Each crystal tends to fracture on a single plane and this plane will vary slightly from one crystal to the next in the aggregate. Brittle fracture surfaces often have a characteristic "chevron" or "herringbone" pattern which points back towards the fracture origin. Mrs. C.F. Tipper in a paper to the Seventh International Congress of Applied Mechanics in London, September 1948, has given information on the formation of these

"chevrons" (8). Chevrons were produced on the fracture surface of tension tests on notched plates as shown in Figure 2.11. Ahead of the crack is a plastic wedge and sections of this wedge are shown at the right of Figure 2.11. Section A-A shows a large ragged opening at the middle of the plate connected to the plate edges by cracks. Section B-B shows a small opening with no cracks extending to the surfaces. Section C-C shows small holes only. A development of these sections along a plane D-D results in a crack front roughly the shape of a V. Normals to this front would have the shape of chevron marks. These markings can thus be followed back to the point of origin and are very helpful in determining the presence of a flaw or stress concentration that may have initiated a fracture. Figure 2.12 shows examples of chevron markings.

A very major portion of the brittle fracture problem lies with fatigue fracture. Fatigue fracture is essentially the brittle fracture of otherwise ductile materials. Fatigue fractures compose over 90% of all fractures in machine components (10). Consequently, a knowledge of the characteristics of such failures would be of great value. Fatigue fractures usually develop over a relatively long period of time following a succession of load applications and consequently the surface will often have a distinctive appearance. Generally, failures start at the surface at some point where the shear stresses first exceed the shear strength. The failure may start at a single location or at multiple locations, depending on the shape of the section and the type of loading. This statement is supported by the failure surfaces in Figure 2.13. An analysis of a fatigue fracture in the light of the knowledge from this figure would enable the designer to make a very good estimate of the degree of improvement required to prevent

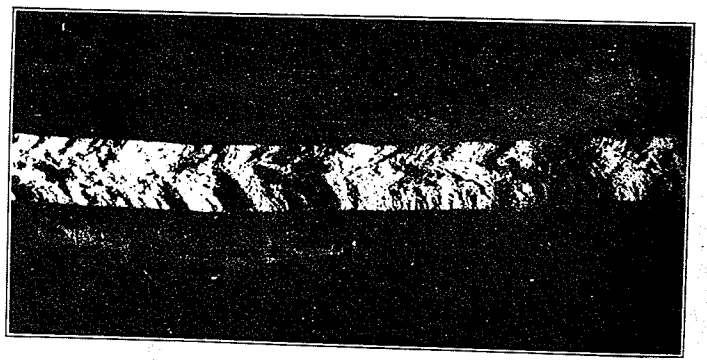

Figure 2.12 An example of chevron marks (8)

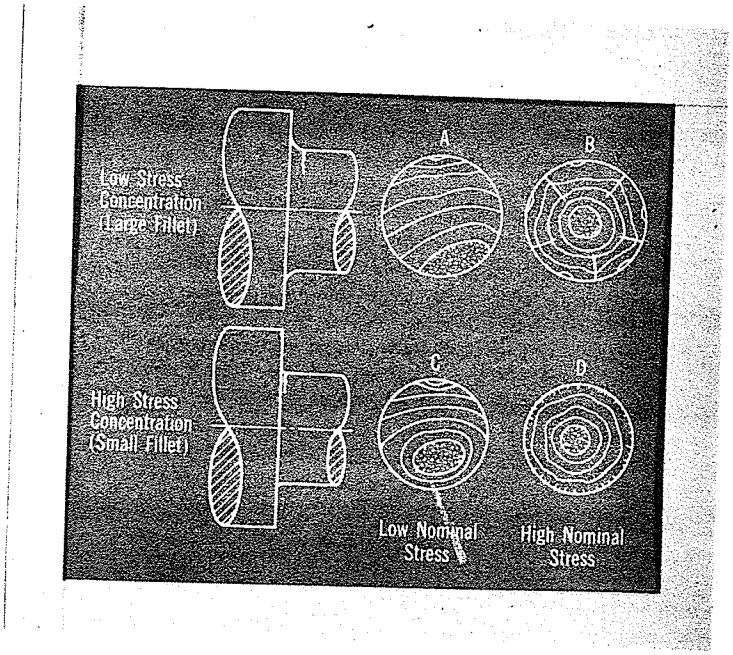

Figure 2.13 The effect of degree of loading and stress concentration on the appearance of fracture surfaces of rotating bending fatigue failures (10)

similar failures from recurring.

When analyzing a fatigue fracture, surface indications such as beach marks, ratchet marks, and the location of final rupture area provide valuable information concerning the loading history imposed on the failed component. Fatigue cracks usually start parallel to the maximum shear stress at the surface but soon turn and advance perpendicular to the maximum tensile stress. As the load fluctuates, the crack grows and continues to weaken the section. Load variations and environmental effects cause small ridges or "beach marks" to form. These beach marks then indicate the position of the advancing crack tip at a particular time. As the section weakens, the crack growth rate increases, causing the beach marks to become farther apart, larger, and thus more distinct. Figure 2.14 shows clearly the presence of beach marks.

When fatigue causes initiation of failure in several locations of a filleted shaft in rotating bending, the junction of progressing fractures usually results in "ratchet marks". The mechanism of their formation is shown in Figure 2.15 and an example of the development of ratchet marks is shown in Figure 2.16.

Figure 2.14 reveals another feature of a fatigue fracture. As is indicated, the final rupture area is not directly opposite the fracture origin but is offset somewhat by the effect of rotation. This can be helpful in analyzing the operation of a component as the final rupture area is offset opposite to the direction of rotation.

The appearance of a fatigue fracture surface can be affected by the notch sensitivity of the material. As discussed in (11) a fatigue crack in

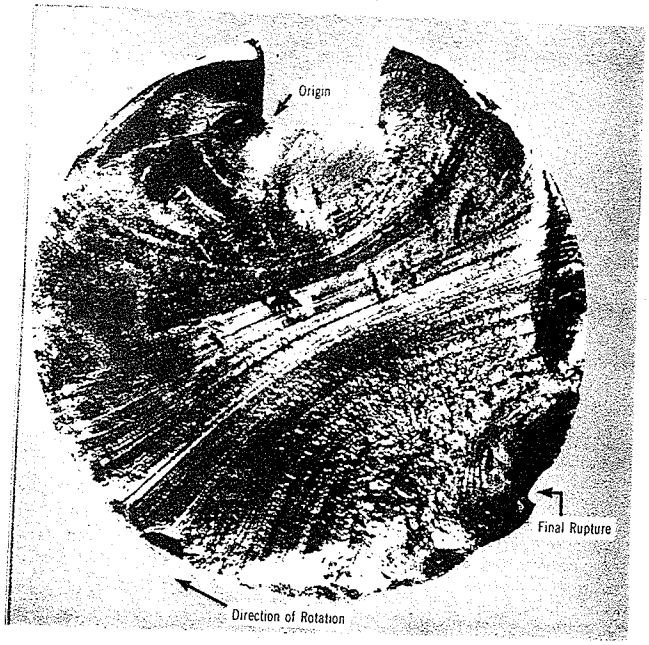

Figure 2.14 The offsetting effect of rotation on the zone of final failure (10)

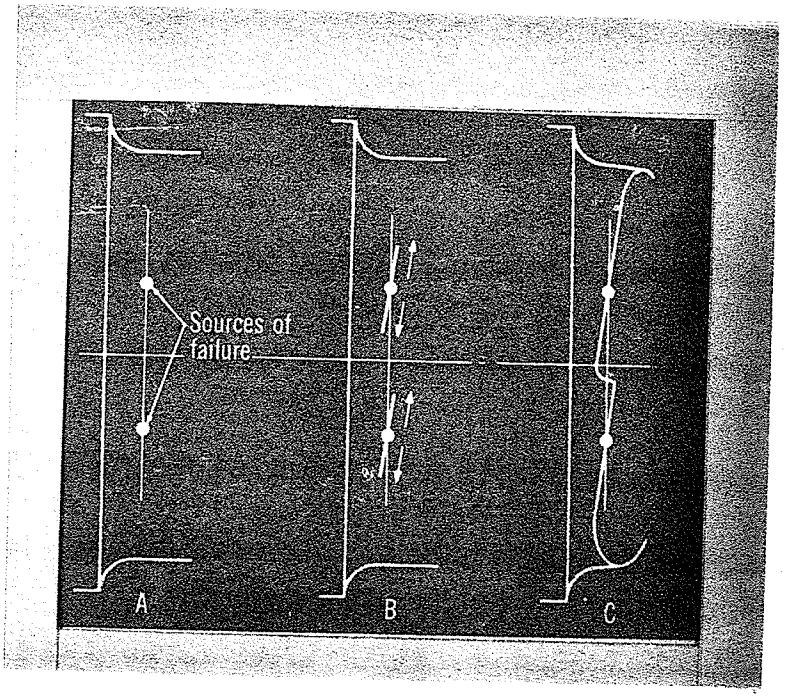

Figure 2.15 The formation and development of "ratchet marks" on the surfaces of fatigue failures (10)

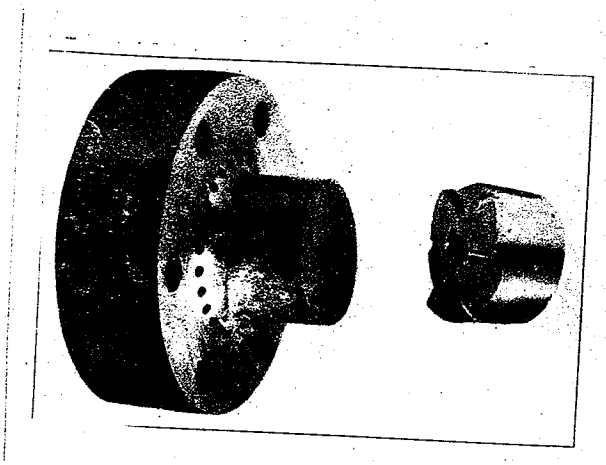

Figure 2.16 Helical crack development and ratchet marks in laboratory test of rotor model (8)

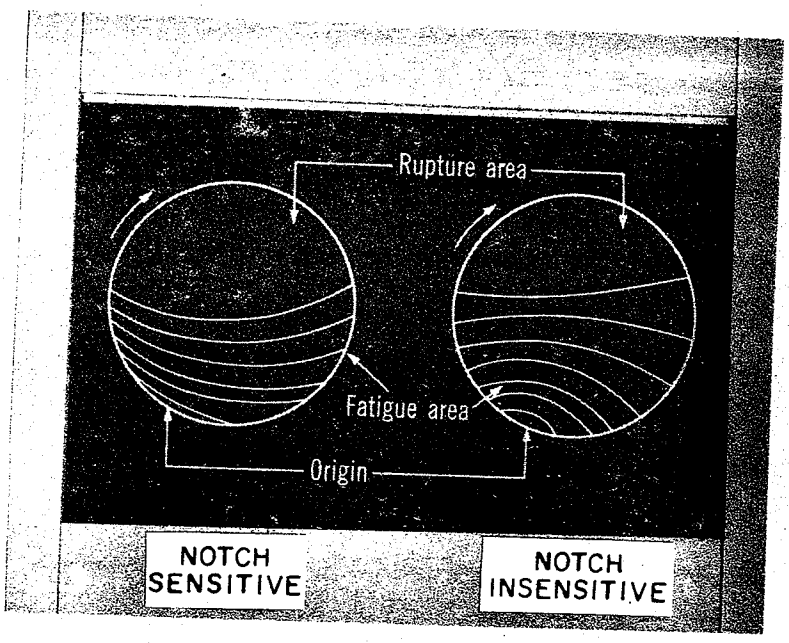

Figure 2.17 An illustration of the effect of degree of notch sensitivity on the development of beach marks (10)

a notch-sensitive material will tend to grow more rapidly at the highly stressed surface. Consequently, in rotating bending, beach marks will curve away from the origin because the rate of crack growth is greater along the periphery than in the interior. On the other hand, in a less notch-sensitive material, a crack will progress at a lower rate along the periphery producing a concave pattern from the origin. Both effects are demonstrated in Figure 2.17.

Fatigue fractures that originate in longitudinal stress concentrations can often be a source of concern. Figure 2.18 shows (a) how keyways and splines may act to concentrate stress and (b) that fatigue cracks tend to propagate perpendicular to the lines of maximum stress. Figure 2.19 shows the typical "starry" fracture that occurs when multiple cracks lead to fracture of a spline shaft. Keyways in shafts may also lead to a "peeling" fracture, as shown in Figure 2.20. Such fractures are usually indicative of a loosely fitting component in which nearly all the torque is transmitted through the key. Failure starts at the bottom corner of the key and progresses parallel to the surface. Figure 2.21 reveals the tendency of a fatigue crack to curve inward towards the larger section at an abrupt change of cross section, again following the normal to the maximum stress.

Fatigue failures may start below the surface if the combination of applied and residual stress exceeds the sub-surface fatigue strength of the metal. In such sub-surface fractures, a circular pattern of beach marks may form around the origin, giving a "fisheye" appearance as shown in Figure 2.22.

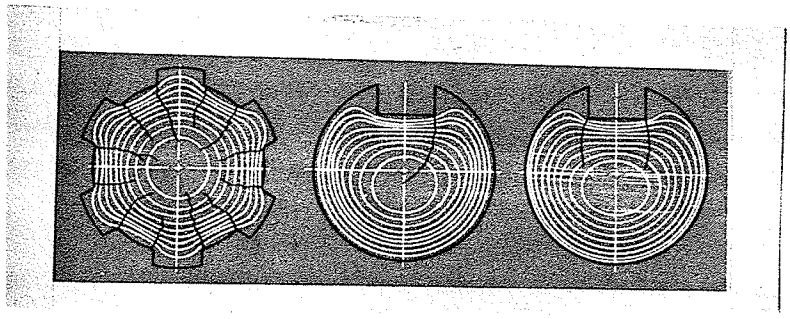

Figure 2.18 Stress lines (white lines) and resulting cracks (dark lines) from stress concentrations in keyways and splines (10)

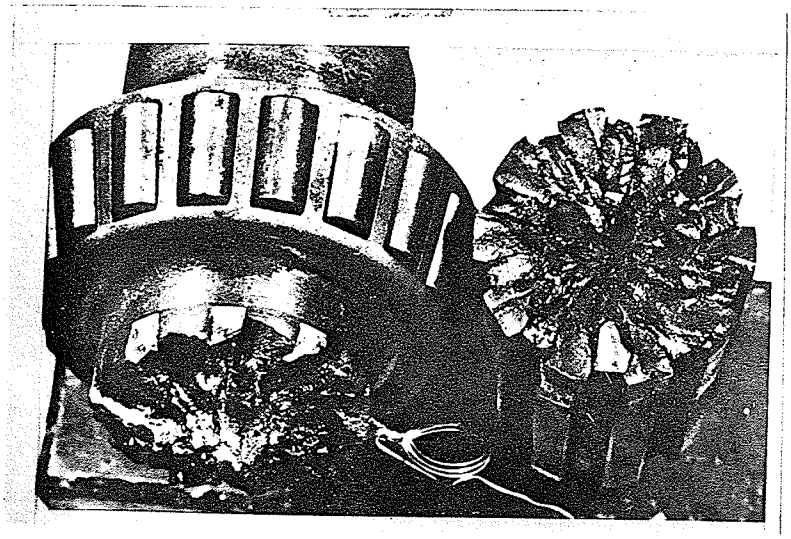

Figure 2.19 The "starry" fracture surface of a spline shaft which failed in reversed torsional fatigue (10)

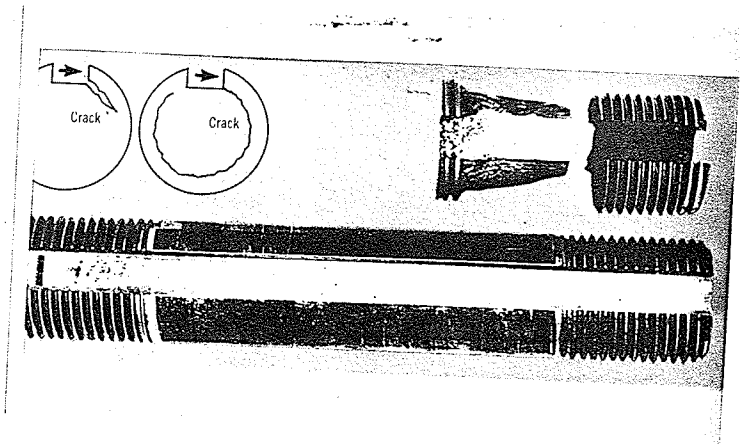

Figure 2.20 A peeling failure around a shaft under the surface resulting from fatigue cracks in keyways of loosely fitting members (10)

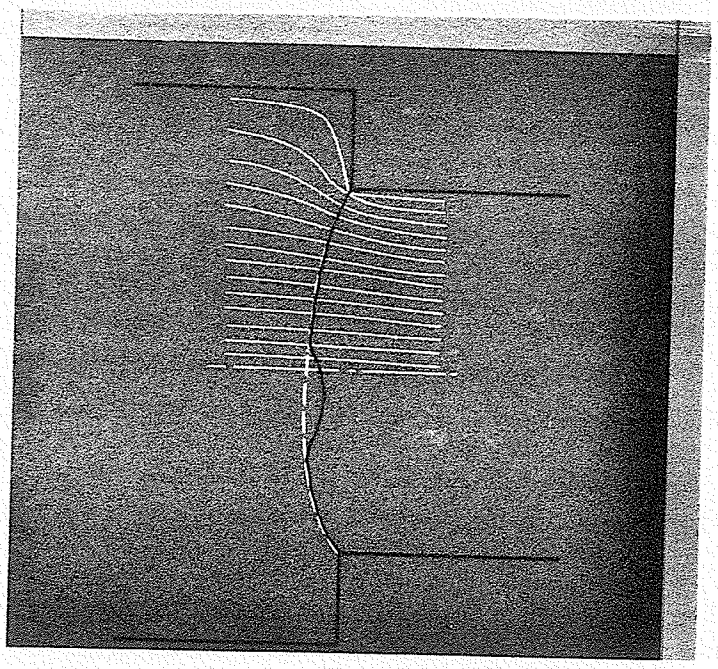

Figure 2.21 Fatigue failure in sharply filleted sections tend to follow the zone of highest stresses (10)

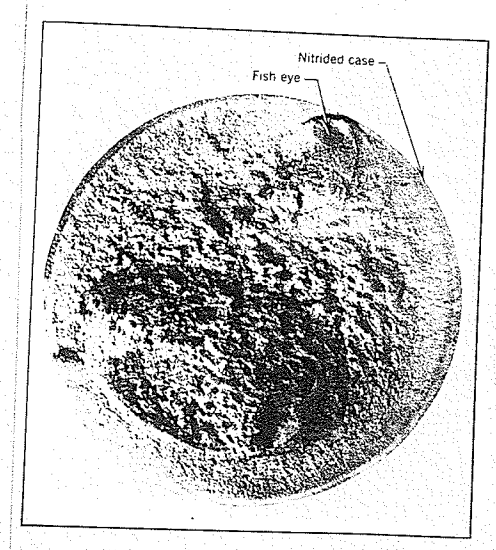

Figure 2.22 "Fish-eye" under nitrided case of a fatigue test specimen (8)

Figures 2.23 and 2.24 illustrate how a fracture would originate in the absence or presence respectively of a stress concentration for a uniform material and a surface hardened material. Figure 2.23 shows that in the absence of stress concentrations, subsurface failures may develop when a component's strength drops abruptly below the surface. However, when a stress concentration is present, the gradient of applied stress drops sharply near the surface and then more gradually to the neutral axis. Under these conditions, failure will almost always start at the surface.

Figures 2.25, 2.26, 2.27 and 2.28 illustrate various type of fatigue fractures that were induced by bending. As pointed out by Wulpi (10): "Fracture caused by bending stress is usually not difficult to analyze if it is remembered that (1) the crack is perpendicular to the tensile stress which occurs on one side of the bend, and (2) the maximum applied stress is located at the surface."

However, fractures not originating at the surface may complicate the problem as pointed out in the preceding part of this section (Figure 2.29). Reversed bending fatigue without rotation may cause cracks on opposite sides of a shaft since each side undergoes alternate tensile and compressive stresses as shown in Figures 2.25 and 2.26. Rotating bending, on the other hand, tends to initiate fatigue cracks starting at numerous locations, as indicated in Figure 2.27.

Axial fatigue of shafts is relatively uncommon in comparison to bending or torsional fatigue. However, certain parts may be subjected to elastic wave reflection of axial stresses (11). In the absence of stress concentrations, these waves may start fatigue cracks anywhere in the section.

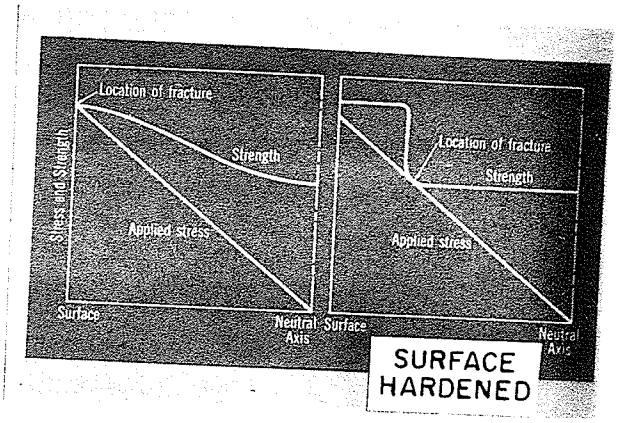

Figure 2.23 Illustration of location of fracture in the absence of stress concentrations (10)

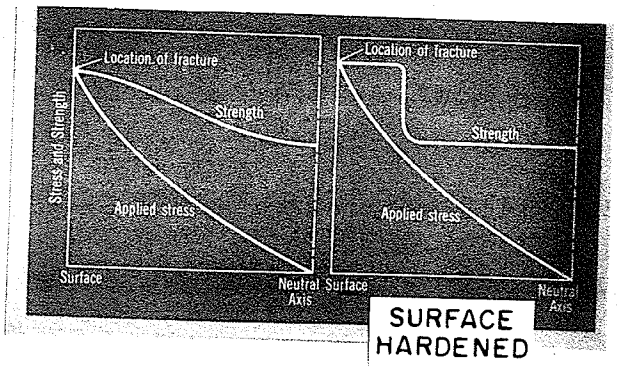

Figure 2.24 Illustration of location of fracture when a stress concentration is present (10)

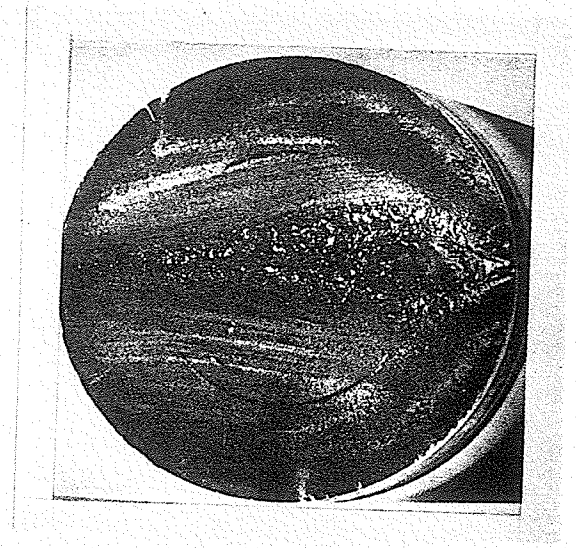

Figure 2.25 A bending failure of a cylindrical shaft when subjected to reversed loading as a cantilever beam (10)

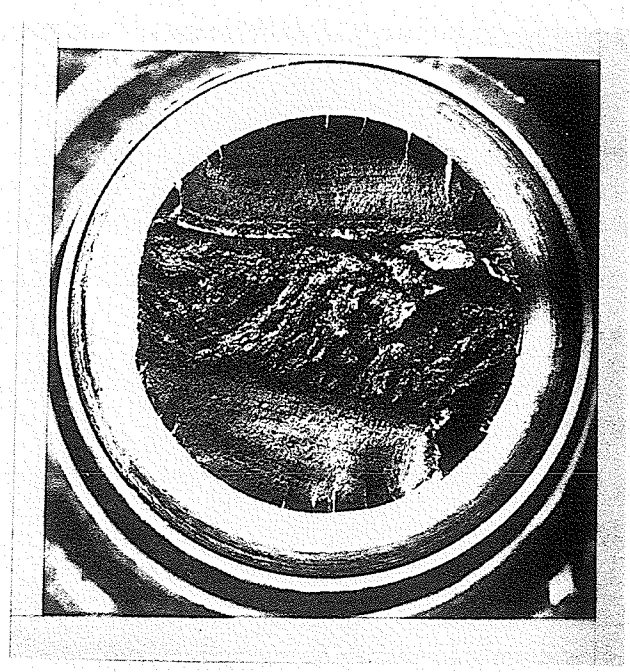

Figure 2.26 A reversed bending fatigue fracture resulting from stress concentrations in a sharp fillet (10)

Figure 2.27 A shaft failure in rotating bending fatigue due to stresses concentrated by a sharp snap ring groove (10)

Figure 2.28 Bending type of service failure of a diesel engine crankshaft (8)

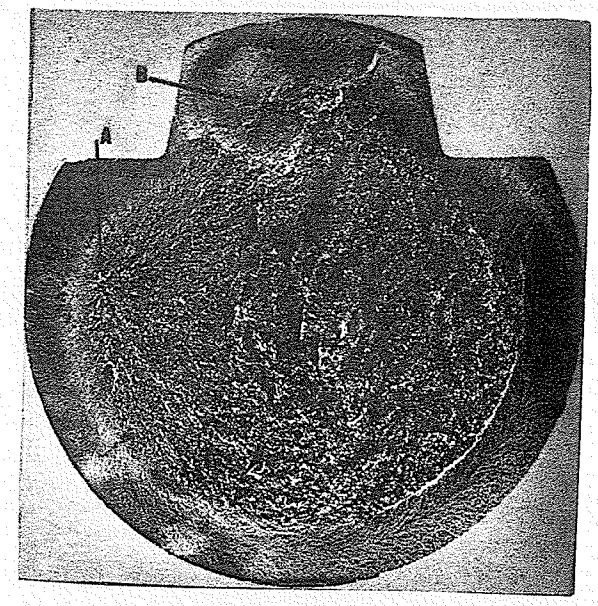

Figure 2.29 A rotating bending failure which began beneath the surface. Chevron marks point to both origins, A and B, and indicate brittle sudden final failure (10)

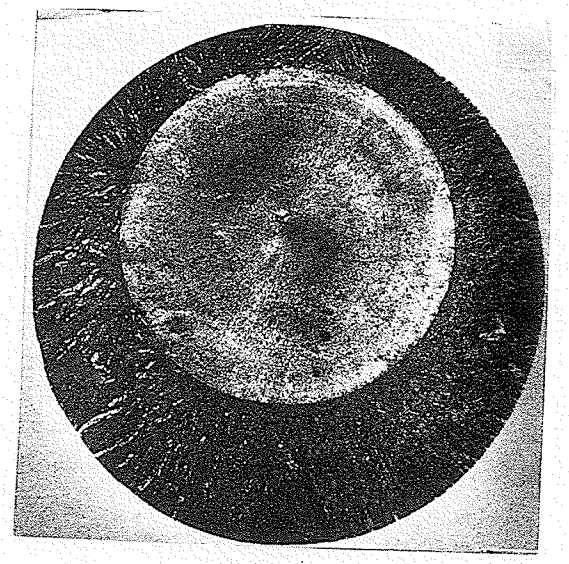

Figure 2.30 A tensile fatigue fracture which occurred in a piston rod of a forging hammer from the "flake" near the center (10)

Figure 2.30 illustrates a "flake" which acted as an internal stress raiser and led to axial fatigue fracture.

Torsional fatigue fracture occurs in such components as crankshafts, torsion bars, coil springs and axles. Keyed or splined shafts and shafts with holes in cylindrical surface may fail in torsion when overloaded. As pointed out by Wulpi (11), shafts under a pure torsional load have five important characteristics:

(1) There are two directions of planes on which maximum shear stresses form. One is perpendicular, the other parallel to the axis of the shaft.

(2) There are two directions of planes on which the maximum normal stresses occur. Both are a 45^{o} to the axis and are perpendicular to each other.

(3) At any given point on shaft surface, the magnitudes of all the maximum stresses - shear, tensile, and compressive - are equal to one another.

(4) All principal stresses are maximum at the surface and zero at the axis.

(5) No normal stresses act on maximum shear planes and, conversely, no shear stresses act on the maximum stresses which are normal to the flat planes.

Consequently, torsional cracks may follow the transverse or longitudinal shear planes, the diagonal planes of maximum tensile stress, or combinations of these. This is shown schematically in Figure 2.31. Therefore, torsional fractures will illustrate a strong dependence on load history and material properties of the shaft in question. Figures 2.32, 2.33 and 2.34 illustrate examples of torsional fracture of service components.

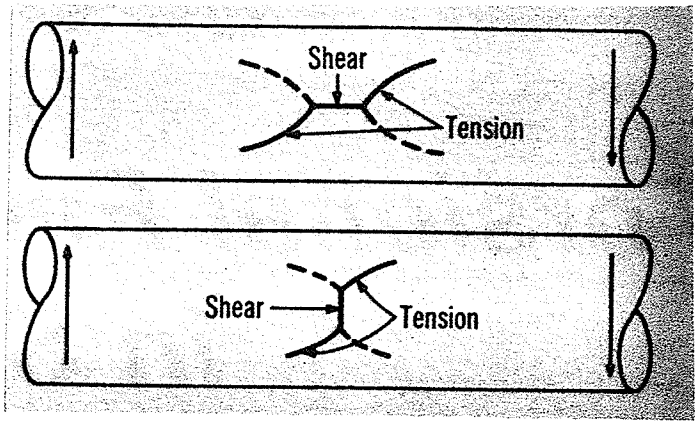

Figure 2.31 Torsional cracks may begin in longitudinal (top) or transverse shear (10)

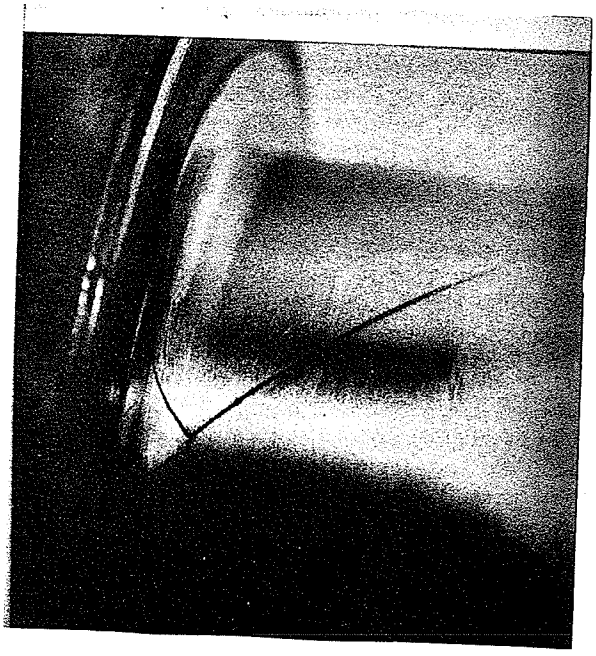

Figure 2.32 Crack formation at the base of a fillet during a reversed torsional fatigue test (10)

Figure 2.33 Holes in shafts sometimes concentrate stresses, resulting in torsional fatigue failures (10)

Figure 2.34 Torsion type of service failure of a diesel engine crankshaft (8)

2.3.2 Ductile Fracture

Ductile fracture, in contrast to brittle fracture, is preceded by a large amount of permanent strain. The limiting case of separation by plastic flow until the cross-section vanishes is called rupture. When appreciable plastic flow occurs but a fracture surface exists and the deformation is less than that required for rupture, the process is termed ductile fracture.

Initiation of ductile fracture can be caused by a number of mechanisms. Often during a normal tensile test, an internal crack can be revealed by sectioning the test specimen after the test has been terminated just prior to fracture as shown in Figure 2.35. Closer examination of such a sectioned area may reveal voids opening up, as in Figure 2.36, from oxide inclusions. In steels, the crack source may be the relatively brittle pearlite. Another source of initiation of ductile failure may be impurities or inclusions trapped in grain boundaries.

Fracture of ductile material may also be initiated by geometrical constraints placed on the material. A good example of geometrical constraint is the severe notch conditions placed on high strength steels to initiate low stress fracture.

Once a ductile fracture has been initiated, its mechanism of development becomes important. Ductile fracture which has been initiated by cracks in brittle phases or inclusions will have a critical development stage because the initiating cracks soon become blunted and leave a number of small holes. The growth and coalescence of these holes to final fracture will depend on the amount of further plastic strain and on the transverse stress which will tend to open up the holes. Fracture initiation due to

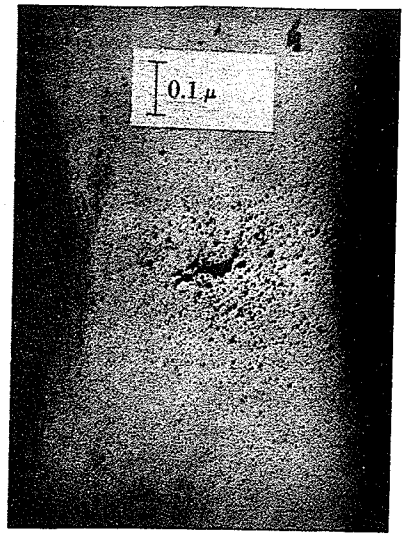

Figure 2.35 Internal crack at neck of tensile specimen of 99.9% pure, tough pitch electroytic copper (26)

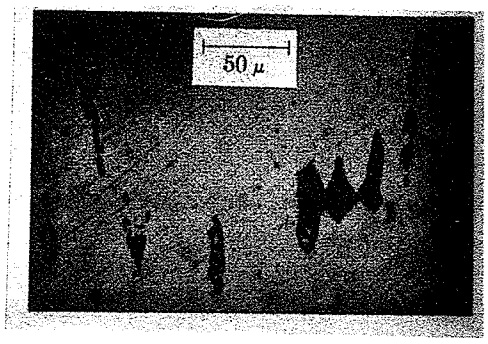

Figure 2.36 Holes growing from inclusions in the copper of Figure 2.35 (26)

very localized strain concentrations, such as may result from strain-softening, will develop simply by a continuation of the initiating mechanism. Thus, ductile fracture initiation and development do not follow one criterion but several competing ones, depending on the combination of stress, strain, and load history.

2.4 Microscopic Features of Fracture Analysis

2.4.1 Low Magnification Analysis

This section will deal with the microscopic features of fracture analysis in the range of magnifications from 1 to 5x for examination of the entire fracture surface and up to about 1000x for examination of the area surrounding a crack tip. The following section will deal with high magnification analysis accomplished by the electron microscope.

Magnification of an entire fracture to a power above 10x is not practical for an optical microscope because of the limited depth of field of such a microscope. However, magnification up to 10x will enable the examiner to look more closely at a specific area in order to try to understand the mechanism that may have initiated the fracture. Figure 2.37 shows an application of the optical microscope to enlarge a specific area of interest.

Small areas of a fracture section may be polished and etched to reveal the nature of the material surrounding the crack that led to failure. Figures 2.5 and 2.6, referred to in 2.2, show mechanisms which can cause failure. During the investigation of the Tanners Creek turbine wheel fracture, photomicrographs (Figure 2.38) revealed grain boundary films which, it was determined subsequently, did not contribute to the failure. Figure 2.39 illustrates the use of an optical microscope in following a crack which

Figure 2.37 Distinctive circular mark on primary fracture surface of a generator rotor failure (5)

Figure 2.38 Photomicrograph showing grain boundary films in Tanners Creek turbine wheel (7)

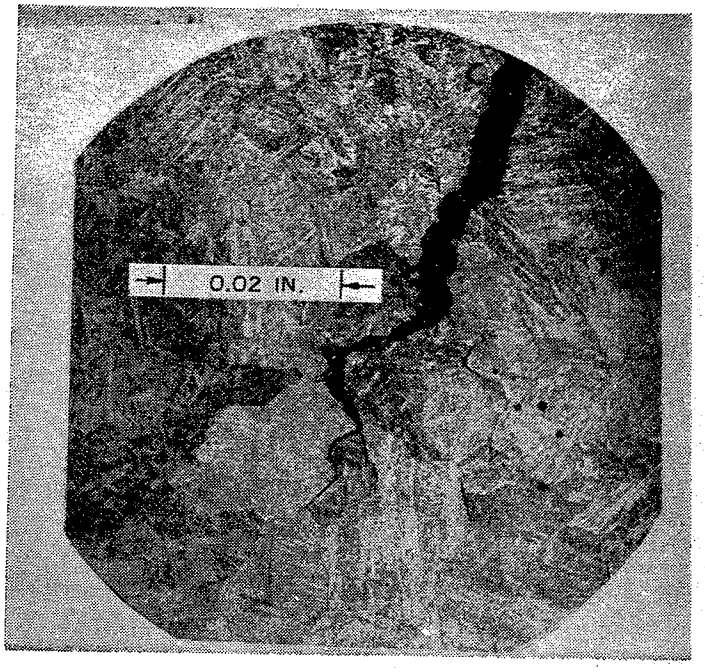

Figure 2.39 Photomicrograph of termination of crack in turbine wheel rim specimen after 2812 hours at 960°F (7)

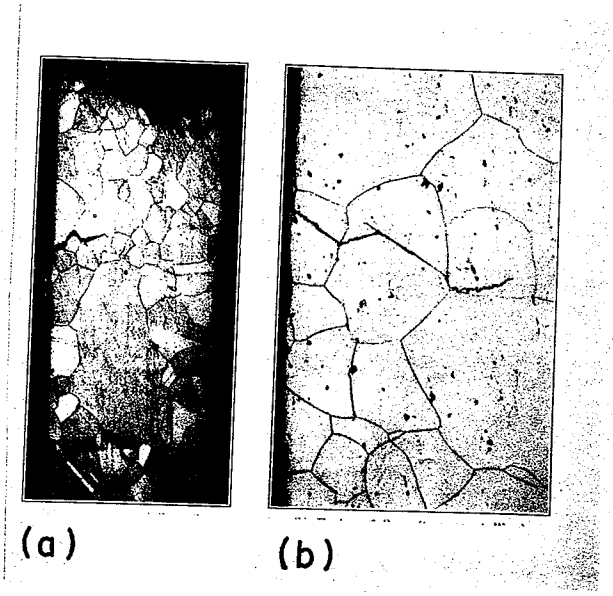

Figure 2.40 (a) Creep-rupture failure (intercrystalline)
(b) Fatigue failure (transcrystalline) (8)

caused fracture in a simulated turbine rim wheel test. Intercrystalline creep-rupture failure is contrasted to transcrystalline fatigue fracture in Figure 2.40. These photographs illustrated the use of optical microscopy in fracture analysis.

2.4.2 High Magnification Analysis

In recent years, the electron microscope has been employed as a helpful instrument in studying the nature of fracture surfaces and revealing the nature of macro-mechanisms that lead to failure. Such a study of fracture surfaces on the microscale has been termed fractography. Unlike the optical microscope which employs reflected light to form an image, the electron microscope relies on the transmission of electrons through the specimen onto a fluorescent screen to produce an image.

Since metal films must be of the order of 1000 angstroms or less for transmission of electrons, fracture surfaces as such cannot be examined. However, replicas can be made of the surface and they can be examined in the electron microscope. The two most widely used techniques for making replicas are (1) the direct carbon technique and (b) the cellulose acetate - metal shadow - carbon technique.

The direct carbon technique consists of placing the fracture specimen directly into a vacuum apparatus, lowering the pressure to 10^{-4} to 10^{-6} torr and then causing carbon to evaporate from two carbon electrodes and deposit on the fracture surface. The specimen is then removed from the vacuum chamber and the metal is dissolved away, leaving the carbon replica which can then be mounted and examined in the electron microscope. A problem inherent with this technique is that, by dissolving the specimen, nothing is

left to fall back on if any errors were made.

The second technique involves softening a piece of sheet plastic such as cellulose acetate in a suitable solvent. The softened plastic is then forced down upon the fracture surface, causing the plastic to assume the shape of the fracture surface. The plastic is permitted to harden and is then pulled off the fracture surface. The plastic replica is then placed in a vacuum apparatus where it is shadowed first by a heavy metal such as palladium to improve the contrast and then carbon to act as a base. The replica is now placed in a solvent to dissolve the plastic and then the carbon-heavy metal replica may be examined. This latter technique preserves the fracture surface for re-use.

The replica techniques outlined above can be used to study the fracture modes such as cleavage or shear or to study the progress of fatigue loading across a surface. Cleavage fractures are low energy, low deformation, transgranular fractures. The fracture surface is composed almost entirely of one or more flat facets. Figure 2.41 shows a cleavage fracture of iron broken at dry ice temperature. This figure shows cleavage steps at the horizontal arrows and river patterns between the oblique arrows. Cleavage facets have a definite and predictable angular relationship with the crystallographic reference planes of the underlying crystall structure.

Certain quenched and tempered steels do not exhibit this "definite and predictable angular relationship" and have been placed in the category of quasi-cleavage. Figure 2.42 shows a quasi-cleavage facet in a quenched and tempered steel. The arrows indicate river patterns which show the local fracture origin to be in the interior of the facet.

Plastic deformation processes usually involve slip. Slip processes leave distinct surface markings on the fracture surface which are rounded

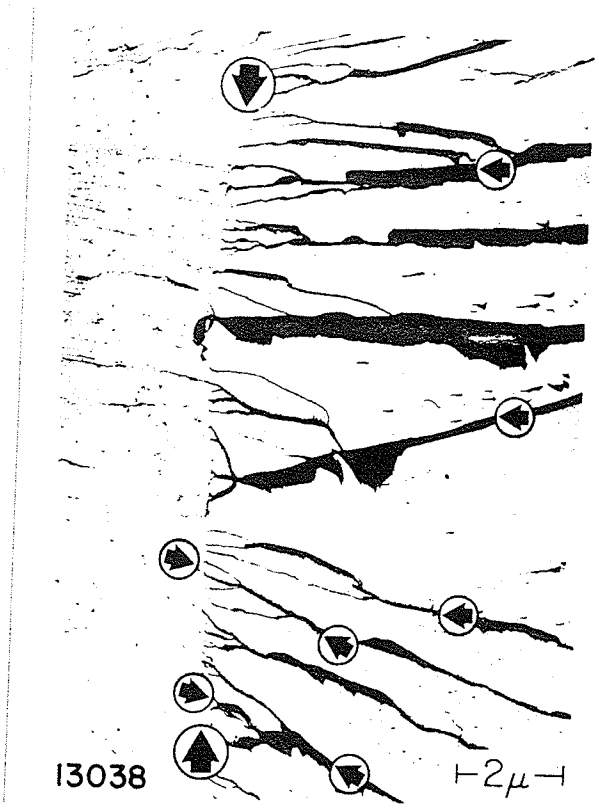

Figure 2.41 Cleavage in iron broken at dry ice temperature (12)

Figure 2.42 A quasi-cleavage facet (bounded by large arrows) in a quenched and tempered steel (12)

Figure 2.43 Ripples (between arrows) in a wrought iron fracture surface (12)

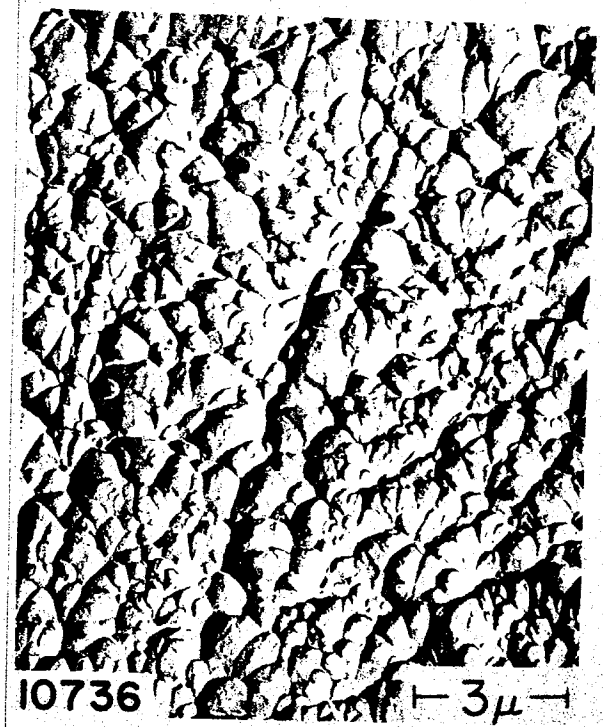

Figure 2.44 Equiaxed dimples resulting from microvoid coalescence (12)

out during latter stages of deformation, leaving the surface smoothly undulating, as shown in Figure 2.43.

Weak boundaries, brittle particles, and microcracks serve as mucleation sites for microvoids. These voids will grow in size with rising stress until either the applied stress is relaxed or fracture relieves the local stresses. The voids appear as dimples on the fracture surface. The nature of the dimples gives an idea of the type of fracture that occurred. Figure 2.44 shows equiaxed dimples resulting from normal fracture while Figure 2.45 shows shear dimples formed by shear fracture with Figure 2.46 illustrating tear dimples resulting from tearing.

Intergranular fracture is revealed in Figure 2.47. Propagating cracks from fatigue, environmental influences or improper heat treatment may follow grain boundaries.

Beach markings, as referred to earlier, were macroscopic features of a fatigue fracture surface. A detailed examination of such beach marks with the electron microscope has revealed that each beach mark is composed of many smaller parallel lines referred to as fatigue striations (Figure 2.48). Forysth and Ryder (13) proved that each load excursion was responsible for one striation and that the size of a striation (that is, the distance between markings) depended strongly on stress amplitude. Hence use of the electron microscope has shown there is a clear distinction between macroscopically observed beach marks, which represent periods of growth during thousands of load cycles, and the microscopically observed striations, which represent the extension of the crack front during one load cycle.

To summarize, the electron microscope can be used to study (a) fracture modes such as cleavage, quasi-cleavage, plastic deformation processes, microvoid coalescence and intergranular fracture and (b) the mechanisms of fatigue.

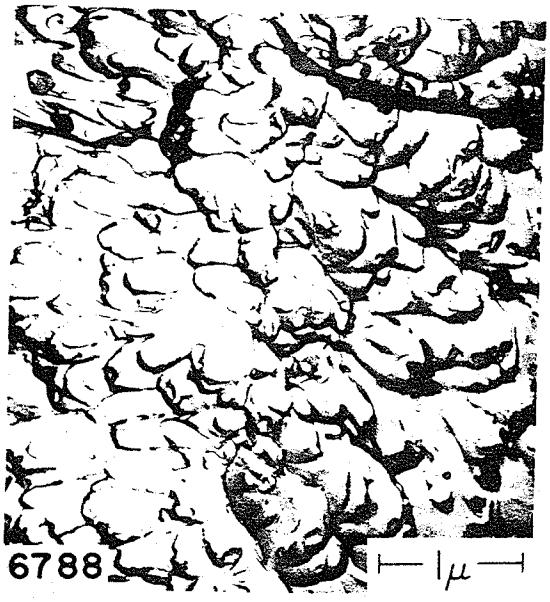

Figure 2.45 Shear dimples on the surface of a shear lip of a stainless steel specimen (12)

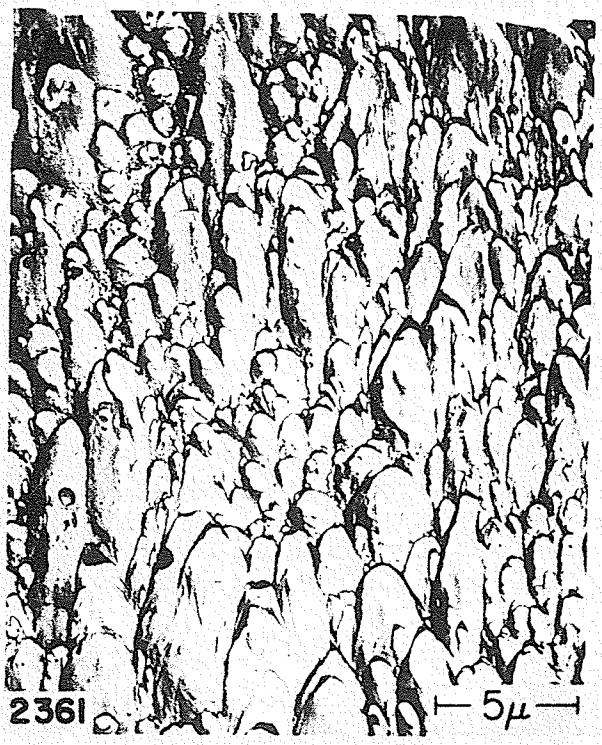

Figure 2.46 Tear dimples in A.I.S.I. Type 410 stainless steel (12)

Figure 2.47 Intergranular fracture surface caused by stress corrosion cracking in tap water (12)

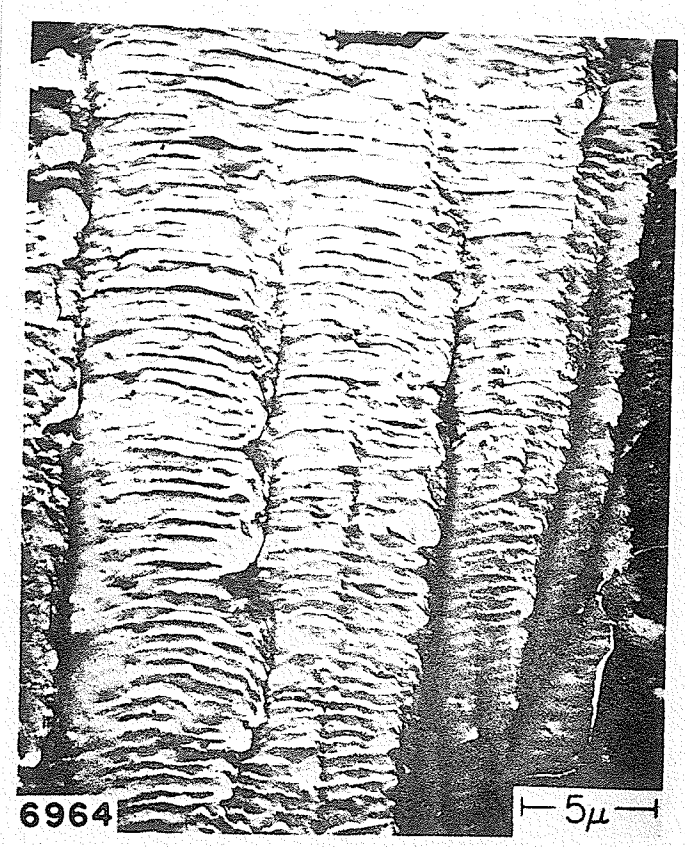

Figure 2.48 Striation patches in 2024 aluminum (12)

2.5 Variables Affecting Fracture

2.5.1 Stress Concentration Effects

Most component parts and assemblies contain notches, fillets, holes, and other geometrical irregularities which tend to increase, or concentrate, the surface stress. Stress concentrations may be introduced by inadequate caution in design procedures or by tool tears when machining is not performed carefully or ordinary tool marks in regions of high stress may cause damage by increasing the stress level imposed on the part. In addition to the stress raising effects of the notch or discontinuity, a triaxial state of stress will develop in the region immediately behind the notch.

This second factor, the triaxial stress state, inhibits yielding. It is known from the theory of elasticity that, for an elastic material loaded in tension normal to a crack in a very thin plate, a biaxial stress state will exist with two nearly equal principal stresses. One of these principal stresses is directed parallel to the crack and the other is directed normal to the crack plane. However, for a thick plate, the depth dimension is generally large compared to the crack root radius and a third principal tensile stress is developed at the center of the plate, normal to the plate surface. This triaxial stress state inhibits plastic flow and promotes brittle behaviour.

Stress concentrations are particularly dangerous in fatigue loading situations. Under a static load, the highly stressed metal yields at the crack tip and passes the stress on to adjacent sections until fracture occurs. However, fatigue loads usually stress the metal below the elastic limit, yielding is localized on a much smaller scale, and work hardening can occur. This can lead to crack growth and progressive deterioration of

the section with no external appearances of forthcoming fracture. Figure 2.49 illustrates the effect of severe notches in steel specimens subjected to fatigue loading.

2.5.2 Specimen Size Effects

Size effect is a particularly important factor to consider in the brittle fracture of components. The strength of a brittle material is governed by the stress at the root of the most dangerous crack and hence it becomes more and more likely to find a dangerous crack in thicker specimens.

Size effect has been observed and measured in various materials. Reinkober (26) in 1931 showed the effect of size by breaking glass fibers, then the two fragments, then the fragments of fragments and each time observed higher strength values. Lubahn (27) recorded a size effect in notched beam specimens. Notched beams 4 inches deep and varying in thickness from 1/8 inch to 4 inches, were fractured in a slow bend test and the nominal net fracture strength was measured. Figure 2.50 shows the results of Lubahn's experiment. Such an effect could be expected, as explained previously, because of the restricting effect on plastic flow of specimen thickness.

Size effect varies with the material involved but is primarily dependent on the distribution and severity of flaws throughout the material. In some brittle materials, such as inorganic glasses, cracks are formed only at the free surfaces, in other such as cast iron, cracks are uniformly distributed in the volume, in still others, such as polymers, different types of flaws exist in the surface and in the volume.

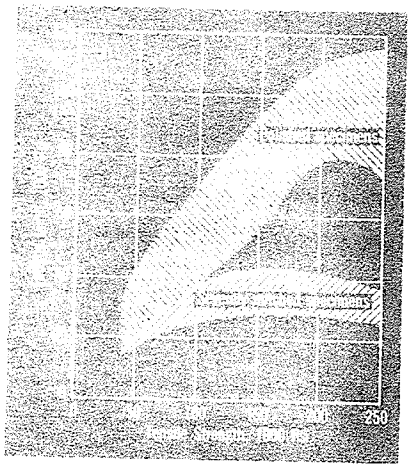

Figure 2.49 Influence of notches on the fatigue life of steel specimens (10)

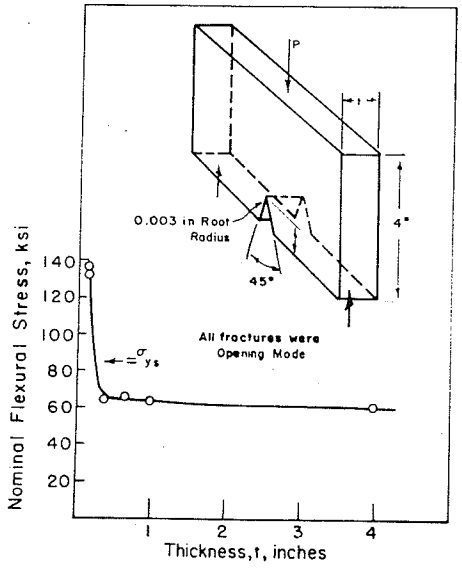

Figure 2.50 Influence of thickness on the flexural strength of notched beams (3)

The recognition of the existence of a size effect is of importance because it places additional emphasis on the interpretation of results of model testing. The smaller test model will have a statistically higher strength and may exhibit plane stress behaviour while the actual component may behave in plane strain. Consequently the application of fracture strengths measured in the laboratory to actual components must be done with the acknowledgment of possible size effects.

2.5.3 Enviromental Effects

2.5.3.1 Temperature

Temperature has often been considered to be among the most influential factors affecting fracture. Generally, decreasing the operating temperature of a material will raise the yield strength, tensile strength and hardness while decreasing the ductility. The cohesive strength of the material will rise as the temperature is lowered but not as rapidly as the rise in the yield strength. Hence the ratio of cohesive strength to flow strength decreases as the temperature decreases. Consequently, the fracture mechanism may change from a high energy shear fracture to a low energy, low deformation brittle fracture. The sensitivity of metals to this temperature transition effect varies and is usually less for the very high strength materials. However, most of the medium or low carbon steels (typical of construction materials for many applications for many years) do exhibit a marked transition in fracture behaviour as the temperature is lowered.

Because many of the commonly used steels do exhibit a transition temperature effect, it becomes important to determine reliable tests to predict the transition temperature. Transition temperature testing will be dealt with more extensively in a following section but it can be said here that the problem is not a simple one as many materials are strain rate and notch sensitive and consequently the transition temperature may vary

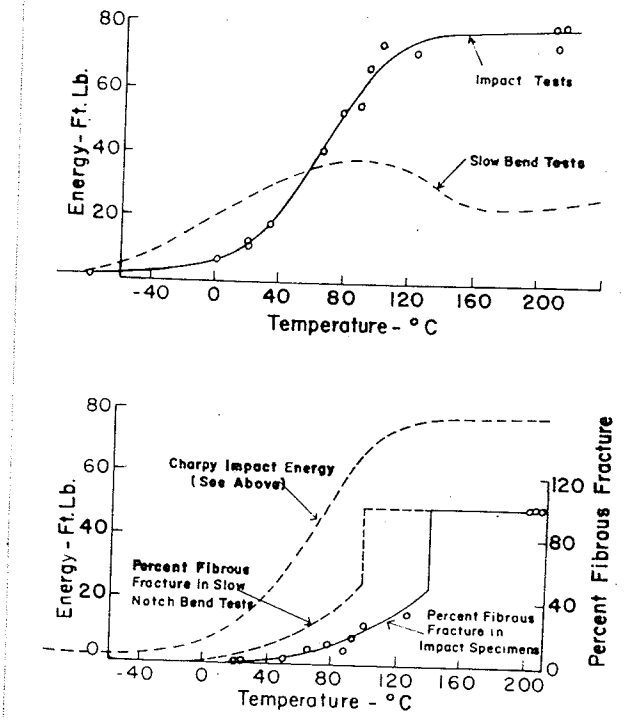

Figure 2.51 Comparison of V-notch Charpy impact characteristics with slow bend test results (3)

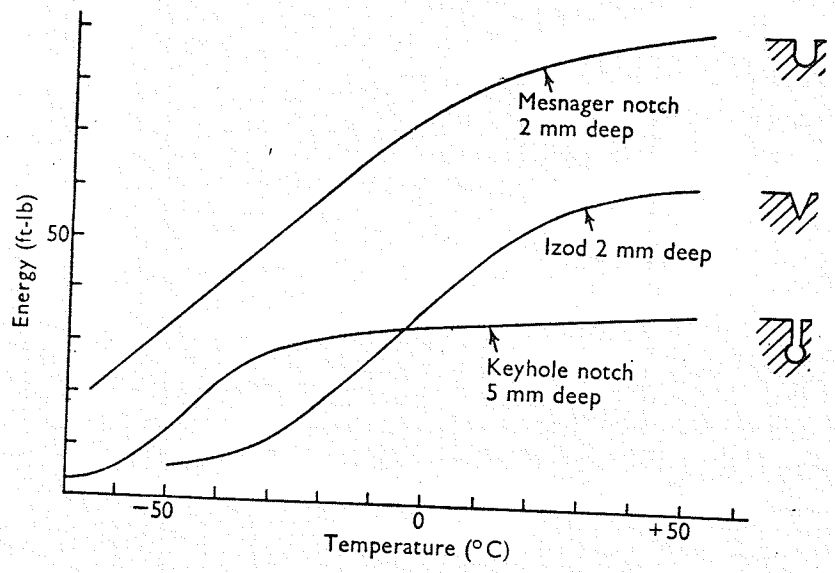

Figure 2.52 Effect of notch shape on energy - temperature curves (9)

depending on the type of test used. Figure 2.51 illustrates a strain rate effect and Figure 2.52 shows the effect on notch type on mild steel. Also, for materials exhibiting a gradual change in fracture behaviour with temperature, the selection of a transition temperature criterion becomes important. Therefore, the designer must select his information from a test procedure simulating the load history expected for his component. When satisfied with the type of test, he should then select a material whose transition temperature is well below the expected operating temperature and in this manner will reduce the possibilities of brittle fracture.

2.5.3.2 Heat Treatment

The heat treatment received by a metal, whether intentionally or accidentally, will have a definite effect on its fracture behaviour. Generally, steels which are heat treated by quenching to martensite and tempered to Brinell 200 to 400 are considered to have the best combination of mechanical properties. As higher strength steels are developed, proper control of heat treatment becomes vital because of the general trend for initiation of low stress fracture from smaller cracks and flaws in higher yield strength materials. However, many factors may interrupt the heat treatment procedure and affect the mechanical properties.

Decarburization, the depletion of carbon content at the surface of steel parts, occurs when steel is heated in air or some other decarburizing atmosphere. Decarburization usually severely lowers fatigue strength in reversed bending but is not as serious for unidirectional fatigue at high stress levels.

Decarburization of steels also has an important effect on the fracture toughness of a steel. The fracture toughness of high strength steels can be

increased by approximately 50% by decarburizing the surface 10% to 20%. (39)

Poor or inadequate quenching will produce incomplete hardening. This results in improper microstructure and random surface hardness with the lower hardness areas being generally weaker than the higher hardness areas.

Overheating of steels by direct overheating, improper grinding or welding heat will damage the fracture resistance of metals. Figure 2.53 shows a weak, coarse-grained structure with grain boundary damage which resulted when the component was overheated. The resultant fracture occurred when the part was stretched during a heat treatment. Figure 2.54 reveals a surface area which was damaged by improper grinding. Such areas may be transformed to martensite, an extremely hard brittle structure which is susceptible to cracking. Heat from accidental welding, "arc strikes" or poor welding procedure may damage the component metallurgically and lead to hard brittle structures, susceptible to brittle fracture.

Heat treatment procedures can also introduce residual stresses in components by transforming structures, which in itself involves volume changes. These residual stresses from heat treatment are generally favourable but will vary with material, case depth, and quenching rate. However, any processes resulting in high residual tensile stresses at surfaces, particularly carburized surfaces, can be damaging to the fatigue life and fracture resistance. Residual tensile stresses may be produced from weld metal contraction during cooling from the welding temperature. Wulpi (10) records an example of a steel I-beam; 40 ft. long, which split with explosive violence while under no load. The beam had lain on the shop floor for about a day after the ends had been torch cut. Fracture was

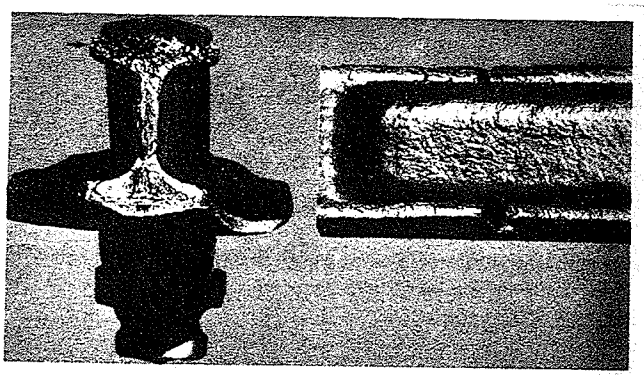

Figure 2.53 An example of "severe overheating", or burning, of a component of steel (10)

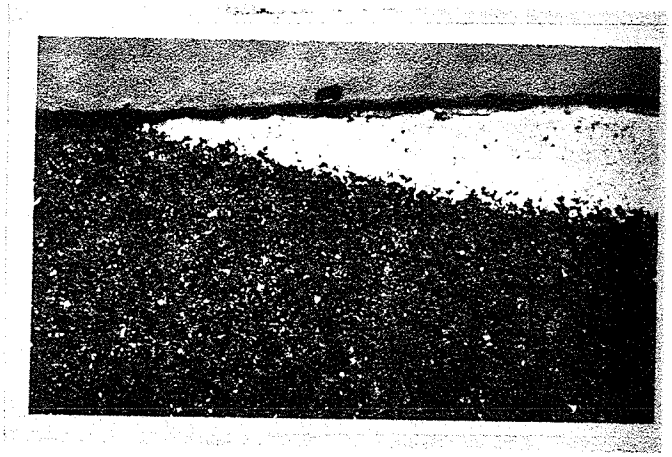

Figure 2.54 An example of a transformation in steel due to heat from excessive grinding (10)

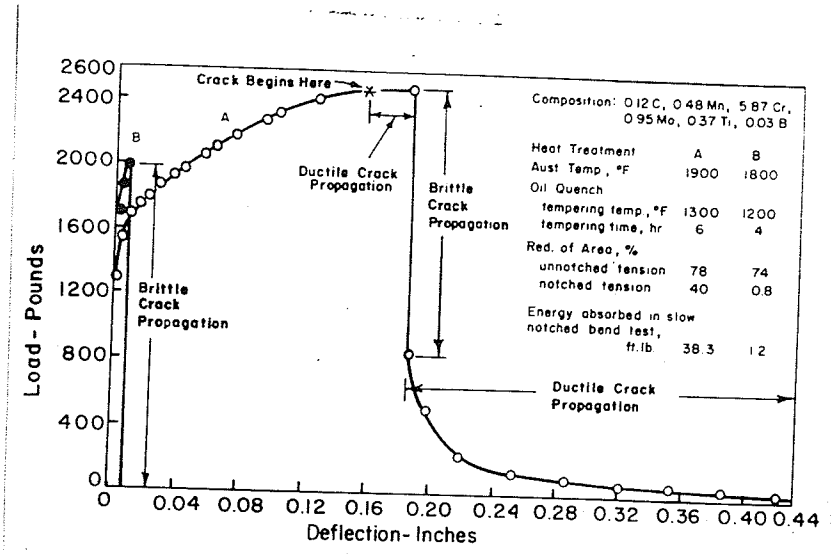

Figure 2.55 Slow-bend data for standard V-notch charpy specimens of a heat treated steel (3)

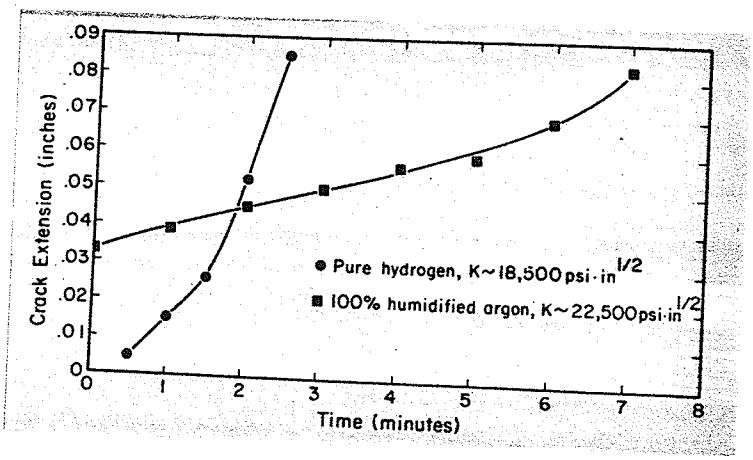

Figure 2.56 Sub-critical crack extension in hydrogen (1 atm.) and humidified argon, H-11 steel (19)

traced to high transverse residual tensile stresses which resulted from a rolling operation. The violent reaction occurred after the complex stress condition was altered by the heat from torch cutting.

As a concluding item on heat treatment, embrittlement may result from several causes, one of which is improper heat treatment. Figure 2.55 shows an example of this for an alloy steel. The composition, two heat treatments, A and B, and the resulting unnotched ductility measurements are shown. Heat treatment B gave a somewhat higher strength than heat treatment A. However, there was little change detected in the ductility measurements on unnotched bars. Figure 2.55 shows the results of the standard Charpy V notch specimens tested in slow bending. Embrittlement is clearly evident for heat treatment B and it must be pointed out that the embrittlement can only be detected by tests of sharply notched members (16). Embrittlement due to damaging atmospheres will be discussed in the following sections.

However, the designer must be conscious of the possible presence of embrittling factors in the material for his structure.

2.5.3.3 Damaging Atmospheres

This section shall be restricted to the effects of various atmospheres on the more commonly used engineering materials such as steels and aluminum alloys. This restriction is necessitated as the field of atmospheric effect on all metal systems is quite voluminous and beyond the scope of this thesis.

Air, the most common atmosphere surrounding structures, has often been used as a reference atmosphere for testing. However, Hartman (14) studied the effects of moisture and atmosphere on the fatigue crack growth of 2024-T3 aluminum alloy at room temperature, using "dry" argon (water

content less than 100 ppm) as a reference environment. He found the presence of moisture in the test environment increased the crack growth rate by a factor of ten for low stress levels. Humid oxygen gave similar effects as humid argon while dry oxygen had only a small if any effect on the rate of crack growth. Spitzig et al (15) studied the effects of dry and humid argon and hydrogen on the fatigue crack growth rate in 18 N_i (250) maraging steel. They found the rate of fatigue crack propagation in this steel was insensitive to moisture. Nearly the same crack growth rates were observed in dry argon, humid argon and humid hydrogen while the rate of crack growth nearly tripled for a dry hydrogen atmosphere. This study appears to verify the findings (28) that impurities such as oxygen, air, or water vapour in hydrogen tend to eliminate the effect of hydrogen on steels. This effect has been attributed to the preferential adsorption of oxygen on the crack surface at the crack tip.

As pointed out just previously, hydrogen has a dangerous embrittling effect on steels. Tetelman (17) has shown that hydrogen introduced in excess of lattice solubility can produce a sufficient stress to cause cracking, but hydrogen must be present and be highly mobile to cause macroscopic embrittlement of polycrystalline aggregates. He concluded that supersaturated hydrogen atoms precipitate as molecular hydrogen gas at the interface between nonmetallic inclusions and the metal matrix. The stresses resulting from the build-up of hydrogen pressure are relieved by the formation of voids, which appear as cleavage cracks in hard materials. The absence of strong barriers such as grain boundaries in single crystals makes crack propagation relatively easy. However, in polycrystals, crack propagation occurs discontinuously and hydrogen must be present and highly mobile in order to restart cracks that are held up at grain boundaries.

These observations and conclusions explain a mechanism for hydrogen embrittlement and cracking of steels.

In several metal-atmosphere systems, the atmosphere may attack the metal and corrosion will occur. When metal components are required to carry loads in aggressive environments, stress corrosion cracking may occur. For most systems, the combination of stress and corrosion is much worse than the addition of the effects of the two factors separately (18). Johnson and Paris (19) make this comment concerning environmental cracking under load:

"High strength steels and titanium alloys are frequently nearly immune to enviromental cracking when tested in smooth sections, perhaps because they do not pit readily. When crack-like flaws are present, however, crack extension under discouragingly low stresses may be evident in seemingly mild environments.".

The embrittling effect of hydrogen is shown in Figure 2.56 by the rapid crack extension in the hydrogen atmosphere. The addition of oxygen to vapor environments is striking in that less 1% by volume of oxygen will essentially terminate a growing crack under a static load, as seen in Figure 2.57. Figure 2.58 shows a similar effect of oxygen when introduced into a hydrogen atmosphere. It has been suggested (19) that oxygen forms an oxide layer which provides a barrier to the passage of hydrogen. For continued crack extension, it is felt the hydrogen would have to reduce the oxide to continue attack on the crack tip or the water vapour would have to dissolve the oxide and thus be able to continue the cracking process.

From the preceding discussion, it becomes obvious that detailed studies into a particular material-environment system should be undertaken

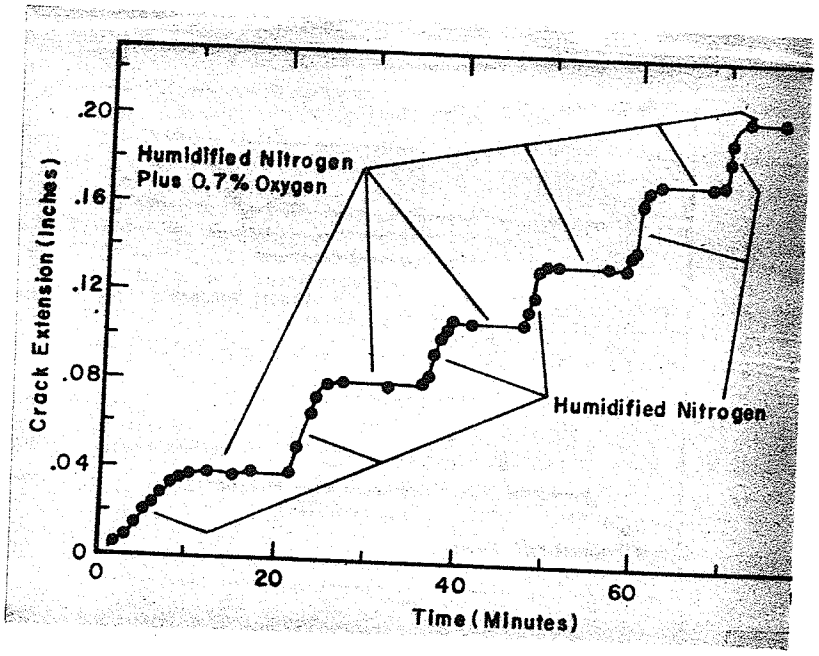

Figure 2.57 Influence of oxygen on sub-critical crack growth in humidified nitrogen, H-22 steel (19)

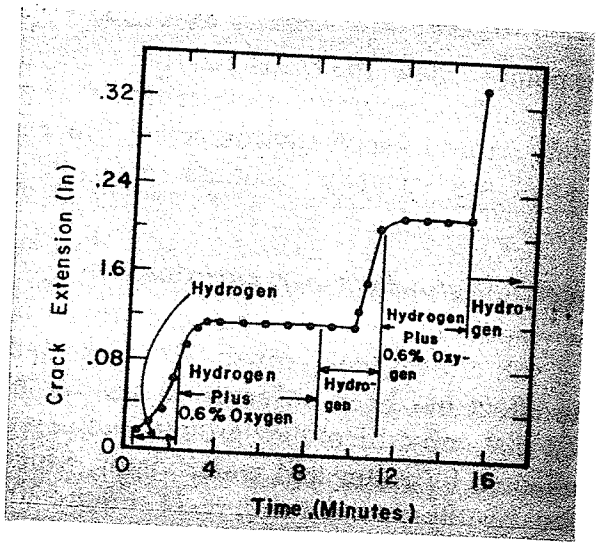

Figure 2.58 Hydrogen-oxygen mixtures and sub-critical crack growth in H-11 steel (19)

before predictions of the fracture behaviour of the material in that particular atmosphere can be made and that "observations and procedures developed on the basis of one material - environment system should not be generalized and applied indiscriminately to other systems". (20)

2.5.4 Load History

The load history of a component can be considered to be of two parts; (1) the type of loading and (2) the rate at which the load was applied. The type of loading may include such common examples as axial, shear, contact, bending, torsional, and random combinations. The loading rate may vary from extremely slow to impact.

Types of loading have been dealt with extensively in sections 2.3 and 2.4 and only a few major points will be emphasized. All types of loads induce normal and shear stresses which must be balanced by the material's cohesive and shear strengths. Because normal and shear stresses are affected differently by stress-concentrating discontinuities, a knowledge of normal stress to shear stress ratios and significant stresses for various types of loads is necessary for a safe design. Also, each type of load causes its own characteristic stress distribution, a knowledge of which is important for proper surface strengthening procedures. Finally, as stated before, characteristics of fracture are directly related to the manner of loading.

The rate of load application and the associated strain rate do have an effect on the fracture behaviour. Figure 2.51 shows the difference in the energy absorbed versus temperature graph which exists for mild steel tested in impact and slow bend tests. In the impact test, the strain rate was approximately 2.5×10^5 times the rate for the slow bend test.

The increased strain rate of the impact test nearly doubled the maximum energy absorbed and appears to have shifted the transition temperature by some 40^{o} C.

Figure 2.59 shows interesting results of strain rate on fracture toughness. The stress intensity factor, K, a measure of fracture toughness, and its time derivative, $\dot{K}$, are plotted for various temperatures as the strain rate is varied over 5 orders of magnitude (3). This indicates that the high toughness exhibited in slow loading tests is appreciably lowered both by decreasing temperature and increasing strain rate. This phenomenon becomes important because a material cannot differentiate between a high strain rate near a crack front produced by rapid loading and that produced by a rapidly propagating crack. Thus either rapid loading or a rapidly propagating crack will cause a marked decrease in the resistance to crack entension. Therefore, when a crack is initiated, the reduced toughness due to the high locally increased strain rate can cause abrupt crack acceleration. The crack could then penetrate through material which had sufficient toughness to prevent crack entension under slow loading rates. Hence a reduction in stress or increase in temperature would be required to arrest the crack.

Because of the effect of load type on stress patterns and of the effect of strain rate on fracture toughness, the load history of a component will have a pronounced effect on its fracture behaviour.

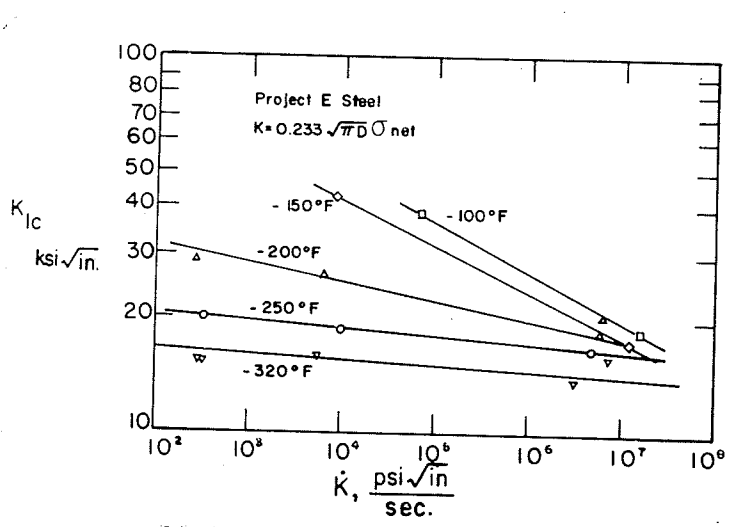

Figure 2.59 Fracture toughness as a function of strain rate at several temperatures (3)

2.6 Approaches to Design Against Fracture

2.6.1 Transition Temperature Approach

2.6.1.1 Introduction

The transition temperature approach to the low stress fracture problem is based on the concept that temperature and strain rate sensitive materials possess a characteristic "transition temperature", below which low stress fracture can occur and above which low stress fracture will not occur. The transition temperature must be determined by a laboratory test with the particular test procedure depending in part on the definition of the transition temperature. Common to all tests is the observation that some aspects of the material's behaviour will change abruptly in a fairly narrow range of temperature.

Most definitions of transition temperature fall into one of the following general categories:

1) The temperature at which the material's capacity for gross plastic deformation in the presence of a sharp notch or crack decreases abruptly to essentially zero. (Tough-brittle transition temperature)

2) The temperature at which the mode of crack propagation abruptly changes with decreasing temperature from full shear to flat. (Fracture mode transition temperature)

3) The temperature at which the fracture strength of a sharply notched or precracked specimen decreases rapidly from values which are above, to values which are below, the conventional yield strength. (Fracture stress transition temperature)

4) The temperature above which a running crack will be arrested. (Crack arrest temperature)

2.6.1.2 Tests for Determining Transition Temperatures

The following section describes some of the more common tests to measure transition temperatures. The nature of the test and the transition temperature criterion involved will be discussed.

For this section, the following nomenclature applies:

T = full plate thickness

t = specimen thickness

b = specimen width

r = radius of notch-bottom

Bend Tests

Bent in plane of plate (Figure 2.60)

The dimensions shown are those used for slow bend tests and are known as the Lehigh test. With somewhat different dimensions, it is used as the Penn State slow bend test. This test is used in the assessment of transition temperature by energy-absorption, contraction below notch, bend angle and fracture appearance.

Pellini drop weight test (Figure 2.61)

The test sample is prepared with a hard weld bead in which a notch may be ground. It is supported and struck by a falling weight. The weight and height of fall is adjusted so that the specimen is broken at one blow. These adjustments can be made after preliminary experiments at room temperature. The height of support is also adjusted to ensure the bend angle at fracture does not exceed 5^{o}. The criterion is the temperature at which fracture occurs with a single blow and minimum deformation.

Bent perpendicular to plane of plate

Charpy V-notch, Charpy Keyhole, and Mesnager tests (Figure 2.62).

The dimensions of the test pieces and the characteristics of the

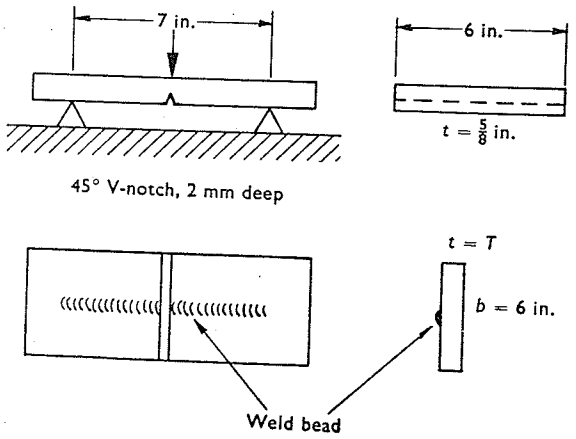

Figure 2.60 Bend test with bent in plane of plate (9)

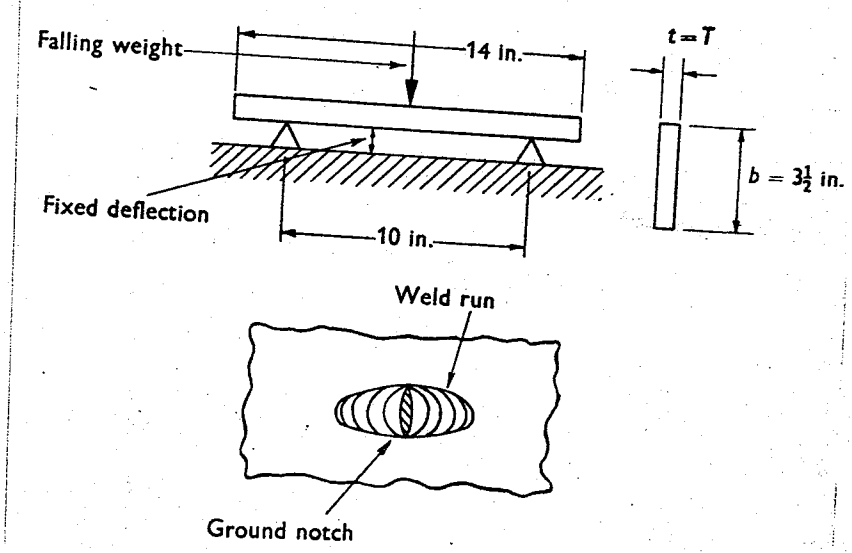

Figure 2.61 Pellini drop-weight test (9)

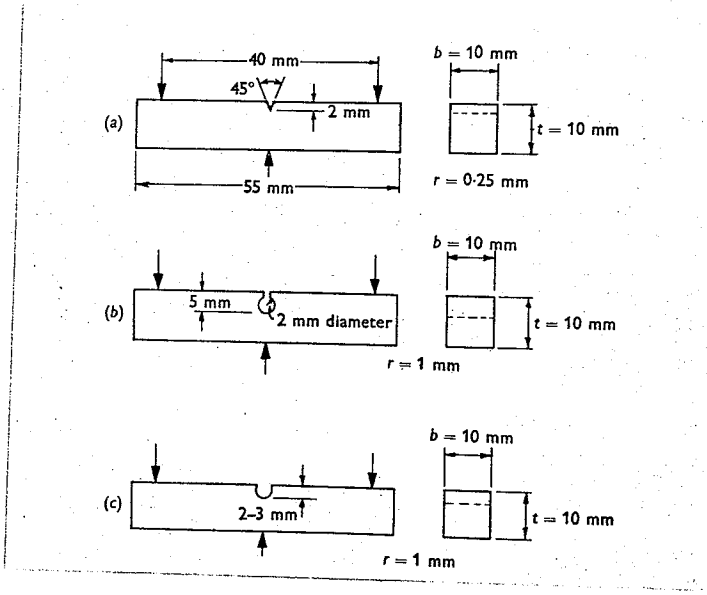

Figure 2.62 (a) Charpy V-notch test

(b) Charpy Keyhole test (9)

(c) Mesnager test

machine are fixed by specifications. Fracture is by single blow impact, but slow bend-tests and other modifications have been made for research purposes. Total energy and fracture appearance is recorded. Transition-temperatures are derived from plotting energy or percent crystallinity curves against temperature. A typical curve is shown in Figure 2.63.

Schnadt test (Figure 2.64)

The standard Charpy V-notch test was modified by inserting a pin on the compression side and by varying the acuity of the notch. Strain rate may also be varied. Total energy is recorded. Tests may be carried out at one temperature with different notches, or at different temperatures with the same notch and at different strain rates.

Hounsfield test (Figure 2.65)

The test pieces are broken in a machine in which the specimen is held in one pendulum and struck by another. They can also be broken by slow bending. Energy and fracture appearance criteria are used.

Izod test (Figure 2.66)

The dimensions of the test pieces and notch are identical with the Charpy V-notch test piece. Loading by cantilever bending avoids damage at the face opposite the notch. Total energy and fracture appearance are recorded.

Tension Tests

Rectangular plate tests (Figure 2.67)

Dimensions of test samples and notches are variable, but width is generally large in relation to thickness, which is plate thickness. Notches are placed on the edges or in the center and may be V-shaped or slits. Measurements of the following are made and plotted against temperature:

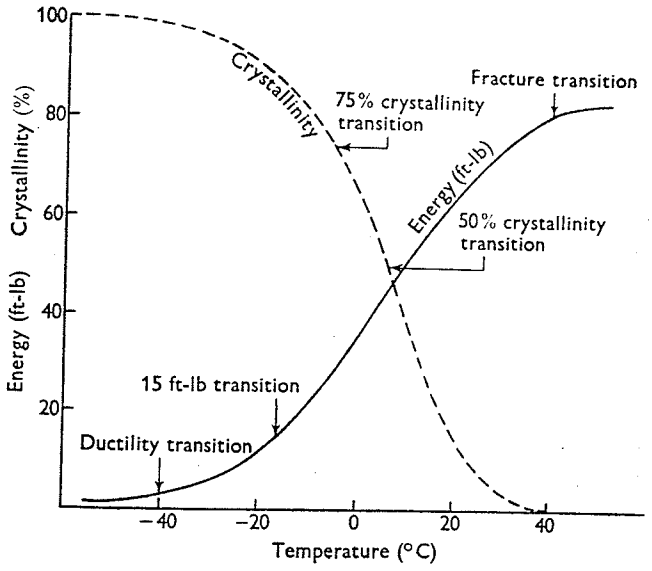

Figure 2.63 Typical energy-temperature and crystallinity-temperature curves for steels (9)

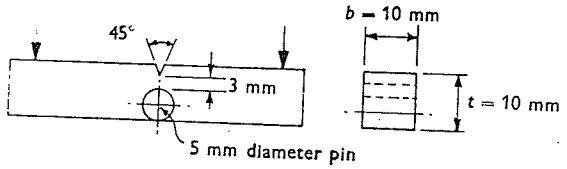

Figure 2.64 Schnadt test (9)

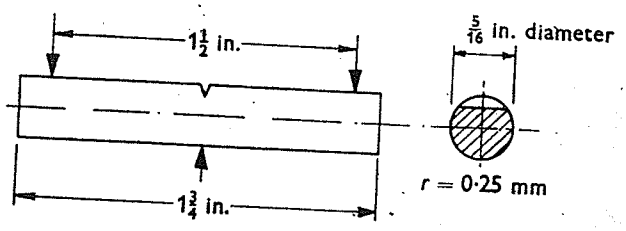

Figure 2.65 Hounsfield test (9)

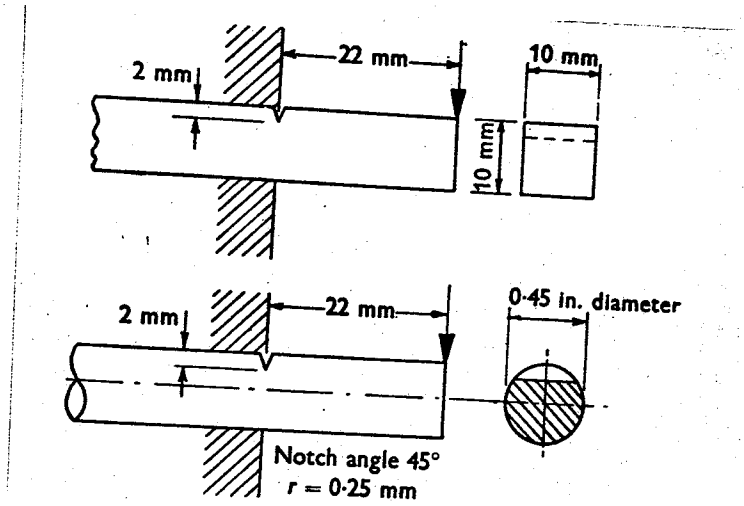

Figure 2.66 Izod test (9)

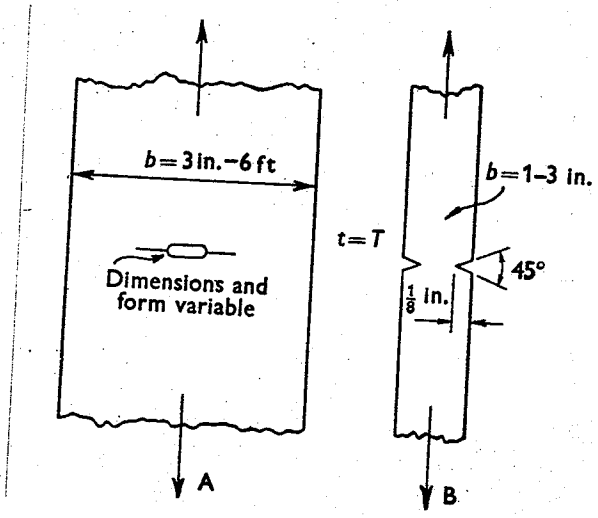

Figure 2.67 "Wide plate" tests (9)

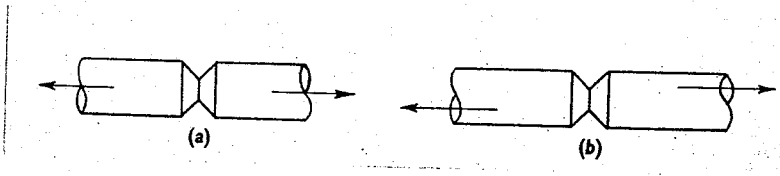

Figure 2.68 Two types of cylindrical tests (9)

ultimate tensile stress, extension, reduction in thickness, energy absorption and fracture appearance.

Cylindrical (Figure 2.68)

Type (a) - Used in the theoretical investigations of notch effects, usually static, but also impact. Breaking stress and reduction in area recorded.

Type (b) - Eccentrically loaded. Load at fracture is recorded. Transition temperature indicated by drop in load at fracture.

Tension-bend Tests

Navy tear test (Figure 2.69) - Load extension records are made from which the energy absorbed to start the fracture and that to propagate it may be plotted. The criterion usually plotted is fracture - appearance, which usually coincides with the sudden drop in energy to cause propagation.

Basgar 'cleavage tear test' - (Figure 2.70)

The dimensions are altered to give varying degrees of eccentricity and the nominal breaking-strength is recorded at different temperatures. Fracture appearance is another criterion.

Robertson Test (Figure 2.71)

With slight modifications, this test was adopted by Standard Oil research workers and is known as the E.B.T. (Esso brittle temperature) test.

A notch is sawcut as shown and a transverse tensile stress of 8-20 k.s.i. is applied. The notched end is cooled by liquid nitrogen and the desired temperature gradient can be maintained. A blow from a bolt-gun on the rounded projection starts a fracture. By knowing the temperature gradient and the position of crack arrest, the crack arrest temperature is obtained.

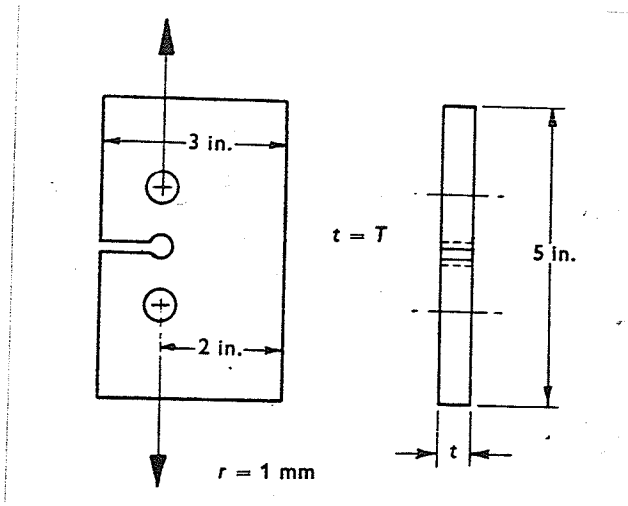

Figure 2.69 Navy tear test (9)

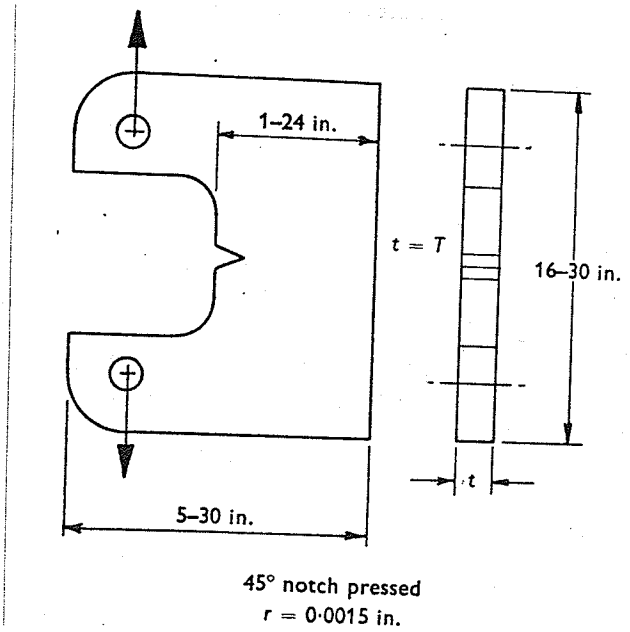

Figure 2.70 Basgar 'cleavage tear test' (9)

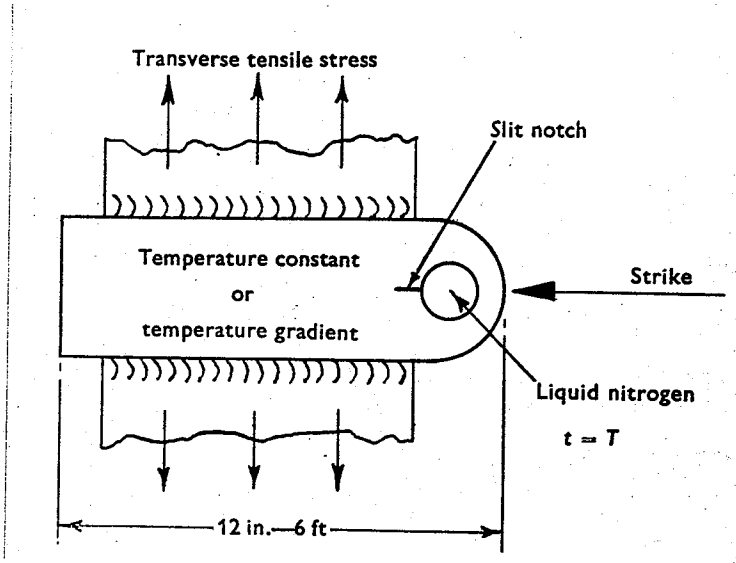

Figure 2.71 Robertson test (9)

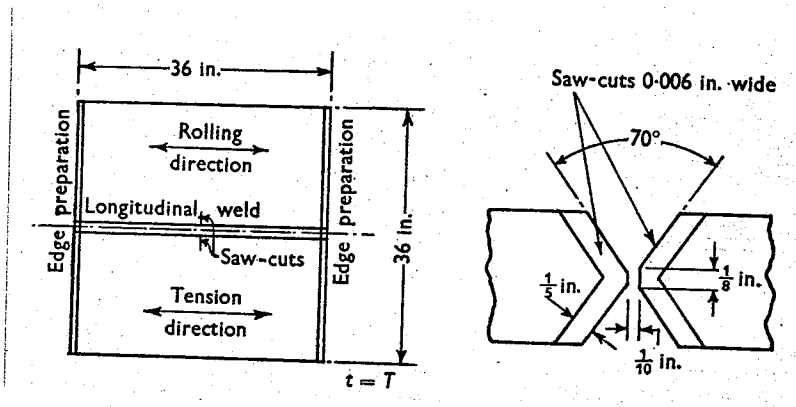

Figure 2.72 B.W.R.A. wide-plate test (9)

British Welding Research Association (B.W.R.A.) wide-plate test (Figure 2.72)

A severe notch coupled with the effects of welding are used to obtain low stress fracture. Measurements of stress at fracture, and strain to fracture, are made and related to crack length and fracture appearance for different materials and temperatures. Low stress fracture is found to occur below certain temperatures. The test is used to investigate welding electrodes, notching procedures, and stress-relieving treatments for different materials.

2.6.1.3 - Application of the transition temperature approach

The applicability and usefulness of the transition temperature approach to the problem of low stress fracture depends on the criterion that is used and the purpose to which it is to be applied. For comparative purposes, almost any one of the various transition criteria may be used directly with a reasonable degree of confidence that the material which exhibits the lowest transition temperature is likely to be the most fracture resistant.

This concept is implemented in design practice either by limiting the operating temperature to values above the transition temperature, or by selecting a material whose transition temperature is lower than the minimum operating temperature. Also, in design situations, the transition temperature approach can be useful for establishing design parameters. However, for complex design, the selection of the appropriate transition temperature criterion and its subsequent translation into useful design information can be very involved.

The transition temperature approach has certain limits. When a material must be used below any of its transition temperatures, then the approach is not useful. Limitations of applicability arise due to size effects of the ultimate structure to the test piece. Also, information on such things as crack arrest temperatures found from plate sections can have little value for design involving heavy sections such as forgings.

In summary, the basic concept of this approach is simple but its application can be quite complex and requires careful consideration. Two primary considerations must be satisfied. The first is the selection of a transition temperature criterion that is appropriate to the needs of the application and is representative of all the embrittling factors that may be present. Then the transition temperature criterion which has been selected must be translated into terms of stress and load capacity of the material, as this is the ultimate information required for design. When these two steps can be satisfactorily achieved, the transition temperature approach can be successfully applied.

2.6.2 Stress Analysis Approach

2.6.2.1 Introduction

The stress analysis approach encompasses a number of concepts and hypotheses concerning fracture of structural components. This approach differs from the transition temperature approach in that the applied load is the quantity of main interest and not the temperature. The temperature enters as a variable since the applied load for fracture is dependent on the temperature.

The concepts in the stress analysis approach can be divided into three main categories.

They are:

(1) Critical stress concepts for the initiation or sustaining of fast fracture.

(2) Critical strain concepts for initiation of fast fracture.

(3) Fracture mechanics concepts involving available and expended strain energy for initiating or sustaining of fast fracture.

The various concepts differ in specific detail but all follow common steps in their general approach to the fracture problem.

2.6.2.2 Critical Stress Concepts

The concept of a critical stress for fracture was first suggested by P. Ludwick (26). On a true stress - true strain diagram, a fracture stress curve is assumed and compared with the flow stress curve as suggested in Figure 2.73. The flow stress curve relates the stress which is required to produce plastic deformation to the strain. The stress required to start fracture for various amounts of strain is depicted by the fracture stress curve. As shown in Figure 2.73, the intersection of the fracture curve with the flow curve defines the fracture condition. Depending on the relative positions of the two curves, fracture would occur with large or small strain and thus ductile and brittle fracture were qualitatively defined.

With the observation that fracture can occur by a normal opening mode and by a shear mode, the critical stress concept was modified to allow for two fracture stress curves, either shear fracture or cleavage fracture. By varying the positions of the flow curve and shear and flat fracture curves,

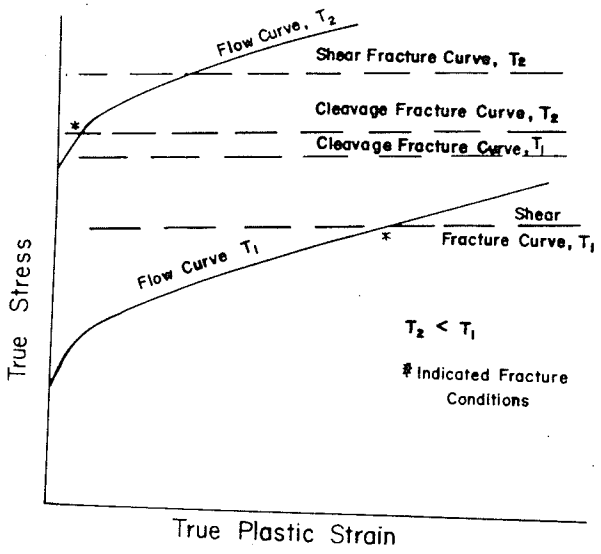

Figure 2.73 Schematic illustration of change from shear to cleavage fracture due to change in temperature (3)

various possibilities of fracture conditions can be seen. Figure 2.73 shows the effect of lowering the temperature. One combination of curves for temperature T_1 results in shear fracture after large plastic strain while the second set of curves for T_2 show flat fracture after very little strain.

Ludwik's fracture stress concept does not deal with the possibility of the dependence of the fracture curve on the flow stress curve. For most metals, some plastic deformation appears necessary to initiate any fracture. Hence factors affecting the flow curve would affect the fracture curve correspondingly.

Modifications of the fracture stress concept have been made to allow the calculation of the applied load for fracture by using elastic-plastic stress analysis methods of varying complexity. A further modification calculates the nominal stress for fracture by dividing the critical fracture stress by a stress concentration factor which has been corrected, where necessary, for the finite nature of material structural units, for plasticity effects, and for specimen configuration and loading condition. However, all the critical fracture stress concepts assume that the fracture stress is a known value for the material.

2.6.2.3 Critical Fracture Strain Concepts

Critical fracture strain concepts presume that some plastic deformation, even though it may be very localized, precedes low stress fracture. The localized deformation is analyzed in an appropriate manner and equated to the critical value to determine the fracture conditions. The load and nominal stress at fracture are obtained from the associated

stress analysis. Thus the fracture stresses are thought of as the result and not the cause of fracture.

In the critical strain concepts, the fracture strain is not single valued for a material, independent of stress state or stress distribution. Hence introducing biaxiality reduces the plastic flow at fracture. Thus the application of the fracture strain concept requires a knowledge of critical fracture strain for a material as a function of the degree of multiaxiality and a complete elastic-plastic strain analysis to determine fracture conditions.

Sach (21) adopted the critical fracture strain concept on the hypothesis that a specific elastic stress distribution will become transformed by plastic flow into a unique strain distribution and triaxiality distribution regardless of the geometry and loading conditions causing the specific elastic stress distribution. He devised a notched test specimen with an elastic stress distribution in the vicinity of the notch which was essentially the same as the pertinent region of the structure under consideration. Then, by utilizing the measured local surface strain at failure in the test piece, he could determine the load carrying capacity of the structure. However, the elastic stress distribution is the important factor in correlating the fracture test with the real structure.

A problem arises with sharp cracks as the elastic stress distribution becomes indeterminate. To overcome this difficulty and avoid measuring surface strain, Lubahn (22) modified Sach's hypothesis. Lubahn assumed that the Sach's hypothesis would be satisfied in both test specimen and actual component provided both had congruent notches and identical gradients of nominal stresses. The congruent notch means that the absolute notch depths

and radii are matched while the use of nominal stresses enables cracks to be handled. When congruent notches and identical nominal stress gradients were present, the nominal stress at fracture would be the same in both parts.

McClintock (23) observed that a strain infinity at the tip of a crack would have no physical meaning as it occurs in an infinitesimally small region. He proposed considering the average strain over a small region at the crack tip and postulated two quantities are required to characterize a fracture strain criterion for a given material: a structural size parameter and a critical value of strain. He analyzed the fracture behaviour of an elastic, perfectly plastic material which had a crack and was subjected to shear stresses. He found he could obtain the nominal stress at instability in terms of the shear yield stress and the crack dimension.

Thus, in summary, the concepts based on critical fracture strain provide insight into certain aspects of low stress fracture, but the exact determination of the critical strain as a function of the stress state is a principal difficulty.

2.6.2.4 Fracture Mechanics Concept

Fracture mechanics is an extension of the fracture instability conditions originally formulated by Griffith (24). A general statement of the fracture process can be derived from the principle of conservation of energy. To proceed from general fracture to fracture instability it is necessary to consider the rates, with respect to crack area, at which the energy is supplied and dissipated. Therefore, a crack in a solid will extend rapidly when an incremental increase in crack area makes available

an increment of elastic strain energy equal to or greater than the increment of work that is dissipated. It has been shown that regardless of the external force variations during crack extension, the rate of release of elastic strain energy with respect to crack area remains unchanged. The symbol G is used to denote the "strain energy release rate", measured in units of in. lb/in.^{2}, also referred to as the "crack extension force" measured in units of lb/in.

The released strain energy is used in the creation of new crack surfaces and includes surface energy and work of plastic deformation which occurs simultaneously with the formation of the crack surfaces. For low stress fracture in metals, surface energy is very small and the dominant contribution comes from plastic deformation in a very localized region adjacent to the crack front. At fracture instability, the critical strain energy release rate, denoted by G_c, is equal to the work rate with respect to crack area, called "fracture toughness". It includes both surface energy and work of plastic deformation.

Griffith studied the problem of an infinite plate containing a crack-like defect. For loads applied remotely from the crack, the energy release rate is proportional to the product of the square of the applied stress and the linear dimensions of the crack. Therefore, for a material with a given fracture toughness, the applied stress for unstable fracture will vary with the inverse square root of the linear dimension of the crack, ie, the larger the crack, the lower the stress. This type of relationship between load and defect has been noted in connection with other previously described fracture concepts.

Irwin (25) has shown the existence of a simple relationship between the energy release rate, G, and the elastic stress components near the crack edge. For the co-ordinates shown in Figure 2.74, the normal stress in the y direction at a point adistance r from the crack front at an angle θ with the crack plane is given by

$$\sigma_x = \frac{K_I}{\sqrt{2\pi r}} \cos\frac{\theta}{2}\left(1 - \sin\frac{\theta}{2}\sin\frac{3\theta}{2}\right)$$

$$\sigma_y = \frac{K_I}{\sqrt{2\pi r}} \cos\frac{\theta}{2}\left(1 + \sin\frac{\theta}{2}\sin\frac{3\theta}{2}\right)$$

$$\tau_{xy} = \frac{K_I}{\sqrt{2\pi r}} \cos\frac{\theta}{2}\sin\frac{\theta}{2}\cos\frac{3\theta}{2}$$

where K is the stress intensity factor. The stresses in the other perpendicular directions can be obtained similarily in terms of the stress intensity factor K and a function of r and θ. This expression is valid for sharp cracks independent of the loading conditions, and thus the square root stress singlularity at the crack tip is also independent of loading conditions. The stress intensity factor, K, provides a single parameter characterization including the effects of specimen configuration, type of load, and magnitude of nominal stress. Since for elastic behaviour, the energy stored in a given volume is uniquely

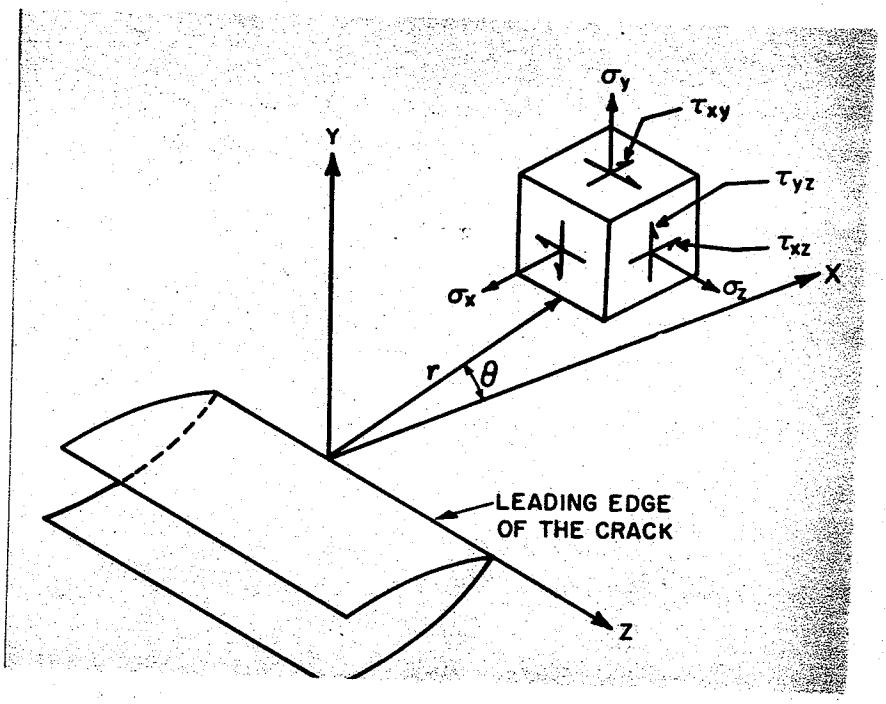

Figure 2.74 Co ordinate system and stress components ahead of a crack tip (18)

defined by the stresses existing in that volume, there exists a simple relationship between the stress intensity parameter, K, and the strain energy release rate, G. For a homogeneous isotropic material the relation is

$$K = \sqrt{GE} \qquad \text{(for plane stress)}$$

and

$$K = \sqrt{\frac{GE}{1-\nu^2}} \qquad \text{(for plane strain)}$$

where E is the modulus of elasticity
and ν is Poisson's ratio

Thus, fracture concepts useful in engineering situations have developed from the original energy balance concept, namely the critical elastic strain energy release rate concept (G_c) or its equivalent, the stress intensity factor concept (K_c). When members are loaded such that opening mode fracture results under plane strain conditions, the critical stress intensity factor is referred to as K_{IC} to avoid ambiguity with other possible critical stress intensity factors. The theoretical analysis of opening mode fracture for specific geometries of interest to this thesis will be developed in Chapter 3 and, as stated in 1.2, it is the intent of the thesis to determine the effect of certain variables on the parameter, K_{IC}.

2.7 Summary

Chapter 2 has attempted to elucidate the problems associated with low stress fracture and show how these problems are being treated. The manner in which post failure analysis is conducted has been reviewed along with the analytical and experimental techniques which are employed to provide more and better knowledge on the brittle behaviour of materials.

The approach which has received most attention recently because it is probably the potentially most useful concept is fracture mechanics. This is so because fracture mechanics can handle flaws, defects and other stress raisers which develop in design situations and mainly because it is a logical extension of present design practices, which customarily deal in terms of nominal stress and are based upon the discipline of the classical mechanics of deformable solids. For these reasons, the thesis attempts to add some additional information to the fracture mechanics concept.

CHAPTER 3

DEVELOPMENT OF THE FRACTURE MECHANICS CONCEPT

3.1 Introduction

Fracture mechanics is based on the concept of applying a reasonable and proper stress analysis to considerations of equilibrium and stability of cracks. The stress analysis employed in fracture mechanics is based, firstly, on the elastic considerations derived from the theory of elasticity with a later accounting for the non-linearity (plasticity) occurring at the crack tip.

As mentioned in Chapter 2, Griffith (24) was the first to consider the equilibrium and stability of cracked, brittle bodies. The ideas of Griffith have been modified to apply to ductile materials such as steels and aluminum by several people including Irwin (25), Paris (1) and Sih (1). The combined efforts of these people have extended the understanding of the behavious of material containing flaws and subjected to various types of loads. The purpose of this chapter will be, therefore, to outline the progress of the fracture mechanics concept from the initial Griffith ideas to the present A.S.T.M. proposals (37) for standardization of plane strain fracture toughness testing.

3.2 Griffith Theory

Griffith (24) gave the first analysis of equilibrium and stability of cracks in 1920. His analysis was based on the consideration of the change in potential energy of a body into which a crack was introduced. His method of analysis is accurate and correct when applied to ideally brittle materials, as he showed by experiments on glass.

Griffith's analysis proceeds as follows:

Consider an infinite sheet of elastic material, as in Figure 3.1, which is subject to uniform biaxial stress, σ , at infinity into which a through crack of length, 2a, is subsequently introduced. Denote the potential energy of the system as U, where Uo is the potential energy prior to introducing the crack. Upon introducing the crack, U may be written as,

$$U = U_o - U_a + U_t \tag{3.1}$$

where U_a is the decrease in the potential energy of deformation (strain energy and boundary force work) and U_t is the increase in surface energy due to the new surface.

Griffith employed the stress analysis of Inglis (38) in computing the potential energy of deformation: It is

$$U_a = \frac{\pi \sigma^2 a^2 t}{E} \tag{3.2}$$

where this the thickness of the sheet and E is the modulus of elasticity of the material. The surface energy term, U_t, is the surface tension of the material, T, times the new crack surface area, 4 a t. Thus,

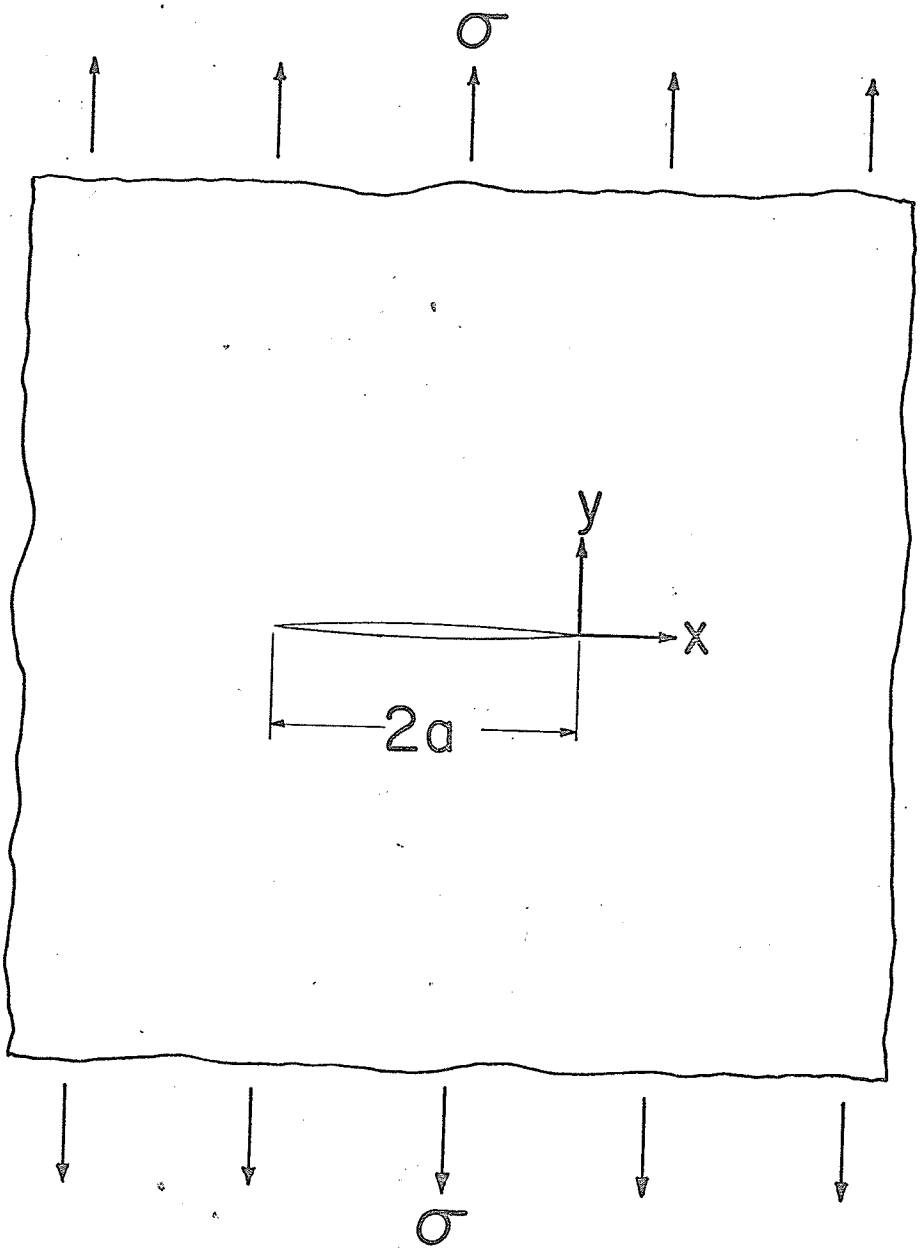

Figure 3.1 The Griffith Crack Problem

$$U_t = 4\ a\ t\ T \tag{3.3}$$

Substituting equations 3.2 and 3.3 into 3.1 gives

$$U = U_o - \pi\sigma^2 a^2 t + 4\ a\ t\ T \tag{3.4}$$

Equation 3.4 now represents the energy balance for the Griffith crack problem.

It is now necessary to examine the variation in the potential energy with respect to crack size, a, noting that a minimum point in the potential energy constitutes a stable equilibrium and a maximum constitutes an unstable equilibrium.

The first derivative of equation 3.4 gives

$$\delta U = \frac{\partial U}{\partial a}\,\delta a = \left(-\frac{2\pi\sigma^2 at}{E} + 4tT \right) \delta a \tag{3.5}$$

For a non zero variation, δa, the bracketed portion in equation 3.5 must be zero. Rearranging gives,

$$\frac{\pi\ \sigma^2 a}{E} = 2T \tag{3.6}$$

or

$$\sigma\sqrt{a} = \sqrt{\frac{2TE}{\pi}} \tag{3.7}$$

Therefore equation 3.6 represents the equilibrium condition for a crack in an ideally brittle material.

The second derivative of U from equation 3.4 is negative, i.e.,

$$\delta^2 U = \frac{\delta^2 U}{\delta a^2}\,\delta a^2 = \left(\frac{-2\pi\sigma^2 t}{E} \right) \delta a^2 = \text{always negative} \tag{3.8}$$

and thus the equilibrium is noted to be unstable. Therefore equation 3.6 represents unstable equilibrium of the crack. In physical terms equation 3.6 depicts the stress and crack length, σ and a, combination

for which failure occurs in a given brittle material, characterized by E and T.

Equation 3.6 has been viewed in a somewhat different way in recent fracture mechanics discussions. The left hand side of this equation may be interpreted to be the elastic energy per unit crack surface area made available for infinitesimal crack extension, denoted G, or

$$G = \frac{\pi\sigma^2 a}{E} \tag{3.9}$$

The right hand side of equation 3.6 is the resistance of the material to crack extension, R, and represents the absorbed energy required to extend the crack per unit area of new surface created. Thus,

$$R = 2T \tag{3.10}$$

for an ideally brittle material. However, non linearity from plasticity in the crack tip region gives additional resistance to the material to crack extension. Equation 3.10 represents the approximate resistance for even very brittle material such as glass. The R term has additive terms due to plasticity for the brittle fracture of ductile materials and these terms are very large compared to 2T. However, it is still possible to use an energy rate analysis of fracture for such cases (1) and view the process as the rate of elastic energy available, G, versus the material's dissipation rate, R, where rapid extension of the crack occurs when G exceeds R.

Griffith used equation 3.7 in order to experimentally verify his theory. The right hand side of equation 3.7 depends only on material

properties. Griffith's measurements gave

$$\sqrt{\frac{2ET}{\pi}} = 137 \quad \text{lbs./in.}^{3/2} \tag{3.8a}$$

He independently ran tests on tubes and spheres of the same glass with prepared cracks and from ten tests obtained

$$\sigma\sqrt{a} = 229 \text{ to } 251 \quad \text{lbs./in.}^{3/2} \tag{3.8b}$$

The comparison of these results is a reasonable verification of his theory of the strength of glass.

3.3 Stress Field Approach

3.3.1 Development

The idea of analyzing crack tips by finding appropriate stress field expansion was initially undertaken by Sneddon (29). He analyzed the typical "Griffith crack" and also the situation of a material which has a penny-shaped crack and which is subjected to stress normal to the plane of the crack. However, it was not until later that Irwin (25) and Williams (30) recognized the general applicability of these field equations and extended them to the most general case for an isotropic elastic body.

The stress analysis of cracks has been reviewed in detail by Paris and Sih (1) and a full development of the stress field approach is beyond the scope of this section. However, the basic concepts will be presented here.

In general, a plane extensional linear elasticity problem may be solved by finding a stress function, $\phi(x,y)$, which satisfies the bihar-

monic equation, i.e.,

$$\nabla^4\phi = \nabla^2(\nabla^2\phi) = \left(\frac{\partial^2}{\partial x^2} + \frac{\partial^2}{\partial y^2}\right)\left(\frac{\partial^2\phi}{\partial x^2} + \frac{\partial^2\phi}{\partial y^2}\right) = 0 \qquad (3.11)$$

and from which the stresses may be computed by

$$\sigma_x = \frac{\partial^2\phi}{\partial y^2}$$

$$\sigma_y = \frac{\partial^2\phi}{\partial x^2} \qquad (3.12)$$

$$\tau_{xy} = -\frac{\partial^2\phi}{\partial x \partial y}$$

and provided that the resulting stresses (and/or displacements) satisfy the boundary conditions of the problem. This stress function approach is fully derived and discussed in any elementary text on the theory of elasticity.

By employing the stress function due to Westergaard (40) it can be shown (Appendix A) that the stresses for an opening mode fracture can be given by:

$$\sigma_x = \text{Re } Z - y \text{ Im } Z^1$$

$$\sigma_y = \text{Re } Z + y \text{ Im } Z^1 \qquad (3.13)$$

$$\tau_{xy} = -y \text{ Re } Z^1$$

where Z is any function of the complex variable $z = x + i\,y$ and $Z^1 = \frac{dZ}{dz}$.

The problem is thus resolved to finding any function, Z(z), which is analytic and which will satisfy the boundary conditions of the particular crack problem.

In the neighbourhood of the crack tip the immediately adjacent stress-free crack surfaces are boundaries which dictate the character

of Z(z) in that vicinity. Taking the origin of the co-ordinates at the right hand edge of a crack parallel to the x - axis, as shown in Figure 3.1, the form which Z must have in this region is

$$Z = \frac{f(z)}{\sqrt{z}} \tag{3.14}$$

where f(z) is well behaved and must approach a real constant at the origin. By applying these conditions to f(z) and substituting equation 3.14 into equations 3.13, τ_{xy} and σ_y approach zero at the crack surface. This then means that the crack surface is stress-free, as expected. The remaining nature of f(z) away from the crack tip is left unspecified and can be adjusted to solve crack problems of the opening mode configuration.

Therefore, in the crack tip region ($|z| \to o$), it is found that

$$\lim_{|z| \to o} Z = \frac{K_I}{\sqrt{2\pi z}} \tag{3.15}$$

where K_I is a real constant and may be thought of as representing the constant term in the series of the Maclaurin expansion for f(z). The constant, $\sqrt{2\pi}$, in equation 3.15 is introduced because it simplifies calculations involved with demonstrating the equivalence of the stress field and energy approaches.

As shown in Appendix A, equations 3.13 can be expressed, using polar co-ordinates and equation 3.15, as:

$$\sigma_x = \frac{K_I}{\sqrt{2\pi r}} \cos\frac{\theta}{2}\left(1 - \sin\frac{\theta}{2}\sin\frac{3\theta}{2}\right) \tag{3.16}$$

$$\sigma_y = \frac{K_I}{\sqrt{2\pi r}} \cos\frac{\theta}{2}\left(1 + \sin\frac{\theta}{2}\sin\frac{3\theta}{2}\right)$$

$$\tau_{xy} = \frac{K_I}{\sqrt{2\pi r}} \sin\frac{\theta}{2}\cos\frac{\theta}{2}\cos\frac{3\theta}{2}$$

Now equations 3.16 represent the "exact" elastic stress field equations as the crack tip is approached (as $r \to 0$), and in the general area of the crack tip, these equations neglect only higher order terms in r in the Maclaurin expansion for f(z). The factor K_I, the crack tip stress intensity factor, is a constant value in the vicinity of the crack tip. Through the unspecified nature of f(z), K_I depends on the configuration of the body and type of loading applied.

The dimensional nature of K_I can be examined now. Since the stresses in linear elasticity must depend linearly upon the load, equations 3.16 imply that K_I contains the load as a linear factor. Subsequent observation of the dimensions involved in equations 3.16 show that K_I must also contain a characteristic length parameter. For most infinite body analyses, the only characteristic length parameter available is the crack length, a. Hence observations lead to

$$K_I \propto \sigma\sqrt{a} \tag{3.17}$$

The result of the Griffith analysis (equation 3.7) contains the term $\sigma\sqrt{a}$ and hence the dependence of K_I on $\sigma\sqrt{a}$ is not unexpected.

Equations 3.16 show that the stress fields (for opening mode situations) which surround the crack tip are always of the same distribution and differ only in their intensity from one situation to another. Consequently, it seems reasonable to suggest that unstable crack extension will take place when the intensity, K_I, reaches a critical value, K_{IC}, i.e., as

$$K_I \rightarrow K_{IC} \tag{3.18}$$

where K_{IC} is a material property which represents the material's ability to withstand a given intensity of crack tip stress field, K_I.

It must be observed that the argument leading to equation 3.18 is not limited to perfectly elastic action. If a small zone (compared to a) of non-linearity is present at the crack tip, it is embedded within the elastic field described by equations 3.16. In a material of given properties, the non-linearity will always disturb the elastic field equations in the same way, and consequently, failure will occur at a given "apparent" field intensity, K_{IC}. The implication is that equation 3.18 applies as a "brittle fracture" criterion for ductile materials.

3.3.2 Modifications

The stress intensity factor, K, which is a measure of the intensity of the applied crack tip stress field, may be obtained for various configurations using the methods of the theory of elasticity. An example of the stress function approach is given in Appendix B for the typical Griffith configuration of Figure 3.1.

The problems involved with stress functions become much more complex as solutions for finite sized specimens are attempted. Analytical solutions to the stress distribution in specimens of complex shape or loading can be obtained by a boundary value collocation procedure (33) applied to an appropriate stress function. The stress function must

satisfy the biharmonic equation (equation 3.11) and the boundary conditions of the specimen. The collocation procedure requires a matrix solution of twice as many equations as the number of boundary stations selected for each combination of the independent variables (load, specimen geometry, and crack length).

The polynomial expressions for the stress intensity factors for the specimens (Figures 4.4 and 4.5) used in this thesis are given below. Both expressions have been obtained by the boundary collocation procedure (31, 32) and have been verified by experimental techniques (33).

For the single edge notched specimen of Figure 4.5,

$$K_I = \frac{P\sqrt{a}}{Bw} * \left[1.99 - 0.41\left(\frac{a}{w}\right) + 18.70\left(\frac{a}{w}\right)^2 - 38.48\left(\frac{a}{w}\right)^3 + 53.85\left(\frac{a}{w}\right)^4\right] \quad (3.19)$$

For the compact tension specimen of Figure 4.4,

$$K_I = \frac{P\sqrt{a}}{Bw} * \left[29.6 - 185.5\left(\frac{a}{w}\right) + 655.7\left(\frac{a}{w}\right)^2 - 1017.0\left(\frac{a}{w}\right)^3 + 638.9\left(\frac{a}{w}\right)^4\right] \quad (3.20)$$

where P is the load in pounds and a, B, w are specimen dimensions as shown in Figures 4.4 and 4.5.

3.4 Plane Strain Fracture Toughness Testing

The concept of plane strain fracture toughness of materials has been widely used since it was formulated by Irwin in 1958. However, lack of standardization has resulted in considerable differences in K_{IC} values reported by different investigations of essentially the same material. It is now proposed (34) to define K_{IC} as the stress

intensity at which the crack reaches an effective length 2% greater than that at the beginning of the test. The proposed method of establishing K_{IC} has been outlined and published in the 1969 Book of A.S.T.M. Standards, Part 31. The critical part of the test procedure consists of obtaining an autographic plot of the load versus the change of distance across the open end of the notch.

The problems encountered with accurate determination of K_{IC} are not limited to the analysis of the load-displacement record. As discussed in Chapter 2, a size effect exists in fracture and thus the material constraint surrounding the crack is a problem. The thickness of the specimen, the crack length, and the percent of uncracked specimen or ligament length becomes important. The required limits for these variables for accurate measurement of plane strain in fracture toughness are fully discussed elsewhere (2) and it will suffice here to say the experimental procedure will be controlled to keep these variables within the prescribed limits.

Problems concerning the effect of the fatigue cracking history and heat treatment do not seem to be fully resolved. The proposed standards of 1969 suggest:

> "The fatigue cracking shall be conducted with the specimen fully heat treated to the condition in which it is to be tested."

while reference (1) suggests:

> "It would seem reasonable to heat treat after fatigue cracking where possible."

Regarding fatigue, the proposed standards of 1969 state:

> "During the final stage of fatigue crack extension, for at least the terminal 2.5 percent of the over-all length of notch plus crack, the ratio of the maximum stress intensity of the fatigue cycle to the Young's modulus, $K_f(max)/E$, shall not exceed 0.0012 in $^{1/2}$. Furthermore, $K_f(max)$ must not exceed one-half of the KQ_f value determined in the subsequent test if KQ is to qualify as a valid K_{IC} result.
>
> "The stress intensity range should not be less than 0.9 $K_f(max)$."

The 1969 standards allow a larger fatigue stress intensity than that proposed by Srawley (34). He suggested the fatigue stress intensity range be about 0.0005 * E in $^{1/2}$. Reference (2) has this comment:

> "Additional data are clearly needed to better define the influences of the conditions of fatigue crack generation on the plane strain fracture behaviour."

Thus, it is the purpose of this thesis to examine heat treatment and fatigue cracking procedures with the hope of providing additional information for the standardization of K_{IC} testing.

CHAPTER 4

EXPERIMENTAL STUDY

4.1 Introduction

As indicated in Chapter 3, the fracture toughness parameter K_{IC} is affected by the degree of stress intensity employed to produce the fatigue crack. The fracture toughness was also noted to vary depending upon whether final heat treatment preceded or followed fatigue cracking. An experimental program was carried out to investigate the extent of these two effects. To ensure that any observed behaviour was repeatable, the two effects were tested on two materials with two different specimen sizes for each material. It was felt that the use of two different specimen sizes for each material would indicate how well K_{IC} could be measured by each specimen size and whether the two experimental variables would have the same effect on all specimens.

4.2 Materials and Specimens

The materials selected for the experiments were 18 Ni (250) Maraging steel, supplied in 0.7 inch thick plate, and 4340 steel, supplied in 1 inch thick plate. The chemical composition of 18 Ni (250) Maraging steel and 4340 steel is given in Tables 4.1 and 4.2 respectively.

Tensile test samples were prepared and included with each batch of specimens heat treated. Post heat treatment tensile tests and hardness readings were made as in attempt at observing the consistency of heat treatment. Approximately 80 hardness readings were taken from fractured

specimens of maraging and 4340 steels. The readings were quite consistent across the section and from specimen to specimen. The average hardness for the maraging steel was 49 R_C and for the 4340 steel the average hardness was 48 R_C. The tensile test results were also very consistent. The maraging steel has an average yield strength of 232 ksi for 4 specimens with no individual reading exceeding $\pm$ 8 ksi on the average. The 4340 tensile test specimens had a similiar consistency. The average yield was 203 ksi, based on 4 tests, with no individual reading exceeding $\pm$ 6 ksi. These results are presented in Table 4.3.

As an additional check on the consistency of the material used in the testing program, micrographs were prepared from material taken from single-edge notch and compact tension specimens of both steels. Figure 4.1 shows photographs of the microstructure of maraging steel and Figure 4.2 presents photographs of the microstructure of 4340 steel.

The examination of the microstructures revealed that the material appeared to be consistent from specimen to specimen. Figure 4.2 shows a uniform structure of tempered martensite. The maraging steel, shown in Figure 4.1, showed planes of banding which were essentially parallel with the surface plane of the specimen and were directed along the rolling axis. The reasons for the presence of these bands was not studied in any amount of detail as it was not the purpose of this thesis to study the basic structure of such a complex material as maraging steel. However, from the consistency of the bands in the specimens studied and the uniformity of the microstructure of the 4340 steel, it was concluded that any microstructural effects would be common denominator to all specimens.

TABLE 4.1

Chemical Composition of 0.66-Inch-Thick 18Ni Maraging Steel Plate

Chemical Composition-Percent
(Check Analysis)

C	Mn	P	S	Si	Ni	Co	Mo	Ti	Al
0.015	0.05	0.001	0.009	0.032	17.3	8.27	4.88	0.42	0.11

TABLE 4.2

Chemical Composition of AISI 4340 Steel

Chemical Composition-Percent
(Ladle Analysis)

C	Mn	P	S	Si	Ni	Cr	Mo	V
0.40	0.71	0.007	0.013	0.25	1.75	0.78	0.25	0.06

TABLE 4.3

Mechanical Properties of 18 Ni Maraging Steel

Yield Strength 0.2%	232,000 psi
Hardness - Rc	49

Mechanical Properties of 4340 Steel

Yield Strength 0.2%	203,000 psi
Hardness - Rc	48

A

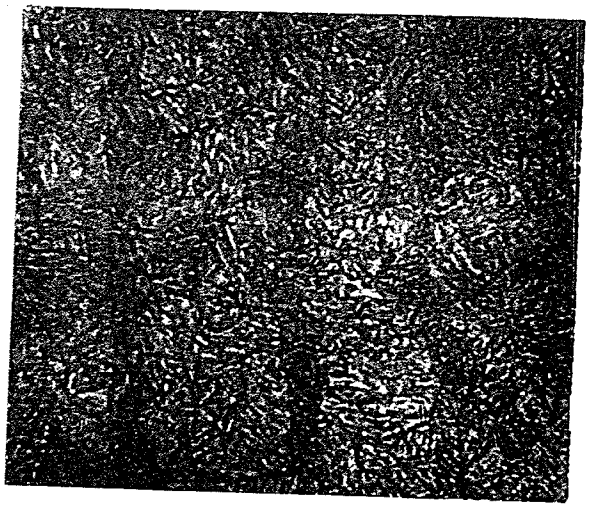

B

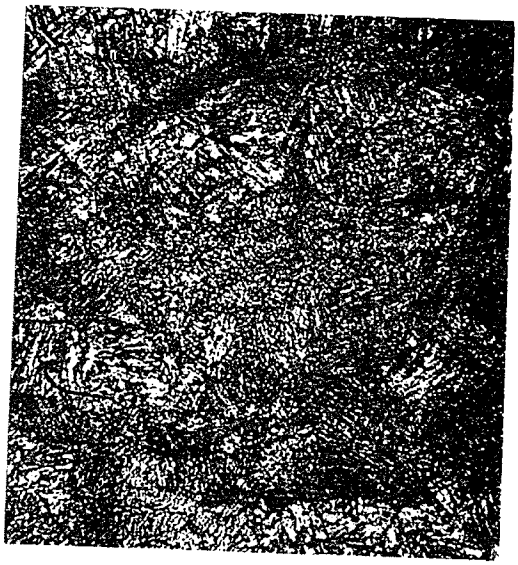

Figure 4.1 (a) Photomicrograph of maraging steel taken from compact tension specimen

(b) Photomicrograph of maraging steel taken from single edge notch specimen

A

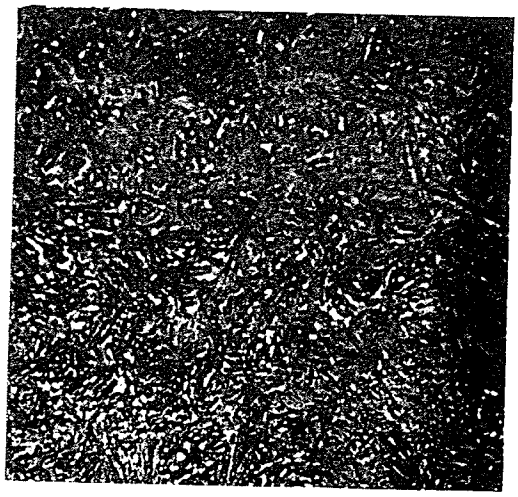

B

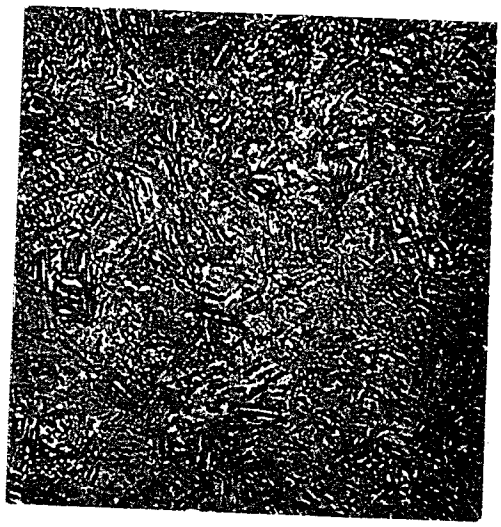

Figure 4.2 (a) Photomicrograph of 4340 steel taken from single edge notch specimen

(b) Photomicrograph of 4340 steel taken from compact tension specimen

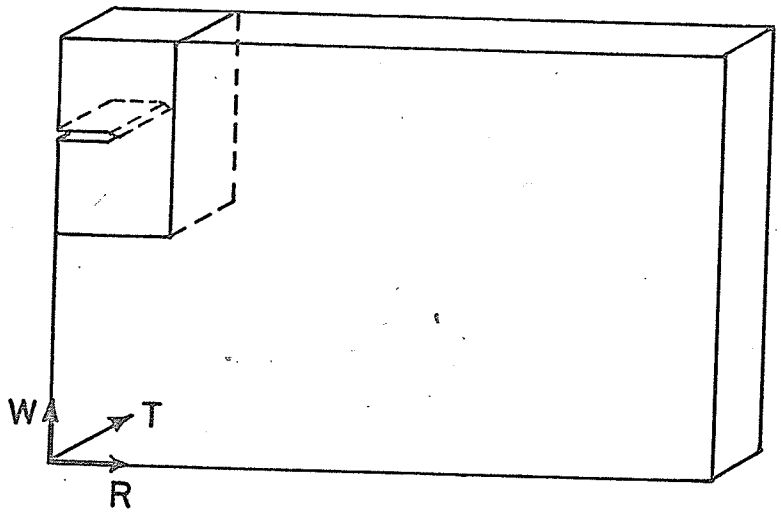

Figure 4.3 GENERAL ORIENTATION OF SPECIMEN IN PLATE

W — WIDTH DIRECTION
R — ROLLING DIRECTION
T — THICKNESS DIRECTION

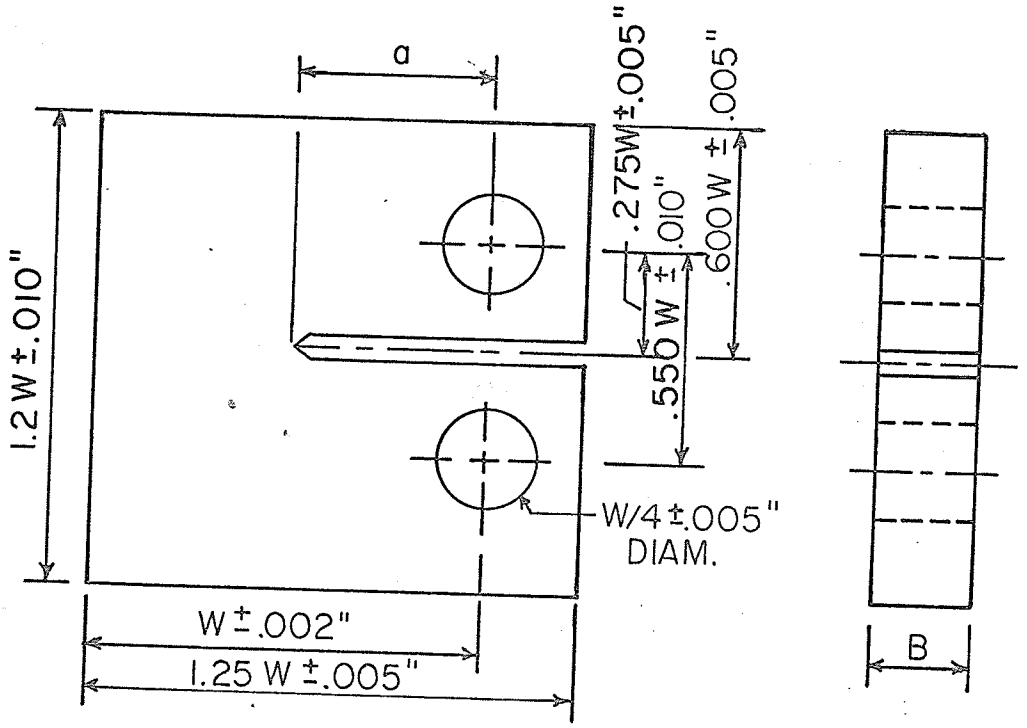

W = 2.000 inch ; a/W = 0.5 ; B = PLATE THICKNESS

Figure 4.4 COMPACT TENSION SPECIMEN

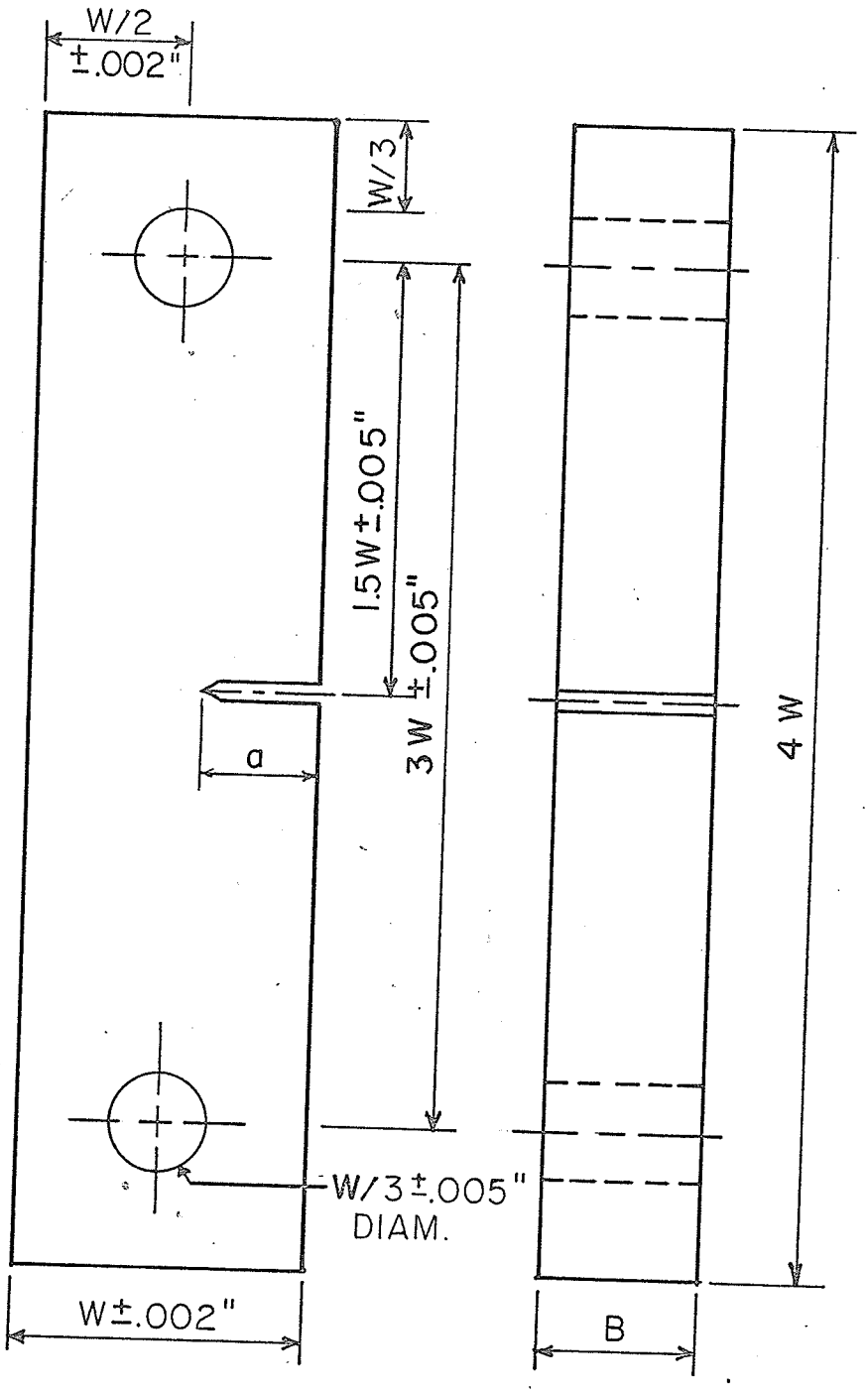

W = 3.000" ; a/W = 0.4 ; B = PLATE THICKNESS

Figure 4.5 SINGLE EDGE NOTCH SPECIMEN

Figure 4.6 Gilmore Universal Testing Machine

4.3 Specimen Preparation

The general orientation of the specimens cut from the plate stock are as shown in Figure 4.3. The crack orientation, related to the co-ordinates of Figure 4.3, is given as WR where the first letter, W, indicates the normal to the crack plane and the second letter, R, indicates the direction of crack propagation. The crack orientation WR is in agreement with that suggested (1) for measuring fracture toughness in sheet and plate products.

The specimens were machined from the stock material to the configurations shown in Figures 4.4 and 4.5. The 45^{o} included angle notch was chosen as the stress raiser configuration because of its relative ease of machining. The main depth of the slot was cut with an ordinary 3/32 inch side and face cutter with the final 0.100 inch being cut with a special 3/32 inch cutter which had been ground to the 45^{o} included angle. This method of machining was employed to keep the notch root radii as sharp and uniform as possible.

Final heat treatment procedures were conducted as specified by the United States Steel Corporation. The single edge notch specimens were heat treated at either Bristol Aerospace Limited or Winnipeg Heat Treating while the compact tension specimens were heat treated in the Metallurgical Engineering Laboratories of the University of Manitoba.

4.4 Testing Equipment

A Gilmore Universal Electo-Hydraulic Closed Loop Material Testing machine with a dynamic capacity of $\pm$ 50,000 pounds was used to fatigue and fracture the specimens. This testing machine had a static capacity of 75,000 pounds and this feature was employed to fracture the single-edge notch specimens.

The machine is shown in Figure 4.6.

To obtain measurements of the surface opening displacements of the crack in the specimen, an extensometer was constructed following the suggestions set forth in the 1969 A.S.T.M. proposed standards for fracture toughness testing (39). The material selected for the cantilever beams was a titanium alloy, Ti-6Al-4V. This material was selected for its relatively high strength and low modulus of elasticity. The spacer block was machined from brass. The specifications of the extensometer are shown in Figure 4.7.

Four Budd Metalfilm strain gages of the type C6-1x1-M50 were mounted on the two titanium alloy beams to provide a full bridge circuit to measure the crack opening displacements. The strain gages had a resistance of 120.0 ± 0.5 ohms with a gage factor of $2.00 \pm 1.0\%$. Extreme care was used to try to ensure the gages were located on the centerline of the beams and equidistant from the ends to be fitted onto the specimen. Two sharp edged supports were machined from mild steel to act as location devices on the specimen. The extensometer, attached to a specimen, is shown in Figures 4.8 (a) and 4.8 (b).

4.5 Test Procedure

As one purpose of the experimental program was to study the effect of the fatigue stress intensity level used to produce a crack on the fracture toughness, it was decided to conduct a series of tests at low fatigue stress intensities and another series at high fatigue stress intensities. The low fatigue stress intensity region chosen was 15% to 30% of the expected fracture toughness while the high fatigue stress intensity region was 50% to 70% of the expected fracture toughness. For 4340 steel

the expected fracture toughness was 55 to 60 k.s.i. $\sqrt{in.}$ (35) while for the maraging steel the expected fracture toughness was 70 to 85 ksi $\sqrt{in.}$ (2).

Using the stress intensity equations of section 3.4, the fatigue loads required to achieve the selected fatigue stress intensities were determined. The specimen was then fatigued in tension at a stress ratio, $R = \frac{\text{Minimum stress}}{\text{Maximum stress}}$, always less than 0.1 until the fatigue crack could be observed to be approximately 0.100 inch beyond the tip of the machine notch. It should be noted that final heat treatment was completed either prior to or following fatigue cracking. This allowed observation of any heat treatment effects on K_{IC}.

When the fatigue crack had progressed sufficiently, the fatigue cycling was then stopped and the extensometer was attached to the specimen. The extensometer output was used to drive the Y - axis for an X-Y recorder while the load signal to the testing machine was used to drive the X - axis. The machine was then programmed to apply a uniform loading rate to the specimen until fracture occurred. In this manner the X-Y recorder gave an autographic display of load displacement opening until final fracture. It should also be noted that loading rate was selected for each specimen to obtain a stress intensity increase rate of 50,000 to 60,000 psi $\sqrt{in.}$ /min. This rate of loading is in agreement with the A.S.T.M. proposed standards. It was felt that by having a common stress intensity rate for all specimens, any effect on K_{IC} by loading rate would be uniform for all specimens.

After the specimen had fractured, the measurement of crack length was taken at 5 stations uniformily spaced across the specimen. These readings were then averaged. If the difference between any two crack length

measurements exceeded 5% of the average, the test was rejected. This criteria was in keeping with the A.S.T.M. proposed standards regarding the linearity of the fatigue crack front.

The load-dispacement plot was analyzed, following the proposed A.S.T.M. standards, to determine the load for proper calculation of the fracture toughness. A straight line was drawn along the straight line portion of the curve and thus nullified any non-linearity at the beginning of the test record which might occur as the extensometer became stationary in its supports. A secant line was drawn which had a prescribed lesser slope than the original straight line. This prescribed lesser slope was 4% for the compact tension specimens and 4.2% for the single edge notch specimens, following the proposed A.S.T.M. standards. The intersection of this secant line with the test record gave the load for the calculation of K_{IC}. Representative load-displacement plots and the accompanying analysis are shown in Figures 4.9, 4.10, 4.11 and 4.12.

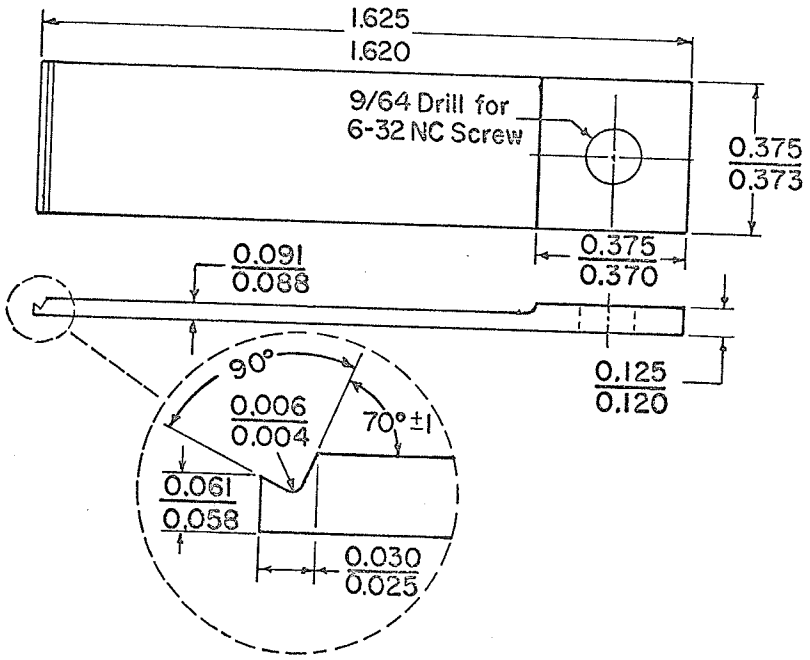

(A)

CANTILEVER BEAMS

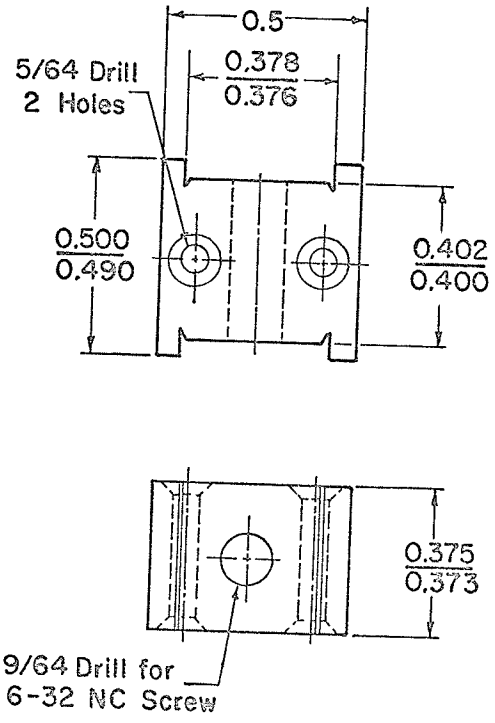

(B)

SPACER BLOCK

Figure 4.7 Specifications for Extensometer

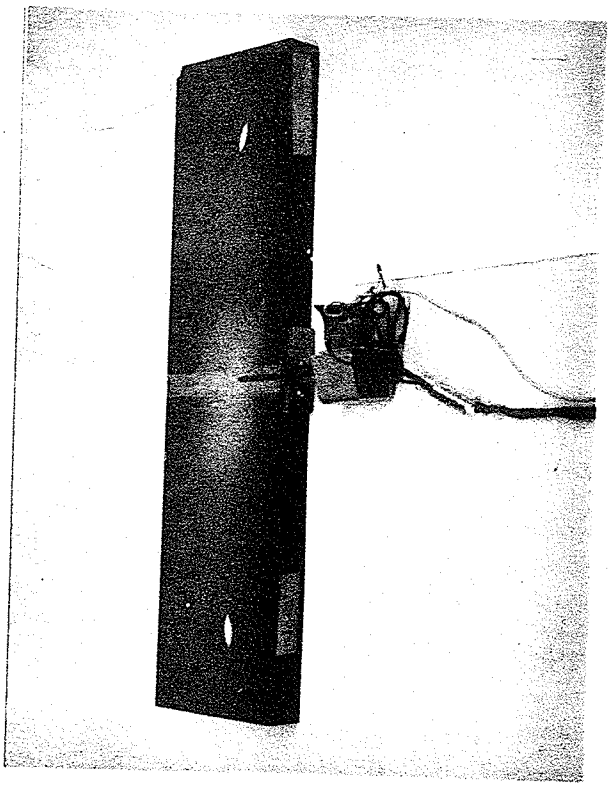

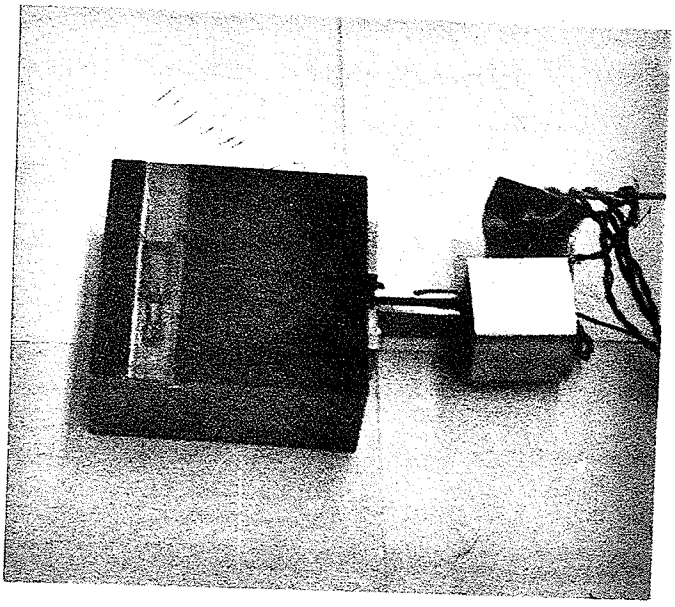

Figure 4.8 (a) Single Edge Notch Specimen and Extensometer

(b) Compact Tension Specimen and Extensometer

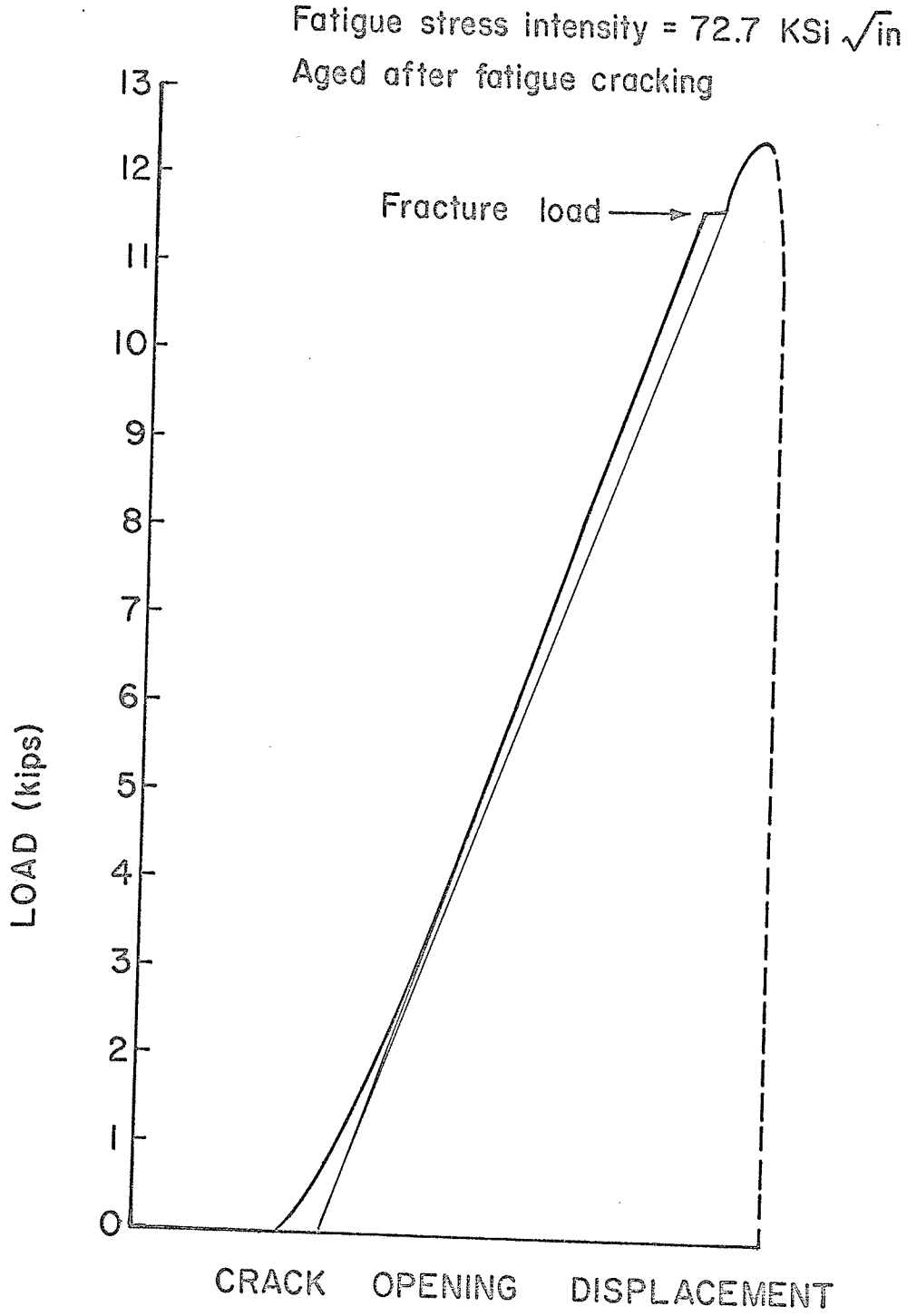

Figure 4.9 Load-Displacement Plot for Compact Tension Specimens of Maraging Steel

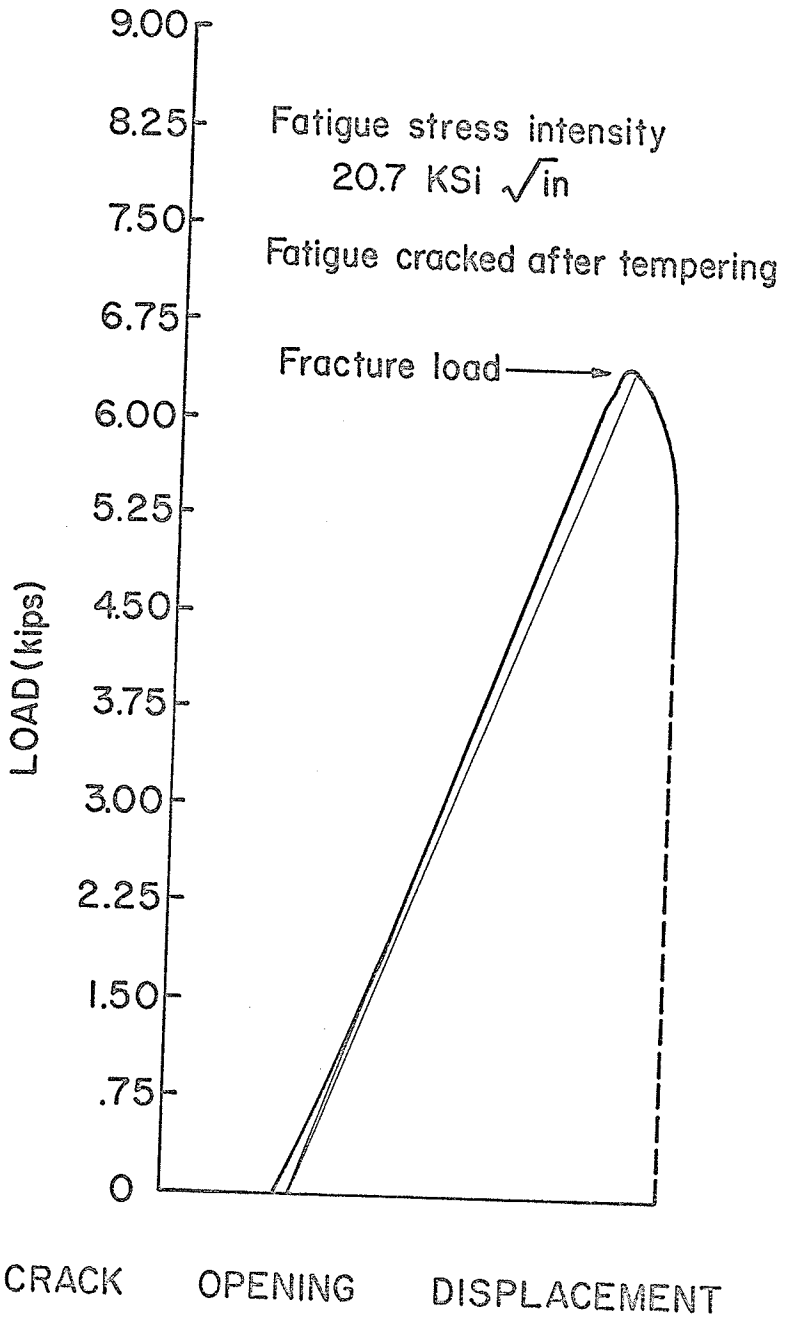

Figure 4.10 Load-Displacement Plot for Compact Tension Specimen of 4340 Steel

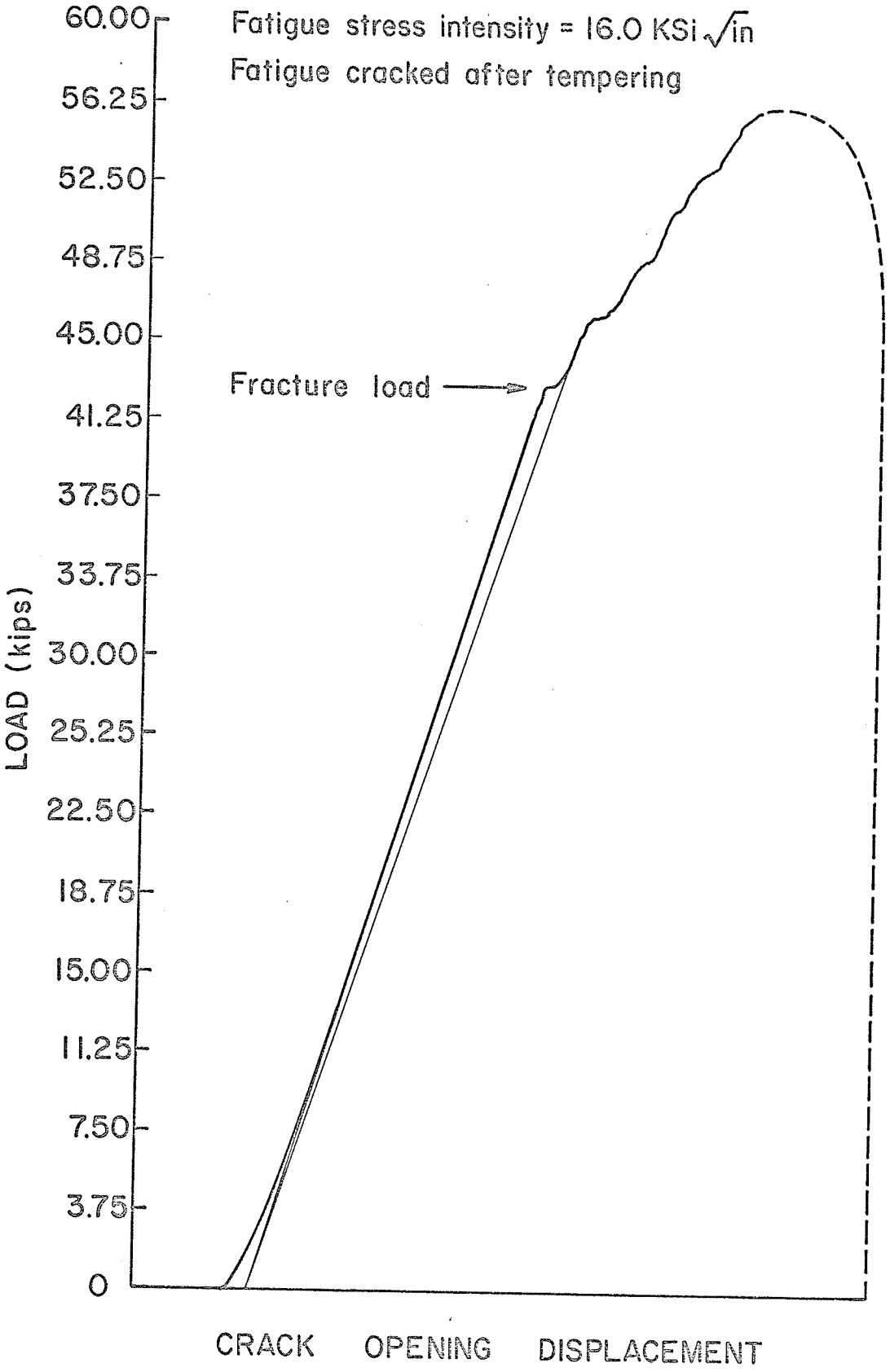

Figure 4.11 Load-Displacement Plot for Single Edge Notch Specimen of Maraging Steel

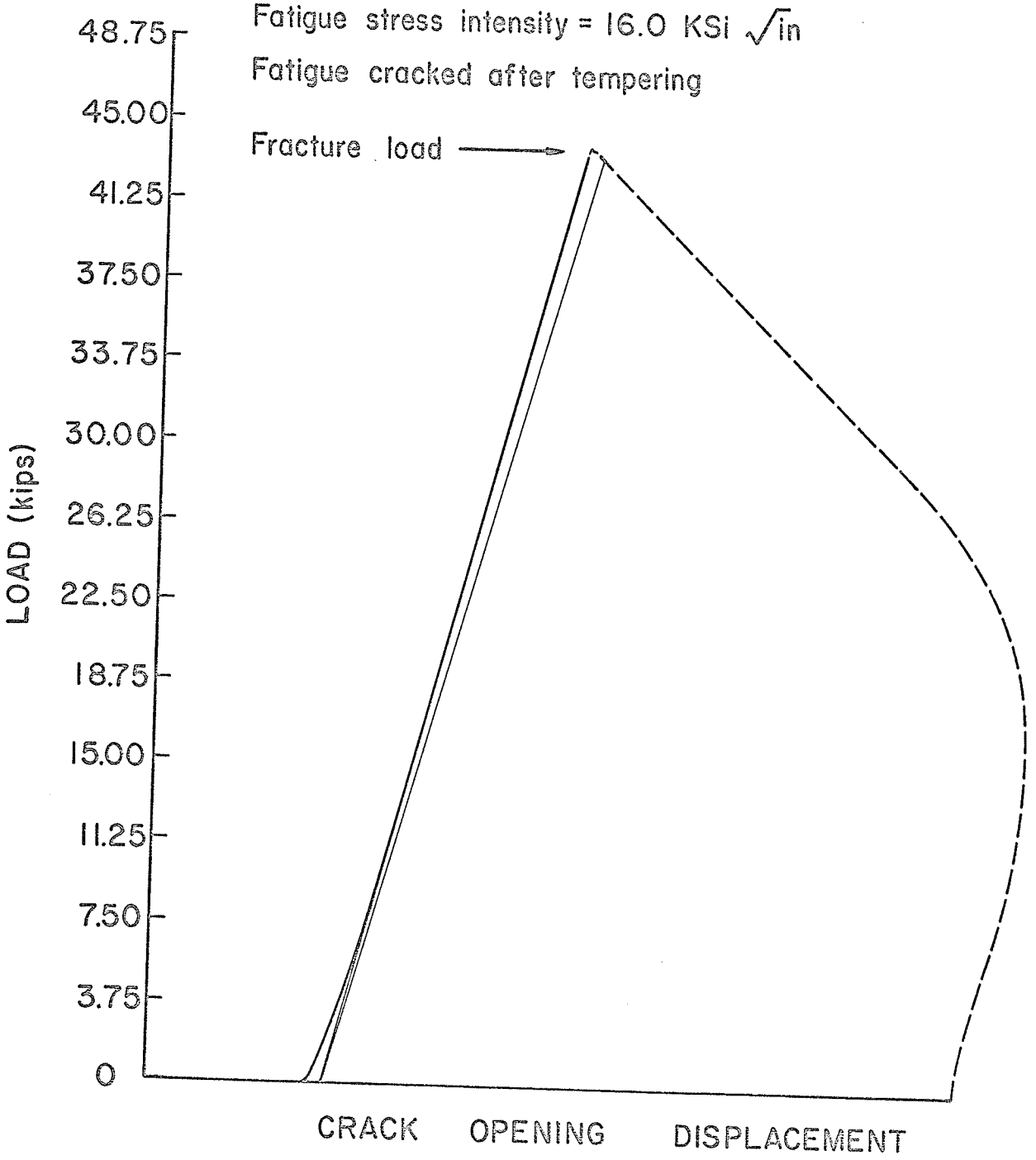

Figure 4.12 Load-Displacement Plot for Single Edge Notch Specimen of 4340 Steel

CHAPTER 5

EXPERIMENTAL RESULTS

5.1 Introduction

Chapter 5 will present the experimental results obtained and attempt to analyze and discuss the significance of the results in the light of previous chapters. It will review all the aspects of the experimental program to ascertain an estimate of the validity of the results and to speculate on the influence of heat treatment, fatigue cracking, and specimen size on fracture toughness.

5.2 Results

Tables 5.1 and 5.2 present the results of the experimental program. The maximum fatigue stress intensity, K_f max, and the fracture stress intensity, K_{IC}, were calculated by a computer program for equations 3.19 and 3.20. The crack length at failure, A, the specimen width, W, the specimen thickness, B, the maximum fatigue load, and the fracture load were used as input information to the program. Equations 3.19 and 3.20, as they appeared in the program, were carefully checked to ensure they were correctly entered into the program. A check of the polynomial portion of equations 3.19 and 3.20 was conducted in the range $a/w = .35$ to $a/w = .55$ in increments of 0.01. The results of this check were in exact agreement with listed values. (37)

The experimental results, as listed in Tables 5.1 and 5.2, are presented graphically in Figures 5.1, 5.2, 5.3, 5.4, and 5.5. These figures

TABLE 5.1

RESULTS FOR SINGLE EDGE NOTCH SPECIMENS

STEEL	CONDITION	NUMBER	A	W	B	FATIGUE LOAD	K_{fMAX}	FRACTURE LOAD	K_{IC}
Maraging	ANN AGE CRK	3B	1.250	3.009	0.715	10.15	20.53	44.060	89.1
Maraging	ANN AGE CRK	2E	1.235	3.061	0.711	10.15	19.53	47.620	91.6
Maraging	ANN AGE CRK	3D	1.280	3.009	0.709	10.15	21.53	41.810	88.7
Maraging	ANN AGE CRK	2A	1.197	3.062	0.706	23.90	44.10	54.100	99.8
Maraging	ANN AGE CRK	1A	1.202	3.154	0.705	24.00	42.08	48.750	85.5
Maraging	ANN CRK AGE	1B	1.213	3.152	0.709	23.75	42.02	47.630	84.3
Maraging	ANN CRK AGE	1C	1.239	3.148	0.698	10.15	18.88	43.120	80.2
Maraging	ANN CRK AGE	1D	1.269	3.149	0.704	10.15	19.41	48.000	91.8
Maraging	ANN CRK AGE	3G	1.238	3.009	0.709	10.15	20.38	40.880	82.1
Maraging	ANN CRK AGE	3F	1.239	3.007	0.708	28.25	56.96	45.000	90.7
Maraging	ANN CRK AGE	3E	1.228	3.007	0.706	28.25	56.30	45.000	89.7
4340	HARD CRK	3H	1.253	3.010	0.708	28.25	57.89	46.880	96.1
4340	HARD CRK	PO	1.223	2.998	1.007	11.25	15.72	42.750	59.7
4340	HARD CRK	P1	1.225	2.999	1.000	11.25	15.86	43.130	60.8
4340	HARD CRK	P2	1.220	2.995	1.002	11.40	15.98	43.880	61.5
4340	HARD CRK	P9	1.228	2.998	1.005	18.40	25.92	41.250	58.1
4340	HARD CRK	P7	1.247	2.997	1.004	18.40	26.62	42.000	60.8
4340	HARD CRK	P3	1.205	3.001	1.009	25.00	33.98	44.910	61.0
4340	HARD CRK	P4	1.207	3.000	1.003	25.50	34.98	44.440	61.0
4340	HARD CRK	P5	1.211	2.998	1.009	25.55	35.07	44.330	60.8

TABLE 5.2

RESULTS FOR COMPACT TENSION SPECIMENS

STEEL	CONDITION	NUMBER	A	W	B	FATIGUE LOAD	K_{fMAX}	FRACTURE LOAD	K_{IC}
4340	HARD CRK	4C5	1.024	1.978	1.010	2.88	20.55	6.340	45.2
4340	HARD CRK	4C4	1.022	1.968	1.007	2.87	20.69	6.450	46.5
4340	HARD CRK	4C1	1.023	1.971	1.009	2.86	20.55	6.260	45.0
4340	HARD CRK	4C6	1.036	1.970	1.007	3.75	27.59	6.550	48.2
4340	HARD CRK	4C2	1.057	1.972	1.009	3.77	28.59	6.750	51.2
4340	HARD CRK	4C0	1.038	1.975	1.010	4.71	34.48	6.710	49.1
4340	HARD CRK	4C3	1.032	1.979	1.013	4.71	33.90	6.830	49.2
4340	HARD CRK	4C7	1.023	1.977	1.009	4.70	33.55	6.910	49.3
Maraging	ANN AGE CRK	HC6	0.715	1.998	0.700	3.08	20.59	10.050	67.2
Maraging	ANN AGE CRK	HC8	0.698	2.001	0.700	3.12	20.42	10.800	70.7
Maraging	ANN AGE CRK	HC5	0.705	1.999	0.700	3.12	20.61	10.000	66.0
Maraging	ANN AGE CRK	HC3	0.725	1.999	0.701	7.04	47.52	9.400	63.5
Maraging	ANN AGE CRK	HC1	0.712	1.998	0.698	7.10	47.44	9.600	64.1
Maraging	ANN AGE CRK	HC2	0.712	1.996	0.698	7.11	47.57	10.100	67.6
Maraging	ANN CRK AGE	CH1	0.717	1.997	0.697	2.85	19.19	8.650	58.3
Maraging	ANN CRK AGE	CH2	0.737	1.998	0.697	2.92	20.12	8.500	58.6
Maraging	ANN CRK AGE	CH3	0.747	1.996	0.699	2.92	20.33	9.800	68.2
Maraging	ANN CRK AGE	CH4	0.789	1.998	0.700	9.95	72.72	11.650	85.1
Maraging	ANN CRK AGE	CH5	0.750	1.997	0.698	9.95	69.58	11.920	83.4
Maraging	ANN CRK AGE	CH6	0.764	1.996	0.698	9.95	70.82	11.180	79.6

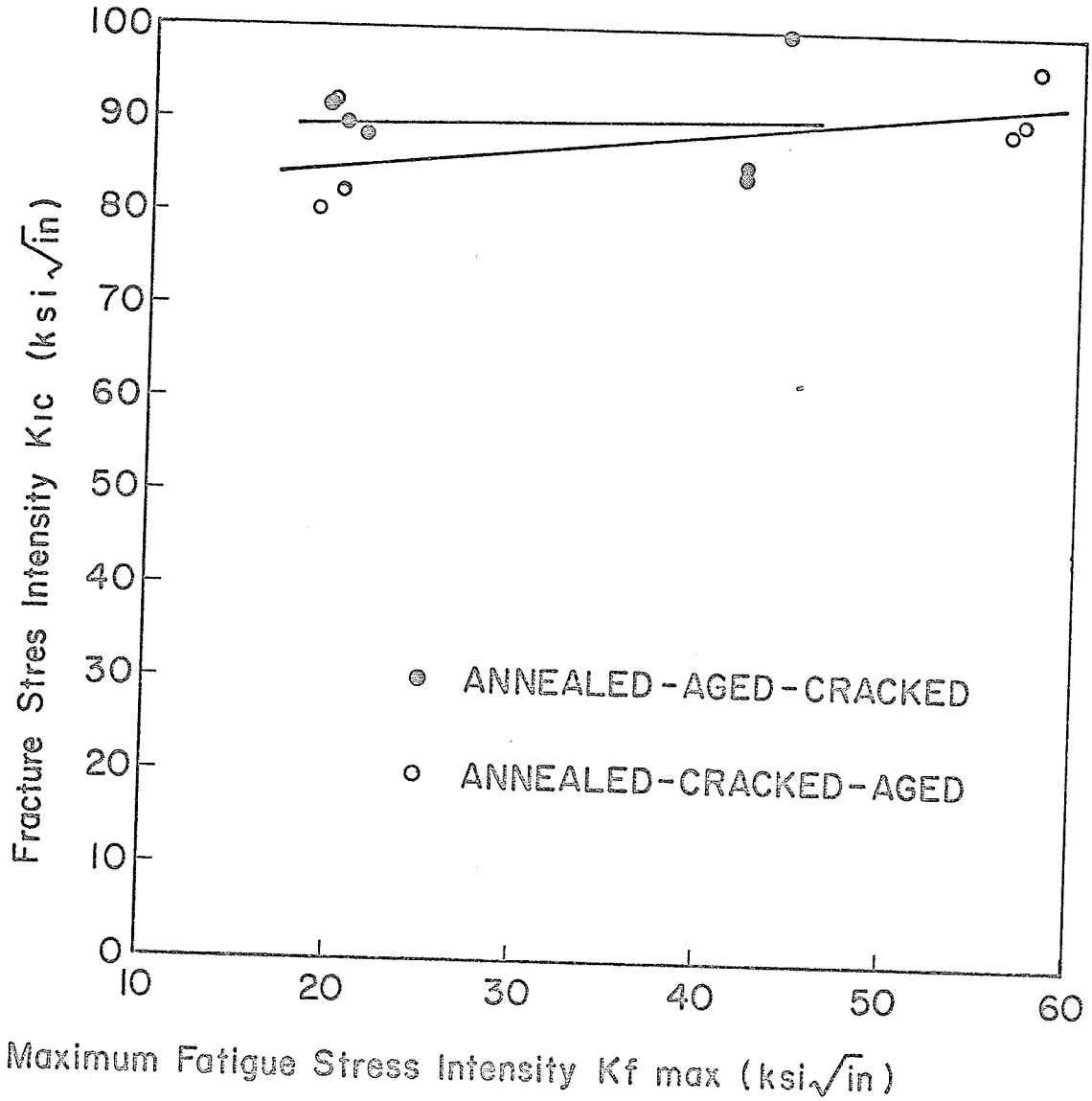

Fig. 5.1 – Kic - Kf max plot for maraging steel
– All specimens are single edge notch

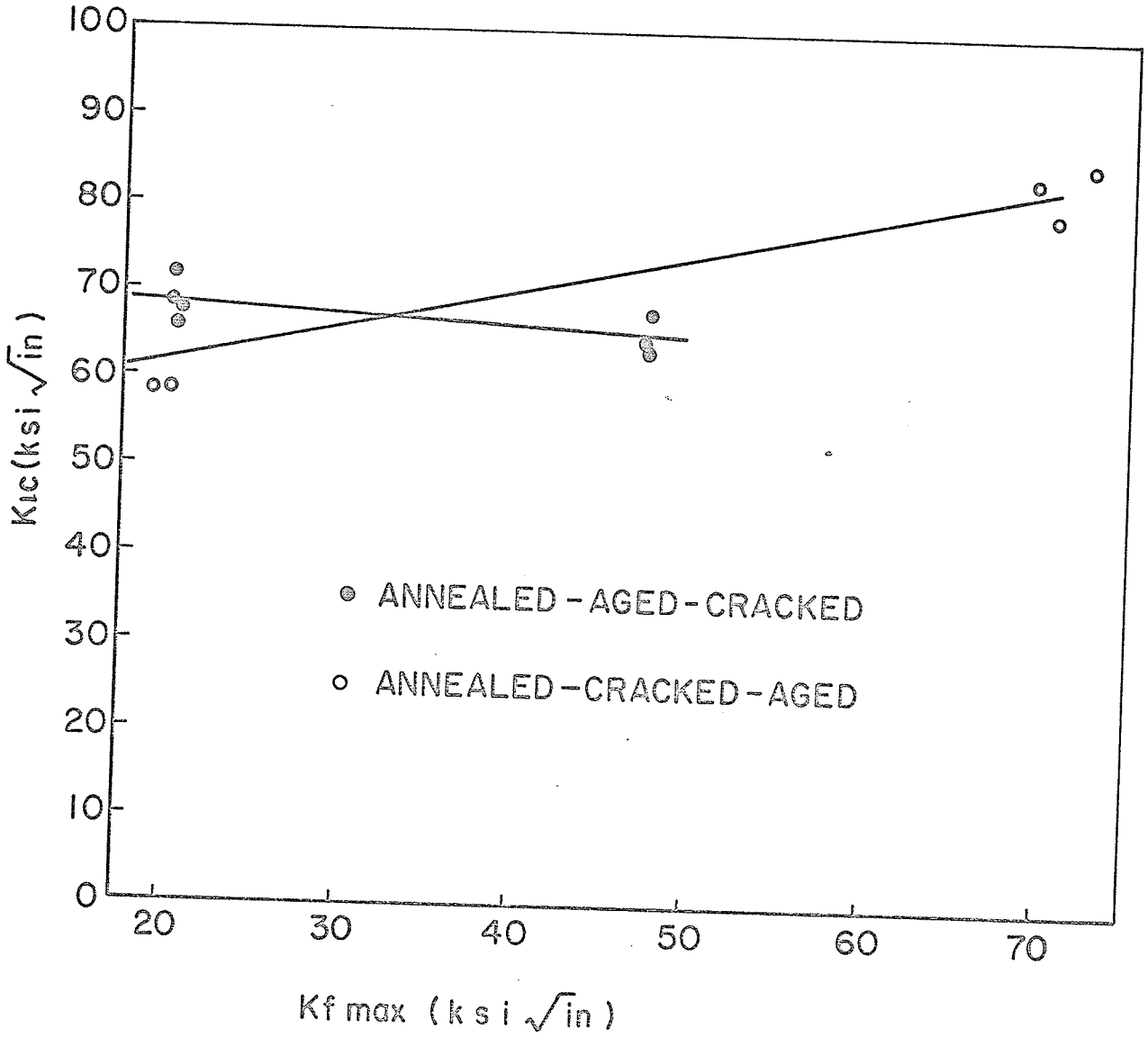

Fig. 5.2 – K_{Ic} vs $K_{f\,max}$ for maraging steel

– All specimens are compact tension

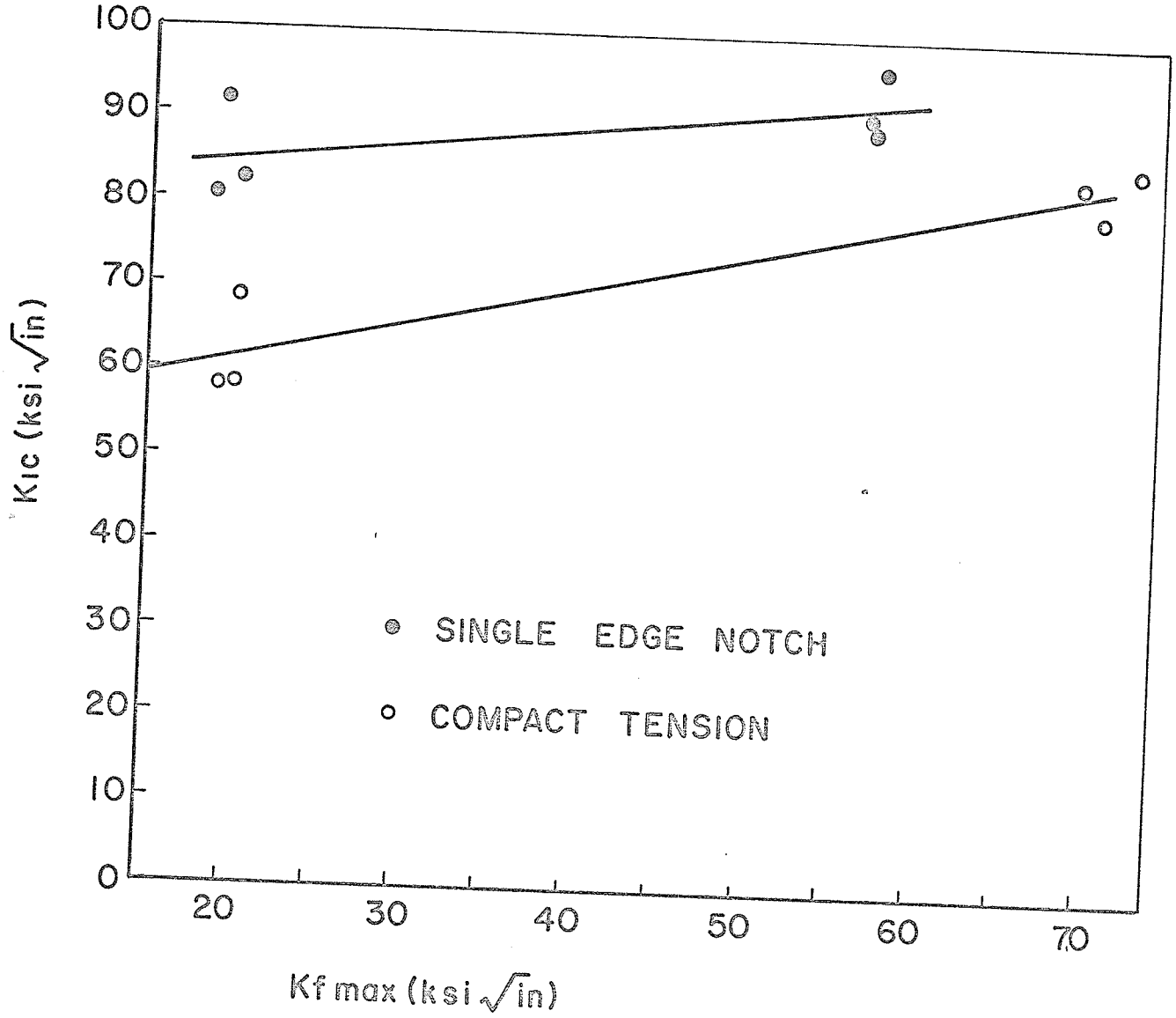

Fig. 5.3 – KIC vs Kf max for maraging steel
– All specimens were annealed, cracked, then aged

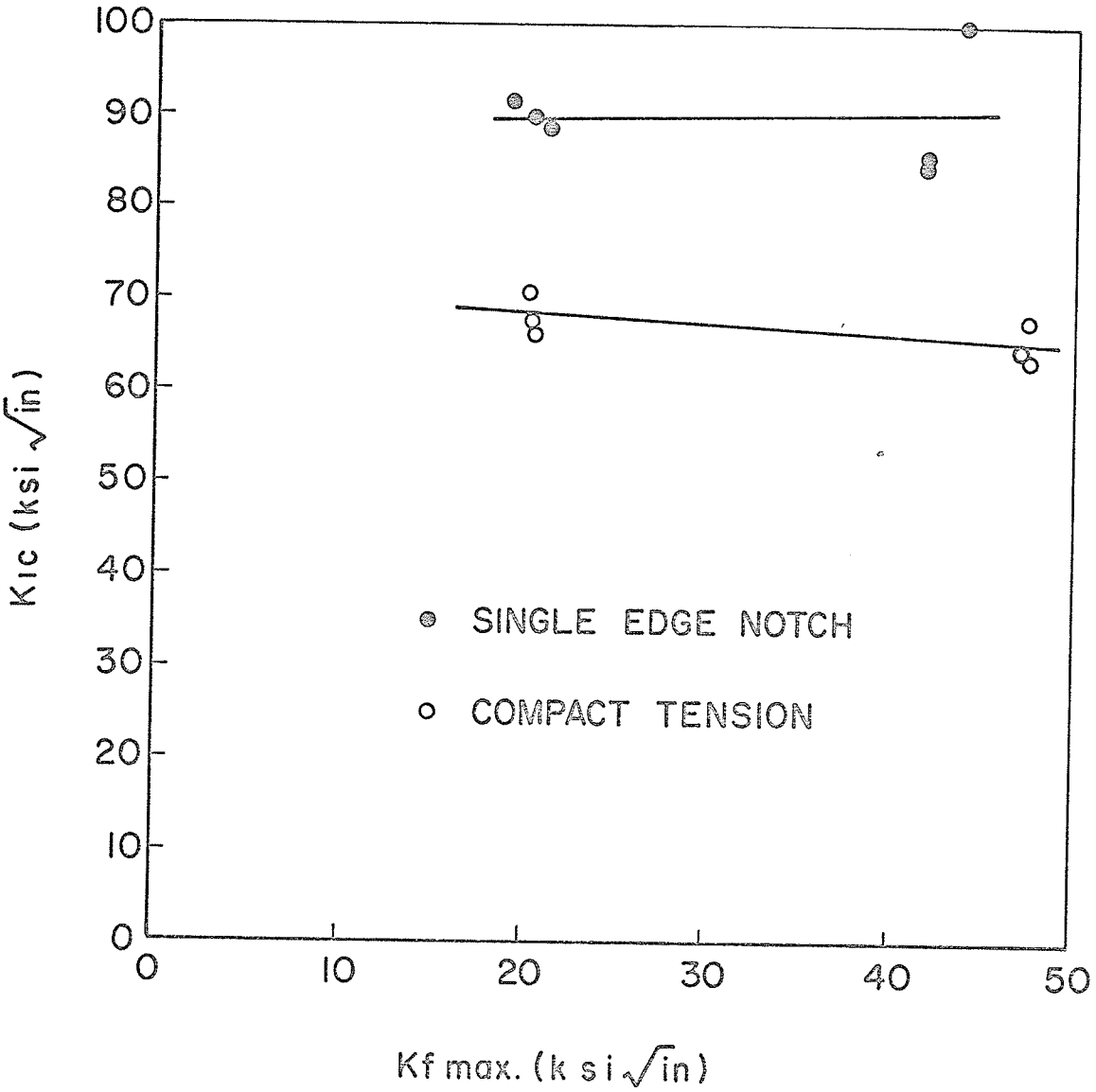

Fig. 5.4 — Kic vs Kf max for maraging steel
— All specimens were annealed, aged, then cracked.

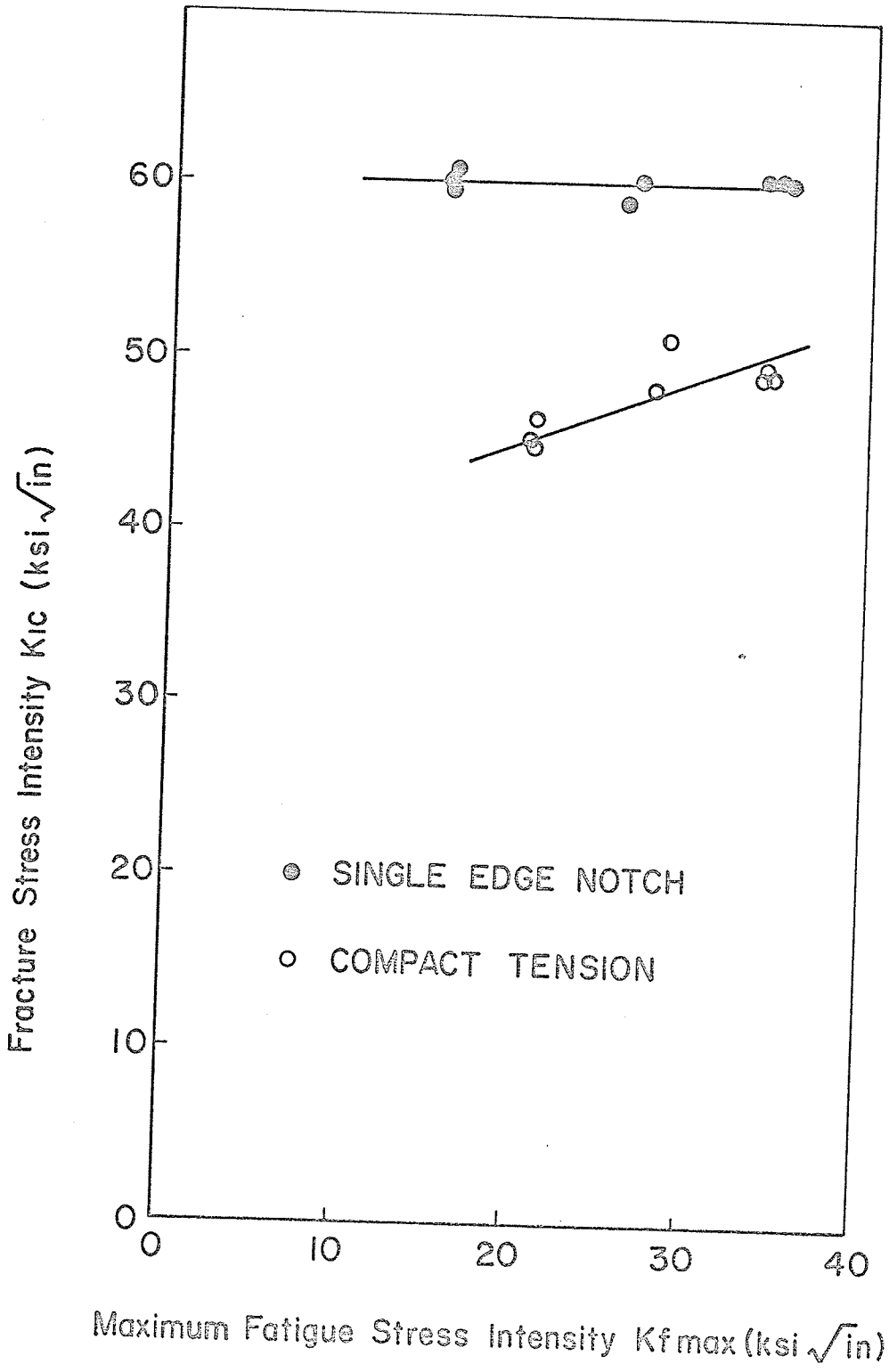

Fig. 5.5 – Kic vs Kfmax for 4340 steel

consist of a plot of K_f max versus K_{IC} and shows how the relationship of K_{IC} to K_f max varies with heat treatment cycle and specimen type.

The trend lines drawn in Figures 5.1 to 5.5 are given as straight lines because only two sets of points were obtained for the majority of tests. The trend lines are based on linear regression analysis of the experimental data. It was felt by the author that these trend lines would be helpful in illustrating the effects of fatigue precracking and heat treatment on fracture toughness. It must be emphasized that a linear relationship between K_{IC} and K_f max has not been assumed or postulated by these results. The linear regression analysis was used because of the limited data and because such analysis would help to reveal any trend which might be obscured by the scatter.

5.3 Analysis and Discussion of Results

The most obvious result of the experiments is the difference in fracture toughness levels for different specimen types of the same material. This result is quite clear in Figures 5.3, 5.4, and 5.5. In all the experiments conducted, the fracture toughness measured by the compact tension specimens was 15% to 20% lower than fracture toughness measured by the single edge notch specimens.

This apparent difference in K_{IC} levels is not easily understood. The fracture toughness of the 4340 steel as measured by the single edge notch specimens was 60 k.s.i. $\sqrt{\text{in.}}$ and was nearly independent of fatigue stress intensity throughout the region tested. This value of fracture toughness is in good agreement with the published data (35). This reference gives a fracture toughness of 53 to 55 k.s.i. $\sqrt{\text{in.}}$ for 4340 tempered for 1 hour at 600° F to a yield strength of 230 Ksi and a value of 68 to 70

k.s.i. $\sqrt{in.}$ for 4340 tempered for 1 hour at 750° F to a yield strength of 213 ksi. These results were obtained by 3 point bend tests of single edge notch plates. The experimental 4340 steel specimens for this thesis were tempered at 600° F for 1 hour to a yield strength 203 ksi.

Brown and Srawley (2) give a fracture toughness of 68.4 k.s.i. $\sqrt{in.}$ for 18 Ni (250) Maraging steel aged at 900° F for 3 hours to a yield strength of 259 ksi. This value is valid when fracture toughness is measured by following the proposed A.S.T.M. standards in all details. The maraging steel for this study was aged at 900° F for 3 hours and reached a yield strength of 232 ksi. It has been observed (35, 2) that the fracture toughness increases as the yield strength decreases. For 18 Ni (300) maraging steel a drop in yield strength from 285 ksi to 242 ksi was accompanied by a fracture toughness increase of 51.75 k.s.i. $\sqrt{in.}$ to 84.5 k.s.i.$\sqrt{in.}$ (2). Hence the fracture toughness of 85 to 90 k.s.i. $\sqrt{in.}$ measured by the single edge notch specimens would seem to be valid.

One possible explanation for the difference in K_{IC} levels as measured by the two specimens could be size effect. This would not be a size effect due to a change in thickness, as thickness was not varied in these experiments. Rather this would be a size effect created by the relative closeness of the loading to the crack in the compact tension specimens as compared to the single edge notch specimens. The compact tension specimens were also subjected to a greater degree of bending and tension than were the single edge notch specimens. The nature of the more severe combined loading on the compact tension specimens may have affected the crack tip stress field in a manner which was not accounted for by the stress intensity equation for this specimen. This could be a possible explanation for the differences in the K_{IC} levels.

The effect of maximum fatigue stress intensity on the maraging steel appears to be closely related to the heat treatment procedure. Figure 5.4 shows that fracture toughness is essentially independent of fatigue stress intensity, in the region tested, for all specimens which were cracked after aging. Figure 5.3 shows that fracture toughness is dependent on fatigue stress intensity for all specimens which were cracked and then aged.

For 4340 steel, the fracture toughness as measured by the single edge notch specimens was independent of fatigue stress intensity. However, as shown by Figure 5.5, the fracture toughness measured by the compact tension specimens was quite dependent of fatigue stress intensity over the same range of fatigue stress intensities. This suggests the compact tension specimens, at least for this material, may be more sensitive to fatigue precracking.

Figure 5.1 and 5.2 show clearly that the heat treatment cycle has an effect on the fracture toughness. The fracture toughness is definitely elevated for all specimens which were subjected to a high fatigue stress intensity and were subsequently aged for 3 hours at 900^{o} F. This would indicate that the heat treatment cycle must receive careful attention during measurements of fracture toughness.

The results of these experiments would seem to support the A.S.T.M. proposed standards regarding fatigue precracking. These proposed standards suggested a maximum fatigue stress intensity for steels of either 36 k.s.i. $\sqrt{in.}$ or one half of the subsequent K_{IC} of the steel. The lesser of the two values should be chosen for the maximum fatigue stress intensity. Following these standards, the maraging steel could be subjected to a fatigue stress intensity of 36 k.s.i. $\sqrt{in.}$ while the 4340 steel would be limited to 30 k.s.i. $\sqrt{in.}$

The 4340 steel results of Figure 5.5 for single edge notch specimens definitely support these recommendations. However, the compact tension results indicate a dependence on fatigue stress intensity even below 30 k.s.i. $\sqrt{in.}$.

The maraging steel results of Figure 5.4 support the independence of K_{IC} from fatigue stress intensity below 36 k.s.i. $\sqrt{in.}$. The results of Figure 5.3 are inconclusive since an accurate estimate of the behaviour of K_{IC} up to a fatigue stress intensity cannot be made.

The A.S.T.M. proposal on heat treatment suggests:

"The fatigue cracking shall be conducted with the specimen fully heat treated to the condition in which it is to be tested".

The results of the experimental study would suggest that the heat treatment should be such that the introduction of the crack would occur at the same point in the heat treatment cycle in both experimental specimen and actual component application.

5.4 Summary

The results of experimental program indicate that the fatigue stress intensity and heat treatment cycle do have an effect on fracture toughness. The extent of the effect of these two variables is interrelated and varies with material and specimen types. However, following the A.S.T.M. proposed standards concerning fatigue precracking should eliminate any fatigue effects on fracture toughness.

The ability of all specimen types to measure fracture toughness accurately and reliably seems questionable as a result of these experiments. More experimental study appears to be required with the compact tension specimen to ensure that it can measure fracture toughness accurately.

CHAPTER 6

SUMMARY AND CONCLUSIONS

6.1 Introduction

This chapter presents a summary of the experimental results and compares them to related results which were found in the literature reviewed. It will also make some recommendations on possible improvement of the experimental approach and give some suggestions for additional investigations.

6.2 Summary

The results of the testing program revealed that the fracture toughness, as measured by the compact tension specimens, was more sensitive to the fatigue cracking stress intensity than was the fracture toughness measured by the single edge notch specimens. The general levels of fracture toughness measured by the compact tension specimens were 15% to 20% lower than the fracture toughness levels measured by the single edge notch specimens.

The literature review had revealed that the fracture toughness was elevated when the fatigue crack was introduced by high fatigue stress intensities (2). However, the published results were computed from specimens fractured in four point bending. Similar evidence for compact tension or single edge notch tension specimens was not found. Also, very little experimental verification of the compact tension specimen was found.

The literature review indicated that all types of fracture toughness specimen geometries should be capable of measuring the fracture toughness

of a material (2, 34). Srawley (34) states:

"It has been established for a number of materials that K_{IC} is independent of size and form of specimen when properly measured; which means, among other things, when the specimen dimensions are adequate". This would seem to imply that the proposed specifications for the compact tension specimen are inadequate or some major inaccuracy occurred in the test program but was not discovered.

6.3 Conclusions

As the experimental program was conducted to investigate certain areas of the A.S.T.M. proposed standards concerning the determination of the fracture toughness of a material, any conclusions will be directed at justification of these standards.

From the experimental study, it can be concluded that the proposed standards concerning fatigue precracking are sufficiently conservative to ensure that the fatigue stress intensity used to initiate a crack will have no effect on the measured fracture toughness of the material.

The use of the recommended compact tension specimen to measure fracture toughness could not be justified by these experiments. The compact tension specimen gave results which were consistently lower than the single edge notch specimen results. The single edge notch specimen results were assumed to be valid as they agreed with published data.

The heat treatment cycle does have an effect on the measured fracture toughness. Consequently, it would seem advisable to subject the fracture toughness specimen to the same sequence of loads and heat treatments which it will receive in service. In this manner, variations in experimental and service fracture toughness could not be attributed to

improper control of the experimental specimen.

6.4 Recommendations and Suggestions for Further Study

To improve the experimental aspects of the thesis, the following suggestion is made:

The minimum number of tests at a given fatigue stress intensity level should be increased from the recommended 3 to either 5 or 6 to increase the confidence in the measured value of fracture toughness.

As a area of further study, this field of fracture toughness testing has many possible areas of exploration. Firstly, more tests should be conducted at immediate fatigue stress intensity levels to obtain a fuller picture of the K_{IC} -K_f max relationship. More study must be conducted with the compact tension specimen to verify its usefulness in fracture toughness testing.

Another very interesting and possible quite revealing study could be conducted into the micro mechanisms of the fracture process. The use of the electron microscope or electron probe to study the development of the fatigue crack, the transition from the fatigue crack tip to fast fracture, and the nature of the mechanism of final fracture could prove to be most rewarding.

BIBLIOGRAPHY

1. Brown, W.F., Jr., and Srawley, J.E., "Fracture Toughness Testing", Fracture Toughness Testing and Its Applications, A.S.T.M. - S.T.P. 381, p. 133, 1964

2. Brown, W.F., Jr., and Srawley, J.E., Plane Strain Crack Toughness Testing of High Strength Metallic Materials, A.S.T.M. - S.T.P. 410, 1967

3. A.S.M.E. subcommittee on Brittle Fracture, "A Review of Engineering Approaches to Design Against Fracture", A.S.M.E., New York, 1964

4. "Lloyd's Survey of Brittle Fracture", Engineering, Vol. 185, p. 497, 1958

5. Schabtach, C., Fogleman, E.L., Rankin, H.W., and Winne, D.H., "Report on the Investigation of Two Generator Rotor Failures" - Trans. A.S.M.E. Vol. 78, p. 1567, Oct. 1956

6. Emmert, H.D., "Investigation of a Large Steam Turbine Spindle Failure" - Trans. A.S.M.E., Vol. 78, p. 1547, Oct. 1956

7. Rankin, A.W., and Sequin, B.R., "Report on the Investigation of the Turbine Wheel Fracture at Tanners Creek" - Trans. A.S.M.E., Vol. 78, p. 1527, Oct. 1956

8. Peterson, R.E., "Interpretation of Service Fractures", Handbook of Experimental Stress Analysis, p. 593, John Wiley and Sons, Inc., 1950

9. Tipper, C.F., "The Brittle Fracture Story", Cambridge University Press, Cambridge, 1962

10. Wulpi, D.J., "How Components Fail" American Society for Metals, 1966

11. Lessels, J.M., "Strength and Resistance of Metals", John Wiley & Sons, Inc., New York, 1954

12. Hertzberg, R.W., "Electron Fractography", Notes for "A Short Course in Fracture Mechanics", Lehigh University, 1969.

13. Forsyth, P.J.E., and Ryder, D.A., "Fatigue Fracture", Aircraft Engineering, Vol. 32, p. 96, April, 1960

14. Hartman, A., "On the Effect of Oxygen and Water Vapour on the Propagation of Fatigue Cracks in 2024-T3 Alclad Sheet", Int. J. of Fracture Mech., Vol. 1, p. 167, 1965

15. Spitzig, W.A., Talda, P.M., and Wei, R.P., "Fatigue Crack Propagation and Fractographic Analysis of 18 Ni (250) Maraging Steel Tested in Argon and Hydrogen Environment", Journal of Engineering Fracture Mechanics, Vol. 1, No. 1, p. 155, 1968

16. Espey, G.B., Jones, M.H., and Brown, W.F., Jr., "The Sharp Notch Strength of Several High Strength Sheet Alloys", Proc. A.S.T.M., Vol. 59, p. 837, 1959

17. Telelman, A.S., "The Hydrogen Embrittlement of Ferrous Alloys", Fracture of Solids, p. 671, Gordon and Breach, New York, 1963

18. Barsom, J.M., "Investigation of Subcritical Crack Propagation", Ph. D. Thesis, The University of Pittsburgh, 1969

19. Johnson, H.H., and Paris, P.C., "Sub-Critical Flaw Growth", Engineering Fracture Mechanics, Vol. 1, No. 1, p.3, June, 1968

20. Wei, R.P., "Some Aspects of Environment - Enhanced Fatigue Crack Growth", Notes for "A Short Course in Fracture Mechanics", Lehigh University, 1969.

21. Lubahn, J.D., "On the Applicability of Notch Tensile Data to Strength Criteria in Engineering Design", Trans. A.S.M.E., Vol. 79, p. 111, 1957.

22. Lubahn, J.D., "Correlation of Tests Using the Congrvency Principle", Proc. A.S.T.M., Vol. 58, p. 678, 1958

23. McClintock, F.A., "Ductile Fracture Instability in Shear", Trans. A.S.M.E., Journal of Applied Mechanics, Vol. 25, p. 582, 1958

24. Griffith, A.A., "Phenomena of Rupture and Flow in Solids, "Philosophical Transactions of the Royal Society",A 221, 1920, p. 163

25. Irwin, G.R., "Analysis of Stresses and Strains Near the End of a Crack Traversing Aplate", Trans. A.S.M.E., Journal of Applied Mechanics, Vol. 79, p. 361, 1957

26. McClintock, F.A., and Argon, A.S., "Mechanical Behaviour of Materials", p. 521, Addison - Wesley Publishing Company, Inc., 1966

27. Lubahn, J.D., "Experimental Determination of Energy Release Rate for Notch Bending and Notch Tension", Proc. A.S.T.M., Vol. 59, p. 855, 1959

28. Hancock, G.G., and Johnson, H.H., "Hydrogen, Oxygen, and Subcritical Crack Growth in a High-Strength Steel", Trans. Metall. Soc. A.I. M.E., Vol. 236, p. 513, 1966

29. Sneddon, I.N., "The Distribution of Stress in the Neighbourhood of a Crack in an Elastic Solid", Proc., Royal Society of London, Vol. A-187, 1946.

30. Williams, M.L., "On the Stress Distribution at the Base of a Stationary Crack", Trans., A.S.M.E., Journal of Applied Mechanics, 1957

31. Srawley, J.E., Jones, M.H. and Gross, B., "Experimental Determination of the Dependence of Crack Extension Force on Crack Length for a Single-Edge-Notch Tension Specimen", NASA TN D-2396, August, 1964

32. Gross, B. and Srawley, J.E., "Stress Intensity Factors by Boundary Collocation for Single-Edge-Notch Specimens Subject to Splitting Forces" NASA TN D-3295, February, 1966

33. Gross, B., Srawley, J.E., and Brown, W.F., Jr., "Stress Intensity Factors for a Single-Edge-Notch Tension Specimen by Boundary Collocation of a Stress Function" NASA TN D-2395, August, 1964

34. Srawley, J.E., "Plane Strain Fracture Toughness", Notes for "A Short Course in Fracture Mechanics", Lehigh University, 1969

35. Srawley, J.E., Jones, M.H., and Brown, W.F., Jr., "Determination of Plane Strain Fracture Toughness", Materials Research and Standards, Vol. 7, No. 6, p. 262, June 1967

36. Ludwik, P., "Dig Bedeutung des Gleit-und Reisswiderstandes fur die Werkstoffprufung", Z. Ver. deut. Ing., Vol. 71, No. 2, p. 1532, 1927

37. American Society for Testing and Materials, "Proposed Method of Test for Plane-Strain Fracture Toughness of Metallic Materials", 1969 Book of A.S.T.M. Standards, Part 31, p. 1099, May, 1969

38. Inglis, C.E., "Stresses in a Plate due to the Presence of Cracks and Sharp Corners", Proceedings, Institute of Naval Architects, Vol. 60 1913.

39. Manning, R.D., Murphy, W.J., Nichols, H.J., and Caine, K.T., "Simulated Service Tests of Steels for Solid Propellant Missile Motor Cases", Materials Research and Standards, June, 1962

40. Westergaard, H.M., "Bearing Pressures and Cracks", Transactions, A.S.M.E., Journal of Applied Mechanics, 1939

APPENDIX A

Stress Field Equations Expressed in Polar Co-ordinates

The stress field equations for opening mode loading were given by equation 3.13 as

$$\sigma_x = \text{Re } Z - y \text{ Im } Z^1 \tag{A.1}$$

$$\sigma_y = \text{Re } Z + y \text{ Im } Z^1$$

$$\tau_{xy} = - y \text{ Re } Z^1$$

where $Z = f(z)$ is an analytic function of the complex variable, $z = x + iy$, and $Z^1 = \frac{dZ}{dZ}$.

Taking polar co-ordinates from the origin, as in Figure 2.74,

$$z = re^{i\theta} \tag{A.2}$$

The stress field in the crack tip region was characterized by equation 3.15 as

$$\lim_{|z| \to o} Z = \frac{K_I}{\sqrt{2\pi Z}} \tag{A.3}$$

then $$\lim_{|z| \to o} Z^1 = \frac{-1}{2} \frac{K_I}{\sqrt{2\pi z}.z} \tag{A.4}$$

expressing (A.3) and (A.4) in polar co-ordinates

$$\lim_{r \to o} Z = \frac{K_I}{\sqrt{2\pi r}} e^{-i\frac{\theta}{2}} \tag{A.5}$$

$$\lim_{r \to o} Z^1 = \frac{-1}{2} \frac{K_I}{\sqrt{2\pi r}.r} e^{-i\frac{3\theta}{2}} \tag{A.6}$$

Applying Euler's identity $e^{-i\theta} = \cos\theta - i \sin\theta$ to (A.5) and (A.6),

$$\lim_{r \to o} Z = \frac{K_I}{\sqrt{2\pi r}} \left[\cos \frac{\theta}{2} - i \sin \frac{\theta}{2}\right] \tag{A.7}$$

$$\lim_{r \to o} Z^1 = \frac{-1}{2} \frac{K_I}{\sqrt{2\pi r}\, r} \left[\cos \frac{3\theta}{2} - i \sin \frac{3\theta}{2}\right] \tag{A.8}$$

Also, $$x = r \cos \theta \tag{A.9}$$

$$y = r \sin \theta \tag{A.10}$$

Substituting (A.7), (A.8), (A.9), (A.10) into (A.1),

$$\sigma_x = \frac{K_I}{\sqrt{2\pi r}} \left[\cos \frac{\theta}{2} - \frac{1}{2} \sin \theta \sin \frac{3\theta}{2}\right] \tag{A.11}$$

$$\sigma_y = \frac{K_I}{\sqrt{2\pi r}} \left[\cos \frac{\theta}{2} + \frac{1}{2} \sin \theta \sin \frac{3\theta}{2}\right]$$

$$\tau_{xy} = \frac{K_I}{\sqrt{2\pi r}} \left[\frac{1}{2} \sin \theta \cos \frac{3\theta}{2}\right]$$

Employing the identity

$$\sin \theta = \sin 2 \left(\frac{\theta}{2}\right) = 2 \sin \frac{\theta}{2} \cos \frac{\theta}{2}$$

in equation (A.11)

$$\sigma_x = \frac{K_I}{\sqrt{2\pi r}} \cos \frac{\theta}{2} \left[1 - \sin \frac{\theta}{2} \sin \frac{3\theta}{2}\right] \tag{A.12}$$

$$\sigma_y = \frac{K_I}{\sqrt{2\pi r}} \cos \frac{\theta}{2} \left[1 + \sin \frac{\theta}{2} \sin \frac{3\theta}{2}\right]$$

$$\tau_{xy} = \frac{K_I}{\sqrt{2\pi r}} \cos \frac{\theta}{2} \sin \frac{\theta}{2} \cos \frac{3\theta}{2}$$

APPENDIX B

The Stress Function Approach to the Griffith Crack Problem

The Griffith crack problem was analyzed in Chapter 3.2 by energy methods. In this appendix, the stress function approach will be used.

The stress field equations, as discussed in Chapter 3.3, were

$$\sigma_x = \text{Re } Z - y \text{ Im } Z^1 \tag{B.1}$$

$$\sigma_y = \text{Re } Z + y \text{ Im } Z^1$$

$$\tau_{xy} = - y \text{ Re } Z^1$$

Consider the Griffith configuration of Figure 3.1. For this configuration, the following stress function is applicable:

$$Z = \frac{\sigma z}{\sqrt{z^2-a^2}} \tag{B.2}$$

where $z = x + iy$ and the origin is at the centre of the crack. It can be verified that this is the correct stress function by observing that:

(1) the function is analytic everywhere except for $- a \leq x \leq a$ on the x - axis,

(2) the boundary conditions of the problem are satisfied.

The boundary stresses are computed by equations (B.1) using equation (B.2) and its first derivative which is

$$Z^1 = \frac{dZ}{dz} = \frac{-\sigma a^2}{(z^2-a^2)^{3/2}} \tag{B.3}$$

At infinity, $|z| \to \infty$, the boundary stresses are

$$\sigma_x = \sigma_y = \sigma$$

$$\tau_{xy} = o$$

On the crack surface, $z = x$, $-a < x < a$, Z is a pure imaginary quantity and gives

$$\sigma_y = \tau_{xy} = o$$

In order to examine the crack tip, the origin is moved from $z = o$ to the right hand crack tip $z = a$. The co-ordinates with respect to the crack tip are related to the previous co-ordinates by replacing z by $z + a$.

With $z + a$ substituted for z, equation (B.2) becomes

$$Z = \frac{\sigma(z+a)}{\sqrt{z^2+2az}} = \frac{\sigma(z+a)(z+2a)^{-1/2}}{\sqrt{z}} \qquad (B.4)$$

Now in Appendix A, it was noted that the stress field at the crack tip was characterized by the equation

$$\lim_{|z| \to o} Z = \frac{K_I}{\sqrt{2\pi z}} \qquad (A.3)$$

By taking the limit, $|z| \to o$ for equation (B.4) and comparing with (A.3), the opening mode stress intensity for the Griffith crack problem is

$$K_I = \sigma\sqrt{\pi a} \qquad (B.5)$$